On the random-matrix theory of Majorana fermions in topological superconductors

Marco Marciani

geboren te Rome (Italië) in 1989

Cover: The illustration symbolically depicts the search for the unpaired
Majorana bound state. The spherical shape is a tribute to the compact
space of scattering matrices, the plane to the linear spaces of Hamiltonians
and time-delay matrices. The central image is a porcelain with an image
from the Dutch painter H. W. Mesdag. Reprinted with small adaptations
with permission of the owner: Kramer Kunst & Antiek, Amsterdam.

To the "families on mission" in The Netherlands

Contents

Contents

Contents

1 Introduction

1.1 Preface

The last decade, solid state materials with topological order have attracted the attention of the scientific community. Topologically protected states can form at the boundaries or defects of these materials and could be used as robust logical units in quantum computers[1,2]. Among these states, Majorana bound states in superconductors, coherent and equal-weight superpositions of electrons and holes with a real wave function, are of particular interest. The corresponding creation operators possess unusual commutation relations, distinct from the bosonic and fermionic commutators, providing the simplest example of quasipartices with non-Abelian statistics. Many models hosting Majorana bound states have been suggested[3–5] and subsequently investigated in great depth theoretically. Experimentally, we are in the stage between the first detection of Majoranas and their reliable reproducibility[6,7].

Beyond the detailed analysis of specific devices, one may ask about the universality of their properties. The question is also motivated by the natural presence of disorder and imperfections in experimental realizations, which call for a statistical "ensemble" description. Already seventy years ago[8] it had been realized by Wigner and Dyson that Random-Matrix Theory[9] (RMT) provides an elegant and rather simple way to obtain the universal statistical properties of ensembles of random Hamiltonians and random scattering matrices[10–12]. Three universality classes were distinguished originally, depending on the presence or absence of time-reversal and spin-rotation symmetry. Relatively recently, twenty years ago, seven more universality classes were added[13,14], to accommodate chiral symmetry and particle-hole symmetry, and it is in these new classes that we can find topological invariants and Majorana bound states. A central objective of this thesis is to describe the topologically nontrivial universality classes at the same level of detail as the original Wigner-Dyson classes, by filling in the gaps in our knowledge of the various distribution functions. Table 1.1 summarizes what we have been able to contribute.

The predictions from RMT can be tested experimentally in quantum dots, confined regions in a two-dimensional electron gas. The electron

		RMT ensembles		
		Wigner-Dyson	Altland-Zirnbauer	chiral
energy levels		[8,18]	[14]	[13]
ballistic coupling	transmission	[19,20]	[21]	[22]
	delay times	[23]	chapter 2	chapter 3
tunnel coupling	transmission	[24]	[25]	?
	delay times	chapter 4	chapter 4	?

Table 1.1: References to papers that have derived various probability distributions in the random-matrix theory of Hamiltonians and scattering matrices of quantum dots. The columns distinguish the symmetry-based universality classes, a total of 10 in groups of 3+4+3. The rows refer to the distributions of the eigenvalues of the Hamiltonian, of the transmission matrix, and of the time-delay matrix. For the latter two distributions the coupling of the quantum dot to the outside world can be via a ballistic point contact or via a tunnel barrier. Contributions developed in the various chapters of this thesis are marked in red; two green entries remain to be done.

dynamics in a quantum dot is chaotic, due to disorder or due to an irregular shape. Much of the theory of quantum chaos developed for electron billiards can be applied to quantum dots. Superconducting quantum dots, also known as Andreev billiards, represent a good platform for the application of the Altland-Zirnbauer ensembles of RMT[15]. Calculations of the probability distributions of thermal and electrical conductances have shown that topology strongly affects transport properties, even determining a pinning, in some cases, to quantized values[16,17].

One application of the new probability distributions obtained in this thesis is to the density of states $\rho(E)$ of an Andreev billiard. A Majorana bound state shows up as a peak at the Fermi energy ($E = 0$) in the density of states, but to detect this peak in a superconducting quantum dot is nontrivial for the following reason: as illustrated in Fig. 1.1, the peak from the Majorana bound state is superimposed on a dip in the background from the other levels. When the quantum dot is coupled to a point contact, the peak is broadened and merges with the background dip, and the net result is close to the density of states of a topologically trivial system, without the Majorana bound state. Remarkably enough, we have found that the cancellation is *exact* for ballistic coupling: an ensemble of quantum dots has the same distribution of the Fermi-level density of states whether or not there are Majorana bound states. To detect the Majoranas either tunnel coupling or chiral symmetry is needed — the corresponding distributions are calculated in this thesis.

In the rest of this introduction, we summarize the background in quantum transport and random-matrix theory, needed to understand the following chapters. For more accurate and self-contained treatments, references are provided throughout the text. In the last paragraph we
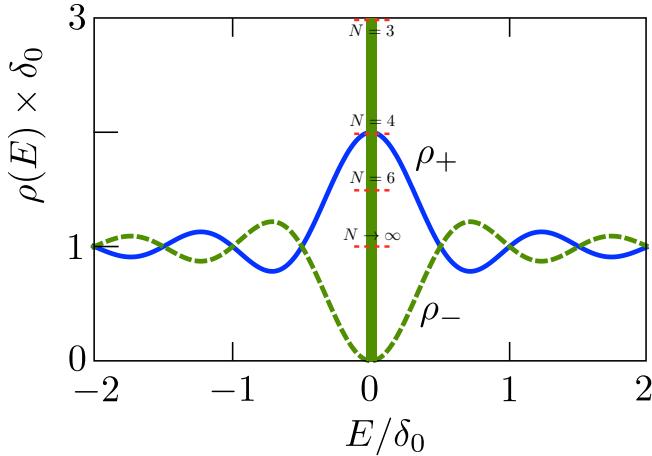
Figure 1.1: Average density of states $\rho(E)$ of an uncoupled superconducting Andreev billiard as a function of the energy E. The labels $-/+$, associated respectively to the green and blue curves, refer to the two topological subclasses of billiards with or without a Majorana bound state. The Majorana delta peak is represented as the green vertical line at the Fermi energy ($E = 0$). The red dashed lines indicate the finite value at $E = 0$ of $\rho(E)$, computed when the billiard is coupled ballistically to N modes. The energy and the functions are rescaled to unit mean level spacing δ_0 of the Hamiltonian ensemble.

present the summaries of the various chapters.

1.2 Scattering formalism in Quantum Transport

To gain information on a physical system, two approaches can be used: an intrinsic or extrinsic one. The first approach consists in working out a mathematical model of the system under investigation, thereby obtaining, at the required degree of depth, a sufficiently detailed understanding of its properties. The second approach consists in coupling the system to another simple and well understood system with fewer degrees of freedom and study how the former system interacts with or respond to the latter. Clearly, the second approach is closer to what experimentalists do in their labs. Inside this working frame, scattering theory is aimed to study the specific case in which the ancillary system consists of probe particles colliding with the main system. Then, many of the properties of the main system can be inferred from the change occurred in the particles state.
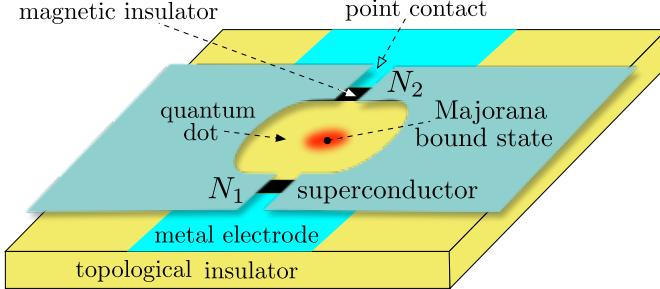
Figure 1.2: Surface states at the edge of a topological insulator form a 2D electron gas. A superconductor is placed on top of the surface and defines a quantum dot (the scattering region) where electrons are allowed to enter from metal electrodes (reservoirs) via two point contacts (the leads). At one side of the bottom- and top-point contact magnetic insulators allow respectively N_1 and N_2 channels to successfully enter the dot. A Majorana zero mode is present in the dot if a magnetic fluxon threads the latter. [From Chapter 4]

In the following we will focus on solid state devices where a satisfactory description of electronic transport phenomena could be obtained assuming a non-self interacting coherent Fermi-liquid of electrons. Electrons are confined, via gating or other potentials, in (ideally long) quasi-1D regions or edges of the device, referred to as *leads* or waveguides, contacted at one end to a *reservoir*, a bigger metallic sample at electrothermic equilibrium. At the other end, the leads is contacted with a small sub-micron region (with characteristic length much bigger than the lead width) with non-regular geometry, where electrons are chaotically scattered. This region is referred to as *scattering region* and can be regarded as zero dimensional. In terms of the description above, the scattering region represents the main system, whose properties are of interest, while the leads the ancillary one. To catch the many essential features of the scattering, it is enough to assume that just two leads are attached to the scattering region. Fig. 1.2 shows one instance of device we will study. Then, the matter of interest is how electronic asymptotic states in the leads shot toward the scattering region are transformed after the interaction into asymptotic states traveling outward.

1.2.1 The scattering matrix S

Let us consider electronic modes in the leads with a specific energy E. Let us call N_1 and N_2 the number of linearly independent modes (sometimes call also channels), with energy E, propagating toward the scattering region respectively in lead 1 and 2. These modes are usually called the *incoming modes*. We will assume the leads to be made of a crystal with inversion symmetry. Therefore, the number of linearly

independent modes propagating outward with the same energy, usually called *outgoing modes*, is the same. For the rest of the thesis we will assume the scattering to be elastic, i.e. with no absorption or dissipation involved.

Let define the two sets of incoming and outgoing asymptotic states respectively as $\{|I_i\rangle\}$ and $\{|O_j\rangle\}$, with $i, j = 0, \ldots, N_1 + N_2$. Using the Schrödinger equation, one can show that the electronic eigenstate at energy E, far away from the scattering region, can be expressed as[28]

$$\psi = \sum_i \alpha_i |I_i(t)\rangle - \sum_{ij} S_{ji}\alpha_i |O_j(t)\rangle \tag{1.1}$$

The full content of the scattering process in contained in the $(N_1 + N_2) \times (N_1 + N_2)$ unitary matrix S. Assuming an incoming wave-packet with small energy broadening, this matrix connects its projections $\{\alpha_i\}$ on the asymptotic states $\{|I_i\rangle\}$, at early times, to its projections $\{\beta_i\}$ on the states $\{|O_i\rangle\}$, at late times, via the relation $\vec{\beta} = S\vec{\alpha}$.

In a two leads problem S can be conveniently block decomposed as

$$S = \begin{pmatrix} r & t' \\ t & r' \end{pmatrix} \tag{1.2}$$

Here r and r' are respectively $N_1 \times N_1$ and $N_2 \times N_2$ matrices, and t, t' are rectangular matrices with the complementing dimensions. The matrices r and r' are referred to as "reflection matrices" relative to the lead 1 and 2, respectively, while t and t' are referred to as "transmission matrices". Generally, such a scattering matrix formalism is used also outside the quantum realm, in systems with wave-dynamics like optics and acoustics[29,30].

1.2.2 Thermal and electrical conductances

The main concern of Quantum Transport is to understand non-equilibrium properties of the systems. Usually, the major goal is the prediction or the understanding of the behavior of currents under variation of an external drive imposed on the system. As straightforward examples, if the drive is a voltage bias between the two leads, one could be interested in the electric current vs voltage bias dependence while, if the drive is a temperature difference, one could be interested in the heat flow vs temperature gradient dependence. Clearly, also cross-responses and more exotic observables could be addressed.

The scattering formalism proves to be a very successful tool for computing all these transport quantities. For example, consider the electrical and the thermal (differential) conductances i.e. the derivative of the

current with respect to the drive. In the most simple case of a normal metal, at low temperature and in weak and constant drive regime, the electrical conductance is

$$G^e := \left.\frac{\partial I}{\partial V}\right|_{V=0} \sim G_0^e \operatorname{Tr} t^\dagger t, \quad G_0^e = \frac{e^2}{h} \tag{1.3}$$

while, similarly, the thermal conductance is

$$G^T := \left.\frac{\partial Q}{\partial T}\right|_{V=0} \sim G_0^T \operatorname{Tr} t^\dagger t, \quad G_0^T = \frac{\pi^2 k_{\mathrm{B}}^2 T}{6h} \tag{1.4}$$

here t is the transmission matrix (cf. Eq. (1.2)) evaluated at the Fermi energy. G_0^{Te}, G_0^T are called respectively electrical and thermal conductance quanta. The interpretation is straightforward: in normal metals currents are made out of electrons filling the incoming modes in one lead and successfully transmitted into the other lead[31]. The quantities $G_0^e \approx 3.37 \times 10^{-5} \Omega^{-1}$ and $G_0^T =\approx (4.73 \times 10^{-13} W/K^2) T$ set the maximum contribution to the conductances one single non-degenerate channel could give. These maxima show an example of quantum upper limit imposed to transport phenomena[32,33].

1.2.3 The Mahaux-Weidenmüller formula

The link between the scattering matrix and the Hamiltonian scattering region is provided by the so-called Mahaux-Weidenmüller formula[28]. The starting point of the derivation is the full Hamiltonian of the scatterer and the leads mode:

$$\mathcal{H} = \sum_{\mu,\nu} |\nu\rangle H_{\mu,\nu} \langle\mu| + \sum_c \int_{E_c}^\infty \mathrm{d}E \, |c(E)\rangle E \langle c(E)|$$
$$+ \sum_{c,\mu} \int_{E_c}^\infty \mathrm{d}E \, |c(E)\rangle W_{c,\mu}(E)\langle\mu| + h.c. \tag{1.5}$$

where H is the scatterer $M \times M$ Hamiltonian, $W(E)$ is a tunneling matrix between the leads modes (both incoming and outgoing) and the scatterer states, E_c is the threshold energy above which a certain channel can gets active i.e. $W(E \leq E_c) = 0$ and $W(E > E_c) \neq 0$.

If the energy dependence of W is sufficiently weak and the energy E is far away from the metallic band edges, the scattering matrix of the channels at that energy is found to be

$$S(E) = \frac{1 - iW(E - H)^{-1}W^\dagger}{1 + iW(E - H)^{-1}W^\dagger} \tag{1.6}$$
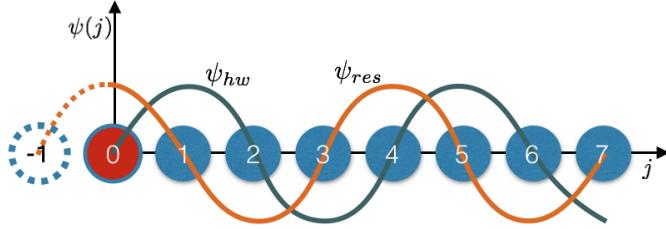
Figure 1.3: Atomic chain with sites positioned at $j = 0, 1, 2, \ldots$. The orbital energy of the 0-th site is assumed to be tunable. An electron with energy $E = \epsilon_0$ is present on the chain and the sketches of its wavefunction in the special cases of hard-wall (ψ_{hw}) and resonance (ψ_{res}) are shown on the vertical axis.

where E is the energy of the incoming electrons and $W(E) \equiv W$.

From this formula one can extract important features of the system. To best highlight them, we consider the case where only one lead is present. In this case electrons can only be reflected back from the scattering region. Energy levels in H which lie far away from E have a small contribution to S because of the term $(E - H)^{-1}$. Moreover, if all of them are far away, S reduces to the identity matrix i.e. the scattering region trivially sends the incoming electrons back to the same channels. On the other hand, if a number of levels are close to E, the associated eigenstates of H have a dominant contribution and an equal number of eigenvalues of S will be close to (-1). If the number of such resonant states equals the number of the attached modes, then $S = -\mathbb{1}$.

A simple example that helps to understand this hard-wall and resonant limit is the following. Consider the semi-infinite atomic chain in Fig. 1.3. All atoms but the first have a single orbital with energy ϵ_0 and the orbital overlap induces a tunneling of amplitude t. We assume the energy of the first atom, ϵ_0', to be tunable:

$$\mathcal{H} = \epsilon_0 \sum_{j=1}^{\infty} c_j^\dagger c_j + \epsilon_0' c_0^\dagger c_0 + t \sum_{j=0}^{\infty} c_j^\dagger c_{j+1} + c_{j+1}^\dagger c_j \qquad (1.7)$$

where c_i is the annihilation operator at the i-th site.

The first atom could be regarded as the scattering region and coupling t between the first and second atom plays the role of W (energy independent). First we check the resonant limit. Let assume the first atom to have orbital energy $\epsilon_0' = \epsilon_0$. The Hamiltonian is readily diagonalized

$$\mathcal{H} = \sum_{k=0}^{\infty} (\epsilon_0 - 2t \cos(ka)) \, c_k^\dagger c_k \qquad (1.8)$$

where a is the lattice constant.

The eigenstates $\psi_k(j) = \alpha \exp(-ikaj) - \beta \exp(ikaj)$ (cf. Eq. (1.1)) must verify the (hard-wall) boundary condition $\psi_k(-1) = 0$. Now, if we consider the eigenstate with energy in resonance with the one of the scattering region (ϵ'_0), its momentum must be $k = \pi/(2a)$. The boundary condition, then, implies $\beta = -\alpha$. Notice that this is in agreement with $S = -1$ as discussed above[*]. To check the hard-wall limit, we increase the energy of the scattering region to make it unaccessible, $\epsilon'_0 \to \infty$. The new boundary condition for the eigenstate, then, is moved on the first atom. The new boundary condition is $\psi_k(0) = 0$. For all eigenstates, and in particular for the previous one, this implies $\beta = \alpha$, compatible with $S = 1$ as discussed above.

1.3 The time-delay matrix Q

The energy dependence of the scattering matrix turns out to be useful to extract information about e.g. low-frequency responses of the system under external drives, the density of state of the system and thermodynamical quantities[34]. A convenient way to work with the derivative of the scattering matrix is to define the matrix

$$Q = -i\hbar S^\dagger \partial S/\partial E \qquad (1.9)$$

The convenience lies upon its mathematical properties (Q is hermitian and closely related to the uniform measure of the space of the matrices S) and its direct physical interpretation. This matrix was first defined by Smith[35], after seminal works[36–38]; its application in Quantum Transport have been reviewed recently by Texier[34]. The matrix Q contains information about the time-delay experienced by the scattered particle with respect to the case in which the interaction is turned off. We show now in some more detail this physical interpretation.

There are essentially two approaches to define and compute time-delays in scattering events. One is a dynamical one, in which a *wave-packet* is shot against the target[36–38]. The other approach[35] considers a *stationary* situation in which a constant particle flux illuminates the target. The central object in this approach is, indeed, the matrix Q in Eq. (1.9).

1.3.1 Wave-packet approach

For simplicity, consider first a one dimensional problem with a scattering region located at $-R \leq x \leq 0$ and a metallic lead, at $x > 0$, with

---

[*]A redefinition of the global phases of the eigenstates $\exp(\pm ikaj)$ may lead to find $S = 1$. The main point, here, is to show opposite values of S in the two cases of resonance and hard-wall barrier.

only one channel. A wave-packet may be constructed on the lead as a superposition of two almost similar monocromatic waves respectively with energies $E_\pm = E \pm \delta E$ and momenta $k_\pm = k \pm \delta k$. The asymptotic form of the wave-packet at $x \gg 0$ can be written as $\psi_{as} = \psi_\alpha - \psi_\beta$ where the incoming wave is

$$\psi_\alpha(x \gg 0, t) = \frac{1}{\sqrt{v}} \left[\exp\left(-i(k_- x + E_- t/\hbar) \right) + \exp\left(-i(k_+ x + E_+ t/\hbar) \right) \right]$$

$$= \frac{2}{\sqrt{v}} \exp\left(-i(kx + Et/\hbar) \right) \cos(\delta kx + \delta E t/\hbar) \qquad (1.10)$$

while the outgoing one is

$$\psi_\beta(x \gg 0, t) = \frac{1}{\sqrt{v}} \left[\exp\left(i(k_- x - E_- t/\hbar + \eta_-) \right) + \exp\left(i(k_+ x - E_+ t/\hbar + \eta_+) \right) \right]$$

$$= \frac{2}{\sqrt{v}} \exp\left(i(kx - Et/\hbar + \eta) \right) \cos(\delta kx - \delta E t/\hbar + \delta\eta)$$

$$(1.11)$$

where v is the channel velocity and η is the phase increment due to the reflection from the scattering region.

The additional phase increment $\delta\eta$ can be understood as the cause of a displacement of the peaks positions of the outgoing wave. With no scatterer action, i.e. hard-wall condition at $x = 0$, $\eta(E) = 0$. If we consider only the peak corresponding to the vanishing trigonometric angle in the cos() function, its position is found to be at $x_0 = \delta E/(\hbar\delta k)\, t - \delta\eta/\delta k = v(t - \hbar\,\delta\eta/\delta E)$. The quantity $\tau := \hbar\,\delta\eta/\delta E$ appears to be retardation of the peak i.e. a *time delay*. Wigner found it to have a lower bound of the order $-R/v$. In our case the scattering region is taken to be 0D, therefore we will find $\tau > 0$. An important remark is that time retardation is associated to the scattering matrix, via η. In particular, it can be expressed in the form of Eq. (1.9) as $\tau = -i\hbar S^\dagger \partial S/\partial E$, as in this case $S = \exp(i\eta)$.

Eisenbud [36] consider this approach in a multi-channel fashion. He found the time-delay of the fraction of an incoming wave-packet in channel i ending up in channel j to be $\tau^{(ij)} = \mathrm{Re}\left[-i\hbar(S_{ij})^{-1}\partial S_{ij}/\partial E \right]$. The quantities $\tau^{(ij)}$ could be used to form naturally a time-delay matrix; however, its connection with S is cumbersome and differs from that of Q in Eq. (1.9).

1.3.2 Steady-state approach

In the steady state approach, the time dependence of the wave is disregarded. Consider the one channel problem analyzed in the previous

paragraph. Smith noticed that the difference in the local density (concentrated around state of the scattering region) in a case under study and in a trivialized situation with vanishing potential disorder is a measure of the time-delay of the scattering process. Indeed, at constant flux normalization of the wave function, higher probabilities in some region correspond to higher dwell times in it. Hence, he defined

$$\tau' = \int_{-R}^{\infty} \mathrm{d}x \ \psi(x)^* \psi(x) - \psi(x)_{as}^* \psi(x)_{as} \qquad (1.12)$$

where $\psi_{as}(x) = \langle x|I \rangle - \langle x|O \rangle$ is the asymptotic superposition of the incoming and outgoing monocromatic waves.

Importantly, he found $\tau' = \tau - \hbar \sin(\eta)/(2E)$ with τ and η as in the previous paragraph. We stress that, in the case relevant for Quantum Transport, scattering happens at high energies ($E_F \gg \hbar/\langle \tau \rangle$), therefore the identity $\tau' \sim \tau$ holds. Inside this frame, also τ may be expressed as a *spatially averaged* local density difference. For technical reasons the generalization to the multi-channel case is best implemented upon the expression for τ, rather then upon τ':

$$\tilde{Q} = \left[\int_{-R}^{\infty} \mathrm{d}x \ \psi_i(x)^* \psi_j(x) - \psi(x)_{as,i}^* \psi(x)_{as,j} \right]_{Av} \qquad (1.13)$$

where $\psi_{as,k}(x) = \langle x|I_k \rangle - \sum_l S_{kn} \langle x|O_n \rangle$.

The equivalence of $\tilde{Q}$ and Q, as in Eq. (1.9), is found to extend also to the multi-channel case. The elements $\tilde{Q}_{ij}$, however, have no transparent physical meaning but the hermiticity of the matrix they form and their bilinear dependence with respect to the modes ψ_k allow for an interpretation.

After diagonalization, one gets the eigenvalues: $\tau_i := \big[\int_{-R}^{\infty} \mathrm{d}x \ \Psi_i(x)^* \Psi_i(x) - \Psi(x)_{as,i}^* \Psi(x)_{as,i} \big]_{Av}$, with $\{\Psi_i\}$ the eigenvector set of $\tilde{Q}$. Comparing with the single channel case, it is evident that the eigenvalues of $\tilde{Q}$ are well-defined dwelling times associated to the eigenvectors of the matrix.

Finally, we remark that Ψ_i has a well-defined time-delay equal to τ_i also in the a wave-packet fashion of Section 1.3.1. Indeed, expanding $S(E)$ in E, one finds that the wave-packets of the form

$$\frac{1}{\sqrt{\hat{v}}} \Psi_i(E) \left[e^{-i(k_- x + E_- t/\hbar)} + e^{-i(k_+ x + E_+ t/\hbar)} \right]$$
$$= \frac{2}{\sqrt{\hat{v}}} \Psi_i(E) e^{-i(kx + Et/\hbar)} \cos(\delta kx + \delta Et/\hbar), \qquad (1.14)$$

where $k_\pm$ and $E_\pm$ defined as in Eq. (1.10), gets scattered into the states

$$\frac{1}{\sqrt{\hat{v}}}\left[S(E_-)\Psi_i(E)e^{-i(k_-x+E_-t/\hbar)}+S(E_+)\Psi_i(E)e^{-i(k_+x+E_+t/\hbar)}\right]$$
$$=\frac{2}{\sqrt{\hat{v}}}S(E)\Psi_i(E)\cos(\delta kx-\delta E(t-\tau_i)/\hbar) \tag{1.15}$$

with well-defined delay times τ_i, (here $\hat{v}$ is the diagonal matrix of the channels velocities). Notice that $\Psi_i(E)$ is not, in general, an eigenstate of $S(E)$.

1.3.3 Time-delay matrix of a 0D system

The matrix Q can be expressed in terms of the scatterer Hamiltonian using its definition, in Eq. (1.9), and the Mahaux-Weidermüller formula Eq. (1.6):

$$Q(E)=W^\dagger\frac{1}{E-H-i\pi WW^\dagger}\frac{1}{E-H+i\pi WW^\dagger}W \tag{1.16}$$

From this expression, the hermiticity of Q is evident, as it has the form of a product $XX^\dagger$. This suggests to consider the dual matrix $Q_D:=X^\dagger X$ which shares with Q the same set of non-zero eigenvalues. We have used this matrix in Chapter 3 to compute the joint distribution of the time-delays $\{\tau_i\}$ in a RMT setting. Moreover, this $M\times M$ matrix has the interesting feature to be also a *dual* of Q also in its physical interpretation. Easily, one can check

$$Q_D(E)=\frac{1}{E-H+i\pi WW^\dagger}WW^\dagger\frac{1}{E-H-i\pi WW^\dagger}$$
$$=-\frac{i}{\pi}\mathrm{Ant}\left[\frac{1}{E-H-i\pi WW^\dagger}\right]$$
$$=\frac{i}{\pi}\mathrm{Ant}\left[G^R(E)\right] \tag{1.17}$$

where $\mathrm{Ant}[\cdot]=1/2\left[(\cdot)-(\cdot)^\dagger\right]$ stands for anti-Hermitian part, and $G^R(E)$ is the retarded Green function of the quantum dot with the self energy $i\pi WW^\dagger$ induced by the coupling with the lead.

The reader may appreciate how, on the one hand, Q is a matrix describing *extrinsic* properties of the scatterer while, on the other hand, Q_D describes it *intrinsically*.

The connection of Q with the density of state of the (coupled) quantum dot [39–41], is made evident by Q_D:

$$\mathrm{Tr}Q(E)=\mathrm{Tr}Q_D(E)=-\mathrm{Im}\mathrm{Tr}G^R(E)=2\pi\,\rho(E) \tag{1.18}$$

where the property $\mathrm{Tr}\mathrm{Ant}[\cdot]=-i\,\mathrm{Im}\mathrm{Tr}[\cdot]$ has been used and the last step is implied by a well known identity in Green function theory.

1.4 Majorana fermions

Majorana fermions[42] are the particles whose field satisfies a real representation of the Dirac equation. The Majorana field must be Hermitian:

$$\psi(r,t) = \psi^\dagger(r,t) \tag{1.19}$$

Such particles are their own antiparticle as it can be seen from the eigenmodes expansion of the field. Bosonic particles with the latter property are easy to be found (photons, pions and so on) while Majorana particles have not been detected so far[43].

In Condensed Matter Physics, Majorana fermions appear in superconducting systems. In this context, the real Dirac equation is replaced by the real Bogoliubov-de Gennes equations in the Nambu space. The latter equation describes the excitations over the nontrivial vacuum of Cooper pairs. Since these excitations, called Bogoliubov excitations, are described by a real field they are actually Majorana fermions. Their particle annihilation operator satisfies

$$d_E = (d_{-E})^\dagger, \tag{1.20}$$

with E the energy of the particle.

As states with negative energy describe antiparticles, the previous relation states the equality between the Bogoliubov particles and their antiparticles. This property implies, for instance, that holes in the Nambu formalism are not really the independent antiparticles of the electrons as opposed to the case of positrons in the high-energy context.

Remarkably, if one is to deal with a model superconductor with an odd number of states - call it an odd-states superconductor - then one excitation is necessarily pinned at $E = 0$. For this special state its creation/annihilation operator satisfies (cf. Eq. Eq. (1.21)):

$$\gamma = \gamma^\dagger, \tag{1.21}$$

where we have defined $\gamma = d_0$.

The γ excitation is profoundly different from the other excitations at finite energy as it verifies

$$\{\gamma, \gamma^\dagger\} = 1$$
$$\gamma^2 = 1/2. \tag{1.22}$$

Remind that, for regular fermions, one expects $d^2 = 0$.

This γ excitation has a fixed occupation $1/2$ and is therefore questionable whether is appropriate to call it "excitation" and not simply a "state" or
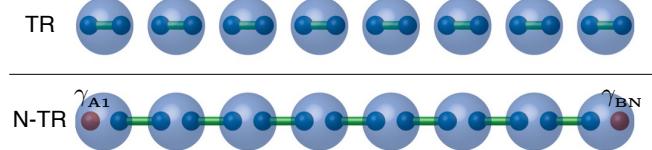
Figure 1.4: Kitaev chain in the topological trivial phase (up) and in the topologically non-trivial one (down), at a special choice of the Hamiltonian parameters as in Ref. 5. Each electron complex state of the chain (big blue circles) can be decomposed into two Majorana states (little blue circles). Bogoliubov excitations involve Majorana states connected by the green lines. In the topologically non-trivial phase unpaired Majorana bound states, γ_{A1} and γ_{BN}, appear and are localized at the two ends of the chain. Different choices of the parameters do not spoil the qualitative feature of these pictures.

"mode". To rescue from misleading physical interpretations, we remark that real superconductors can have only an even number of states as electrons come always in pair with a hole. In Sec. 1.4.1 we will show how some superconductors can be thought as "split" into two odd-states superconductors featuring two distinct γ states, called in this cases "Majorana bound states".

Hermitian Majorana-like operators are usefully exploited for the analysis of generic superconductors. For any fermionic degree of freedom c_n, n being an unspecified quantum number, we can define two "Majorana operators", A and B:

$$\begin{aligned}
\gamma_{An} &:= c_n + c_n^\dagger \\
\gamma_{Bn} &:= i(c_n - c_n^\dagger)
\end{aligned} \tag{1.23}$$

Notice that the property (1.21) does not hold for even-states superconductors for which, in the limit of vanishing E, one has $d_{0^-} \neq d_{0^+}$. Nonetheless, two Majorana (hermitian) operators at zero energy can be defined as in Eq. (1.23) using d_{0^-} and d_{0^+} instead of c and $c^\dagger$.

1.4.1 Majorana bound states and Kitaev chain

The properties of Majorana bound states can be harnessed for quantum computation purposes in some topological superconductors. A qubit can be constructed out of excitations that are robust under local noise and controllable in a deterministic way.

The simplest example of such system came out in the year 2001[5]. Kitaev showed that a p-wave superconducting and spinless electronic chain (of finite length $N \gg 1$) presents a phase transition to a phase which supports an excitation at zero-energy and localized at the two ends of the chain (see Fig. Fig. 1.4). This zero-energy Bogoliubov particle,

$d^{(Kit)}$, can be expressed as the sum of two Majorana operators in this way: $d^{(Kit)} = \gamma_{A1} + i\gamma_{BN}$, where the degree of freedom $n = 1, N$ indicates spatial localization of the corresponding states, respectively around the first and last sites (cf. Eq. (1.23)). γ_{A1} and γ_{BN} are the two "Majorana bound states". Only non-local perturbations can delocalize them and move from zero the energy of the excitation associated to $d^{(Kit)}$. In the following we give an heuristic explanation of these features.

First, notice that in this topological phase all bulk excitations are localized in space (at least for the case of the "special" Hamiltonian parameters chosen by Kitaev). As a consequence, as we are interested in the excitations at the ends of the chain, we can write two distinct Nambu Hamiltonians, H_j ($j = 1, 2$), each describing one edge. Both Hamiltonians can be written as $H_j = iA_j$ with A_j an antisymmetric matrix (cf. Sec. 1.6.2). The crucial point is that the dimensions of both matrices are odd as they must describe the states associated to a certain number of Bogoliubov excitations of finite energy (each requiring two Nambu degrees of freedom) and the one associated to the single Majorana operator, either γ_{A1} or γ_{BN}. Odd antisymmetric matrices have a pinned zero eigenvalue and describe odd-states superconductors. In principle, if we now add local perturbations in the chain, the Hamiltonian of the bulk may become relevant, connect the states of the two ends and break the validity of our Hamiltonian splitting argument. However, if $N \gg 1$ any effective coupling of the two edges is exponentially suppressed, as N increases. Thus local perturbations can only affect the elements of H_j separately and the dimensions of the matrices themselves, but leaving these dimensions with the same (odd) parity.

As the two ends of the chain are effectively decoupled, we have seen a realization of two odd-states superconductors each one supporting an unpaired Majorana bound state γ. We conclude that Majorana bound states are states that are stiffly localized in space. Moreover, they constitute an excitation ($d^{(Kit)}$) bound at zero energy that can be used as a qubit.

Other mechanisms have been found to produce Majorana bound states, they are well described in Ref. 2. Most of the setups considered in this work (cf. Fig. 1.2), exploit the fact that magnetic fluxons threading a 2D electron gas in a p-wave superconducting phase are encircled by a vortexing zero-energy Majorana bound states.

1.5 Random-Matrix Theory

Random-Matrix theory (RMT) finds its origin in the late 19th century[9]. In a nutshell, it is the theory of *matrices ensembles* i.e. matrix spaces

with a given (probabilistic) measures.

A first application of this tool to a physical problem have been discovered by Wigner[47] in 1955. The problem regarded the understanding of general properties of neutron scattering off heavy nuclei. Experiments were showing narrow resonances at certain energies. Inside the compound-nucleus approach[48], a description of such a phenomenon could be done in terms of the so-called R-matrix, function of the energy of the collision and of nucleus excitation energy. However, the complexity of the nuclei Hamiltonians hinder an exact treatment of such R-matrix and suggest that a stochastic approach could be effective. Following Wigner, the problem can be attacked at follows. The nucleus Hamiltonian is, in principle, an operator on a infinite dimensional Hilbert spaces. One can truncate the Hilbert space to a finite dimensional subspace, therefore representing the Hamiltonian operator by a matrix of finite dimension M. At reason, one can assume that all matrix elements should be independently and identically distributed and that eigenvectors rotations should leave the distribution unchanged. These conditions are met only by a *Gaussian measure*[12] of the form

$$d\mu(H) = e^{-\text{Tr}H^2/2\sigma^2}\mathrm{d}H \tag{1.24}$$

Having a probability for the Hamiltonian, one is finally enabled to compute the probability density function (or its momenta) of physical observables (e.g. the R-matrix). To meet physical consistency, the limit $M \to \infty$ has to be performed at the end of the calculation.

The only inputs to this theory are the degrees of freedom of the entries H_{ij}, inferred by the physical symmetries the system possesses, and the energy scale σ. In real applications, however, a more accessible energy scale is the so-called *mean level spacing* δ_0 i.e. the average difference between two subsequent eigenvalues E_i of H in the *bulk* of their joint distribution (that is $|E_i| \ll \sqrt{M}$). A part from a factor c, of order unity and dependent on the symmetry, $\sigma_0 = c\sqrt{M}\delta_0/\pi$ holds.

Motivated by the somewhat arbitrary assumptions giving rise to the above Gaussian ensemble, in a series of important papers[18], Dyson applied the statistical approach directly to the scattering matrices, defining the so-called Circular ensembles. To meet physical consistency only rotational invariance of the distribution is assumed as a chaotic system should not privilege any of the scattering channels. The important gain of this approach is that the specific ensemble describing a system is defined only by the symmetries of the system and no energy scale is needed as an input. The only ensemble measure allowed by the physical requirements is the so-called invariant Haar measure of the space of unitary matrices

$$d\mu(U) = -iU^\dagger \mathrm{d}U \tag{1.25}$$

appropriately restricted to the matrices U *compatible* with the symmetries of the system.

In the following years, the field has rapidly developed. For what concerns this Thesis, we simply underline two important formal results. First, the Gaussian ensemble has been shown to be the simplest in a whole class of ensembles (with a more complex function of H inside the trace in Eq. (1.24)) giving rise, asymptotically in M, to the same eigenvalues correlation functions[49]. Second, for a certain set of symmetries (the Wigner-Dyson one, see Section 1.6.1), the Gaussian ensemble has been proven to be equivalent to the Circular one when dealing with the kind of scattering processes we consider here[24]. These results will allow us to make use of both Gaussian and Circular ensembles interchangeably.

1.5.1 RMT and Quantum Transport

In the context of electronic Quantum Transport in mesoscopic devices, RMT can be applied to study *chaotic quantum billiards* or *chaotic quantum dots*. Usual realization of such billiards are 2D regions of sub-micron size, located at the interface of crystals along the 1D path of a confined 2D electron gases. In the scattering formalism language, the chaotic billiard is the scattering region and the 1D electron path determines the leads (one, two or more). A chaotic quantum billiard is defined as a billiard whose classical description (obtained sending $\hbar \to 0$) would be chaotic. The Hamiltonian of a chaotic quantum billiard is expected to show *level repulsion* as some parameter (e.g. shape, lattice constant) is varied. Such feature is typical of generic Hamiltonians of the Gaussian ensembles. Moreover, transport observables present several features not present in integrable quantum systems. For instance, the electrical and thermal conductances show *universal conductance fluctuations*. These features are signatures of non-deterministic chaotic transport, confirmed by several experiments in the past years. The conclusion is that chaotic billiard can be studied by means of RMT. However, one has to keep in mind there are some limitations in the allowed energy range of the scattered particles (electron or hole) for the applicability. Essentially, if $\tau = \mathrm{Tr}Q/N$ is the channel-averaged dwell time, then RMT is applicable if $t_E, t_{erg} \ll \tau \ll t_\phi$, where t_E is the Ehrenfest time, t_{erg} is the ergodic time, and t_ϕ the dephasing time[51].

	Wigner-Dyson			Altland-Zirnbauer				Chiral		
Class	**A**	**AI**	**AII**	**D**	**DIII**	**C**	**CI**	**AIII**	**BDI**	**CII**
H-name	GUE	GOE	GSE	–	–	–	–	chGUE	chGOE	chGSE
S-name	CUE	COE	CSE	CRE	T_-CRE	CQE	T_+CQE	–	T_+CRE	T_-CQE

Table 1.2: For each symmetry class, the names of the relative Hamiltonian and scattering matrix ensembles are given. The sign "–" indicates that a name has not yet been consensually assigned.

1.6 Symmetry Classes and the ten-fold way

We give now a list of the ensembles of the matrices H, S and Q, relevant for 0D systems[11,14,15].

Consider a one-body electronic Hamiltonian H. When dealing with an electronic chaotic systems (especially 0D systems), four kind of commutation properties have physical relevance (these are usually called *symmetries*). H can commute or anticommute with a unitary or antiunitary operator. Conventional symmetries are unitary operators commuting with H. In the following, we will assume there are none of them in the system, or equivalently, we can assume we are treating separately the sectors of H with different quantum numbers associated to these latter symmetries. The other commuting properties are usually referred to with the name of a prominent element: time-reversal $\mathcal{T}$ (antiunitary commuting); particle/hole $\mathcal{C}$, (antiunitary anticommuting); chiral $\mathcal{S}$, (unitary anticommuting). Notice that the presence of both $\mathcal{T}$ and $\mathcal{C}$ symmetries implies the symmetry $\mathcal{S}$.

In the usual Nambu space (spin 1/2) $\mathcal{T}^2 = -1$ and $\mathcal{C}^2 = 1$ hold. When spin rotational (unitary and commuting) symmetry is present, once H is restricted to one spin-block, the system is effectively spinless. For this reason, the list below contains also ensembles with $\mathcal{T}^2 = 1$ and $\mathcal{C}^2 = -1$.

Three families of ensembles, named Wigner-Dyson, Altland-Zirnbauer and Chiral, are found out of ten independent combinations of these symmetries, according to different values of the squares of the operators. Sometimes, this classification is picturesquely referred to as the *ten-fold way*. Table 1.2 presents the names of the Hamiltonian and scattering matrices ensembles associated to each ensemble - notice that mathematicians usually prefer to call the latter "classes".

1.6.1 Wigner-Dyson ensembles

The time-delay matrix Q in this ensembles has the same structure of the Hamiltonian H.

Class A *(No symmetries).* The Hamiltonian H is a complex hermitian matrix. The associated scattering matrix S is complex unitary.

Class AI *(Time reversal and spin-rotational symmetries, $\mathcal{T}^2 = 1$).* This class contains effectively spinless systems. One can always find a basis where H is real. The matrix S is unitary symmetric and can be written as the product UU^T, with U complex unitary.

Class AII *(Time reversal symmetry, $\mathcal{T}^2 = -1$).* This class contains spin-full systems. The 2×2 Hamiltonian spin blocks, are real quaternions[*]. The matrix S is unitary self-dual (or, equivalently, unitary symplectic), where self-dual means $\sigma_y S^T \sigma_y = S$ with σ_y acting on the spin degree of freedom.

1.6.2 Altland-Zirnbauer ensembles

Particle/hole symmetry is present in these ensembles. Notice that Q has now a different structure from H. Moreover, classes D and DIII carry a $\mathbb{Z}_2$ topological invariant. For more details, check Table II in Chapter 4.

Class D *(Particle/hole symmetry, $\mathcal{C}^2 = 1$).* In the Majorana basis, introduced in Section 1.4, H is a purely imaginary antisymmetric matrix. The matrix S is orthogonal. As in class AI, Q is real symmetric.

Class DIII *(Particle/hole and Time reversal symmetries, $\mathcal{C}^2 = 1, \mathcal{T}^2 = -1$).* In the Majorana basis H is a purely imaginary antisymmetric matrix but now the spin blocks (coupling same Majorana states with opposite spins) are real quaternions (the entries of which are pure imaginary). The matrix S is orthogonal and self-dual. The matrix Q is real symmetric with real quaternionic elements.

Class C *(Particle/hole and spin-rotational symmetries, $\mathcal{C}^2 = -1$).* Similarly to class AI, this ensemble contains effectively spinless systems. In the Nambu basis, the Hamiltonian is the imaginary unit times an anti-hermitian real quaternionic matrix. The matrix S is unitary with real quaternionic elements. The matrix Q is hermitian real quaternionic. For all the matrices H, S and Q, the quaternionic structure is in the particle/hole degree of freedom.

---

[*]A real quaternion $\mathbf{q}$ as the structure $\mathbf{q} = q_0\sigma_0 + i\vec{q}\cdot\vec{\sigma}$.

Class CI *(Particle/hole, Time reversal and spin-rotational symmetries,* $\mathcal{C}^2 = -1, \mathcal{T}^2 = 1$*)*. In the Nambu basis, H is the imaginary unit times the real part of an antihermitian real quaternionic matrix. The associated S is complex unitary with real quaternionic elements and symmetric. As in class DIII, Q is real symmetric with real quaternionic elements.

1.6.3 Chiral ensembles

A chiral operator can square only to 1. The classes DIII and CII in the previous paragraph are also chiral symmetric as they possesses both $\mathcal{T}$ and $\mathcal{C}$ symmetries (notice that $\mathcal{T}^2 \mathcal{C}^2 = -1$ holds in these ensembles). The chiral ensembles comprehends, however, systems with either only chiral symmetry or with all symmetries provided $\mathcal{T}^2 \mathcal{C}^2 = 1$. These systems carry a $\mathbb{Z}$ topological invariant. Moreover, the electronic states can be divided in two groups, say A and B, upon which the chiral operator is represented by $\tau_z = \mathbb{1}_M \oplus (-\mathbb{1}_{M'})$, with $M(M')$ the dimension of the space spanned by the $A(B)$ electrons. Thus, H is a $(M + M') \times (M + M')$ hermitian matrix with vanishing diagonal $M \times M$ and $M' \times M'$ blocks. The scattering matrix in these ensembles is conveniently defined as $\tilde{S} = \tau_z S$, (S being connected to H via Eq. (1.6)). Remarkably, Q commutes with $\tilde{S}$. Hence, time eigenstates are also scattering eigenstates.

Class AIII *(Chiral symmetry)*. The Hamiltonian off diagonal blocks have complex elements. The matrix $\tilde{S}$ is unitary and hermitian. It can be represented as $U \tau U^{\dagger}$, with U unitary and τ a diagonal signature matrix. The matrix Q is hermitian.

Class BDI *(Chiral, Particle/hole and Time reversal symmetry,* $\mathcal{C}^2 = 1, \mathcal{T}^2 = 1$*)*. The Hamiltonian off diagonal blocks have real elements. The matrix $X \tilde{S} X^{\dagger}$, with $X = \mathbb{1}_A \oplus (i\mathbb{1}_B)$ is orthogonal and symmetric and can be written as $O \tau O^T$, with O unitary and τ a diagonal signature matrix. The matrix Q is real symmetric.

Class CII *(Chiral, Particle/hole and Time reversal symmetry,* $\mathcal{C}^2 = -1, \mathcal{T}^2 = -1$*)*. The Hamiltonian off diagonal blocks have quaternionic elements. The matrix $X \tilde{S} X^{\dagger}$ (X as above) is unitary self-dual and can be written as $U \tau U^{\dagger}$, with U is unitary symplectic equivalent (i.e. maps self-dual matrices to self-dual ones) and τ a diagonal signature matrix. The matrix Q is hermitian self-dual.
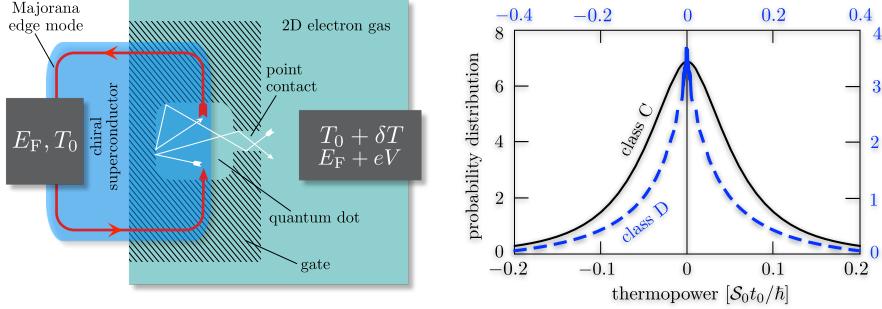
Figure 1.5: (left) Andreev-billiard geometry to measure the thermopower $\mathcal{S}$ of a semiconductor quantum dot coupled to chiral Majorana modes at the edge of a topological superconductor. A temperature difference δT induces a voltage difference $V = -\mathcal{S}\delta T$ under the condition that no electrical current flows between the contacts. For a random-matrix theory we assume that the Majorana modes are uniformly mixed with the modes in the point contact, by chaotic scattering events in the quantum dot. (right) Probability distribution of the dimensionless thermopower $p = \mathcal{S} \times \hbar/t_0\mathcal{S}_0$ in symmetry class C (black solid curve, bottom and left axes), and in class D (blue dashed curve, top and right axes). These are results for the quantum dot of Fig. 2.2 connecting a single-channel point contact to the unpaired Majorana edge mode of a chiral p-wave superconductor (class D), or to the paired Majorana mode of a chiral d-wave superconductor (class C). [From Chapter 2]

1.7 This thesis

1.7.1 Chapter 2

In this chapter we compute (i) the joint probability density function of S and Q related to a chaotic quantum dot in the regime of ballistic coupling for the Altland-Zirnbauer ensembles, (ii) the average density of states in the dot and (iii) the probability density function of the Seebeck coefficient (also called thermopower), $\mathcal{S} = (\partial G(E)/\partial E)/G(E)$. All quantities are computed at the Fermi energy (defined as $E = 0$), as the most characteristic features due to the ensemble symmetries manifest themselves at this energy. The derivation of (i) is a generalization of the one for the Wigner-Dyson ensembles, to be found in Ref. 52. However, some additional care was required to take into account the topological invariant of classes D and DIII. Similarly to the case of the Wigner-Dyson ensembles, S and Q are found to be independently distributed, S with a uniform distribution and Q with a Laguerre-type one. In classes D and DIII, the independence of S and Q implies the remarkable independence of the pd.f. of Q from the topological invariants. As a consequence, also the average density of states is found to be topology independent. In contrast to the case of the Wigner-Dyson ensembles, the quantity is dependent on the number of channels that couple to the dot. As an

application of the previous findings, the thermopower is considered. It depends both on S and Q and has no direct topology dependence. As $\mathcal{S}$ vanishes if $G(E)$ is an even function, a minimal superconducting setup must have a three terminal geometry. The thermopower probability density function have been computed for minimal channels cases, for classes D and C. Finally, we discuss how thermopower could be used for the detection of chiral edge states.

1.7.2 Chapter 3

We complete, here, the calculation of the joint probability density function of S and Q, at the Fermi energy and in the ballistic coupling regime, for all ten ensembles adding the computation regarding the three chiral ensembles. In these ensembles S and Q are not fully independent, as they commute, and a different approach to the computation is required. The computation of the time-delay eigenvalues distribution is made easier using the hermitian-dual of $Q = 2\pi\hbar\Omega\Omega^\dagger$ i.e. $\tilde{Q} = 2\pi\hbar\Omega^\dagger\Omega$. This matrix shares with Q the same non-zero eigenvalues, but has a block diagonal structure. Surprisingly, the finite eigenvalues of the two blocks (i.e the proper delay times) have *independent* Laguerre distributions; moreover, they depend on the topological number ν of the dot. Since the scattering matrix depends on ν only up to a certain saturation value ($\nu = N$), Q has more topological information than S, as opposed to the cases of classes D and DIII (see Chapter 2). Restricting ourselves to a case of equal dimension N of the chiral sectors of the scattering channels, we compute the average density of states in the dot. It is found to diverge at values of the topological number close to the saturation one. Focusing on an Andreev chaotic billiard formed on top of a topological insulator, we compute analytically the different time-delay distributions as the chemical potential is set to the Dirac point or is far away from it. In the former case the system is in the chiral class BDI, in the latter case in class D. The difference in the distribution is striking and, remarkably, could be experimentally measured on the same physical system.

1.7.3 Chapter 4

This chapter is the natural completion of Chapter 2. Here, we analyze the effect of a tunnel barrier at the entrance of a QD on the joint probability density function of S and Q for the Altland-Zirnbauer ensembles. The two matrices get statistically correlated. As a consequence, the marginal distribution of Q, in classes D and DIII, acquires a marked dependence on the topological invariant. For classes D and C, we compute the average density of states of the QD as a function of a generic barrier.
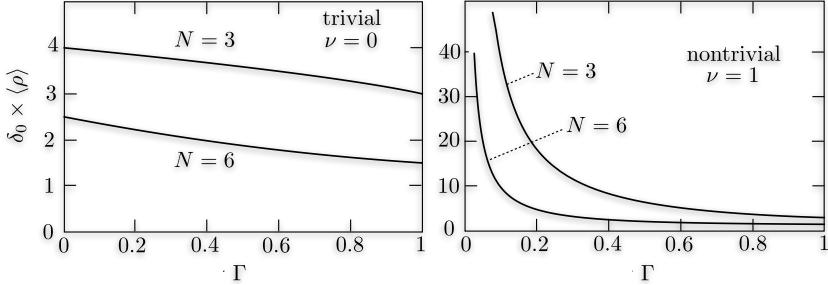
Figure 1.6: Ensemble averaged (Class D) density of states as a function of mode-independent transmission probability Γ through the barrier, in the absence ($\nu = 0$) or in the presence ($\nu = 1$) of a Majorana bound states. [From Chapter 4]

Interestingly, the DoS in the trivial topological phase of class D, calculated in the tunnelling limit does not coincide with the DoS of the closed system. Again for class D, we focus the attention on the Poisson Kernel, the probability density function of S, trying to understand why, at ballistic coupling, many statistical features due to a Majorana bound state disappear. With this task in mind, we consider the thermal and the Andreev conductances. They are observables that depend only on the scattering properties of one terminal. We found that just one channel (of the terminal not engaged by the observable) coupled ballistically is enough to make the effect of the Majorana bound state disappear. Finally, we study the variation of the average Andreev conductance across the topological phase transition in a QD/nanowire geometry.

1.7.4 Chapter 5

This last chapter presents a contribution to a different field of research: the control of nanomagnets composed by "adatoms" (atoms adsorbed on surfaces). One of the main goals is to obtain a sufficient magnetization stability to make them exploitable as bit units. At low temperature and other specific conditions, the adatom can be described as an effective spin with well-defined magnitude. In some systems, the main effect of the substrate crystaline field is to set the ground state to be degenerate and formed by the two states with highest spin projection (in modulo) to the axis perpendicular to the substrate. However, the same field may couple these two states splitting them energetically, an unwanted phenomenon called "ground state splitting". Moreover scattering of substrate electrons off the atom destabilizes the atomic state, creating transitions between the two states. When just one electron is needed for such transitions the process is referred to as "single electron switching". Building on
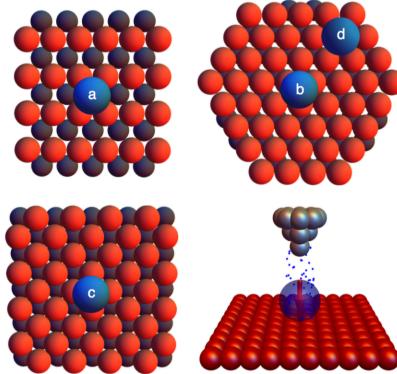
Figure 1.7: (a-d) Atoms deposited on different surfaces with $C_{\chi v}$ symmetry. $\chi = 2, 3, 4, 6$ respectively for the adatoms (a),(b),(c),(d). (e) Sketch of a scanning tunneling microscope current measurement to infer the total momentum of the atom. The tip of the microscope is in grey.[From Chapter 5]

earlier discoveries, we describe rigorously how the point group symmetry of the substrate and the time reversal symmetry forbid either ground state splitting or single electron switching or both, via selection rules. We identify which combinations of rotational symmetries and spin magnitudes are expected to be stable (i.e. with neither ground state splitting and single electron switching mechanisms), time reversal symmetry being present or not. The mirror symmetry is found to produce no selection rules. Finally, we use the same formalism to analyze configurations of adatoms interacting via generic (first-order) Heisenberg interaction. In a setting similar to the known Lieb-Mattis theorem but generalized by the presence of the crystaline field, we prove a theorem about the ground state of the atomic clusters and conjecture its extension. The analytics is supported by numerics that simulates typical outputs of scanning electron microscope measurements.

Bibliography of chapter 1

[1] C. Nayak, S. H. Simon, A. Stern, M. Freedman, S. Das Sarma, Rev. Mod. Phys. **80**, 1083 (2008).

[2] J. Alicea, Rep. Progr. Phys. **75**, 076501 (2012).

[3] G. Volovik, JETP Lett. **70**, 609 (1999).

[4] N. Read and D. Green, Phys. Rev. B **61**, 10267 (2000).

[5] A. Y. Kitaev, Phys.-Usp. **44**, 131 (2001).

[6] V. Mourik, K. Zuo, S. M. Frolov, S. R. Plissard, E. P. A. M. Bakkers, and L. P. Kouwenhoven, Science **336**, 1003 (2012). M. T. Deng, C. L. Yu, G. Y. Huang, M. Larsson, P. Caroff, and H. Q. Xu, NanoLett. **12**, 6414 (2012). L. P. Rokhinson, X. Liu, and J. K. Furdyna, Nat. Phys. **8**, 795 (2012). A. Das, Y. Ronen, Y. Most, Y. Oreg, M. Heiblum, and H. Shtrikman, Nat. Phys. **8**, 887 (2012).

[7] J. Alicea, Nature Nanotech. **8**, 623 (2013).

[8] E.P. Wigner, Gatlinberg conference on neutron physics, Oak Ridge National Laboratory Report ORNL 2309 59 (1957).

[9] Persi Diaconis, Peter J. Forrester, arXiv:1512.09229.

[10] C. W. J. Beenakker, Rev. Mod. Phys. **69**, 731 (1997).

[11] Handbook on Random Matrix Theory, edited by G. Akemann, J. Baik, and P. Di Francesco (Oxford University Press, Oxford, 2011).

[12] P. J. Forrester, Log-Gases and Random Matrices (Princeton University Press, 2010).

[13] J. J. M. Verbaarschot, Phys. Rev. Lett. **72**, 2531 (1994).

[14] A. Altland and M. R. Zirnbauer, Phys. Rev. B **55**, 1142 (1997).

[15] C. W. J. Beenakker, Rev.Mod.Phys. **87**, 1037 (2015).

[16] C. W. J. Beenakker, J. P. Dahlhaus, M. Wimmer, and A. R. Akhmerov, Phys. Rev. B **83**, 085413 (2011).

Bibliography of chapter 1

[17] M. Diez, J. P. Dahlhaus, M. Wimmer, C. W. J. Beenakker, Phys. Rev. B **86**, 094501 (2012).

[18] F. J. Dyson, J. Math. Phys. **3**, 140; 157; 166; 1199 (1962).

[19] H. U. Baranger, and P. A. Mello, Phys. Rev. Lett. **73**, 142 (1994).

[20] R. A. Jalabert, J.-L. Pichard, and C. W. J. Beenakker, Europhys. Lett. **27**, 255 (1994).

[21] J. P. Dahlhaus, B. Béri, C. W. J. Beenakker, Phys. Rev. B **82**, 014536 (2010).

[22] A. F. Macedo-Junior, and A. M. S. Macêdo, Phys. Rev. B **66**, 041307(R) (2002); **77**, 165313 (2008).

[23] P. W. Brouwer, K. M. Frahm, and C. W. J. Beenakker, Phys. Rev. Lett. **78**, 4737 (1997).

[24] P. W. Brouwer, Phys. Rev. B **51**, 16878 (1995).

[25] B. Béri, Phys. Rev. B **79**, 214506 (2009).

[26] V. A. Gopar, P. A. Mello, and M. Büttiker, Phys. Rev. Lett. **77**, 3005 (1996).

[27] P. W. Brouwer, S. A. van Langen, K. M. Frahm, M. Büttiker, and C. W. J. Beenakker, Phys. Rev. Lett. **79**, 913 (1997).

[28] C. Mahaux and H. A. Weidenmüller, Shell-model approach to nuclear reactions (North-Holland, 1969).

[29] M. Born, E. Wolf, Principles of optics: electromagnetic theory of propagation, interference and diffraction of light (Oxford, Pergamon Press, 1964).

[30] Varatharajulu and Pao, J. Acoust. Soc. Am. **60**, 556 (1976).

[31] R. Landauer, IBM Journ. of Res. and Dev. **1**, 223-231 (1957).

[32] J. B. Pendry, J. Phys. A **16**, 2161-2171 (1983).

[33] K. Schwab, E. A. Henriksen, J. M. Worlock, and M. L. Roukes, Nature **404**, 974 (2000).

[34] C. Texier, Physica E **82**, 16-33 (2016).

[35] F. T. Smith, Phys. Rev. **118**, 349 (1960).

[36] L. Eisenbud, dissertation, Princeton, June (1948) (unpublished).

[37] D. Bohm, Quantum Theory, (Prentice-Hall, New York, 1951).

[38] E. P. Wigner, Phys. Rev. **98**, 145 (1955).

[39] M. Sh. Birman and M. G. Krein, Soviet Math. Dokl. **3**, 740 (1962).

[40] E. Akkermans, A. Auerbach, J. E. Avron, and B. Shapiro, Phys. Rev. Lett. **66**, 76 (1991).

[41] N. Lehmann, D. V. Savin, V. V. Sokolov, and H.-J. Sommers, Physica D **86**, 572 (1995).

[42] E. Majorana, Nuovo Cimento **14**, 171-184 (1937).

[43] F. Wilczek, Nature Phys. **5**, 614-618 (2009).

[44] M. Leijnse and K. Flensberg, Semi. Sci. Tech. **27**, 124003 (2012).

[45] T. D. Stanescu, and S. Tewari, J. Phys. Cond. Matt. **25**, 233201 (2013).

[46] C. W. J. Beenakker, Annu. Rev. Con. Mat. Phys. **4**, 113 (2013).

[47] E.P. Wigner, Ann. of Math. Second Series **62** 3, 548-564 (1955).

[48] N. Bohr, Nature **137**, 344 (1936).

[49] Chap. 6 in Ref. 11 and references therein.

[50] S. Oberholzer, E. V. Sukhorukov, C. Strunk, C. Schönenberger, T. Heinzel, and M. Holland Phys. Rev. Lett. **86**, 2114 (2001); S. Oberholzer, E. V. Sukhorukov, C. Schönenberger, Nature **415**, 765-767 (2002); Washburn, S., and R. A. Webb, Adv. Phys. **35**, 375 (1986) and I. H. Chan, R. M. Clarke, C. M. Marcus, K. Campman, and A. C. Gossard, Phys. Rev. Lett. **74**, 3876 (1995).

[51] P. G. Silvestrov, M. C. Goorden, and C. W. J. Beenakker, Phys. Rev. B **67**, 241301(R) (2003); J. Tworzydło, A. Tajic, H. Schomerus, P. W. Brouwer, and C. W. J. Beenakker, Phys. Rev. Lett. **93**, 186806 (2004).

[52] P. W. Brouwer, K. M. Frahm, and C. W. J. Beenakker, Waves in Random Media **9**, 91 (1999).

2 Time-delay matrix, midgap spectral peak, and thermopower of an Andreev billiard

2.1 Introduction

A semiconductor quantum dot feels the proximity to a superconductor even when a magnetic field has closed the excitation gap that would open in zero magnetic field: The average density of states has either a peak or a dip,[1]

$$\rho_{\pm}(E) = \delta_0^{-1} \pm \frac{\sin(2\pi E/\delta_0)}{2\pi E}, \tag{2.1}$$

see Fig. 2.1, within a mean level spacing δ_0 from the Fermi level at $E = 0$ (in the middle of the superconducting gap). The appearance of a midgap spectral peak or dip distinguishes the two symmetry classes C (dip, when spin-rotation symmetry is preserved) and D (peak, spin-rotation symmetry is broken by strong spin-orbit coupling). These Altland-Zirnbauer symmetry classes exist because of the $\pm E$ electron-hole symmetry in a superconductor, and are a late addition to the Wigner-Dyson symmetry classes conceived in the 1960's to describe universal properties of nonsuperconducting systems.[2]

Electron-hole symmetry in the absence of spin-rotation symmetry allows for a nondegenerate level at $E = 0$, a socalled Majorana zero-mode.[3,4] The class-D spectral peak is then converted into a dip, $\rho_+ \to \rho_- + \delta(E)$, such that the integrated density of states remains the same as without the zero-mode.[5,6] The entire spectral weight of this Fermi-level anomaly is $1/2$, consistent with the notion that a Majorana zero-mode is a half-fermion.[7]

Here we study what happens if the quantum dot is coupled to M conducting modes, so that the discrete spectrum of the closed system is broadened into a continuum. We focus on the strong-coupling limit, typically realized by a ballistic point contact, complementing earlier work on the limit of weak coupling by a tunnel barrier or a localized
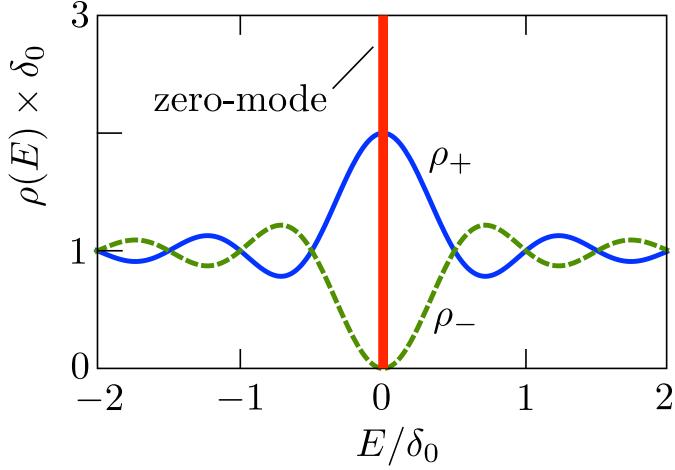
Figure 2.1: Ensemble-averaged density of states (2.1) of an Andreev billiard in symmetry class C (ρ_-, dashed curve), or class D without a Majorana zero-mode (ρ_+, solid curve). The class D billiard with a Majorana zero-mode has the smooth density of states ρ_- together with the delta-function contribution from the zero-mode. In this chapter we investigate how the midgap spectral peak or dip evolves when the billiard is opened via a ballistic point contact to a metallic reservoir. We find that the distinction between class C and D remains, but the signature of the Majorana zero-mode is lost.

conductor.[8–15] The simplicity of the strong-coupling limit allows for an analytical calculation using random-matrix theory of the entire probability distribution of the Fermi-level density of states — not just the ensemble average. Using the same random-matrix approach we also calculate the probability distribution of the thermopower of the quantum dot, which is nonzero in spite of electron-hole symmetry when the superconductor contains gapless Majorana edge modes.[16]

The key technical ingredient that makes these calculations possible is the joint probability distribution of the scattering matrix S and the time-delay matrix $Q = -i\hbar S^\dagger dS/dE$, in the limit $E \to 0$. This is known for the Wigner-Dyson ensembles,[17] and here we extend that to the Altland-Zirnbauer ensembles. The Fermi-level density of states then follows directly from the trace of Q, while the thermopower requires also knowledge of the statistics of S. We find that these probability distributions depend on the symmetry class (C or D), and on the number M of conducting modes, but are the same irrespective of whether the quantum dot contains a Majorana zero-mode or not. A previous calculation[14] had found that the density-of-states signature of a Majorana zero-mode becomes less evident when the quantum dot is coupled by a tunnel barrier to the continuum. We conclude that ballistic coupling completely removes any trace of the Majorana zero-mode in the density
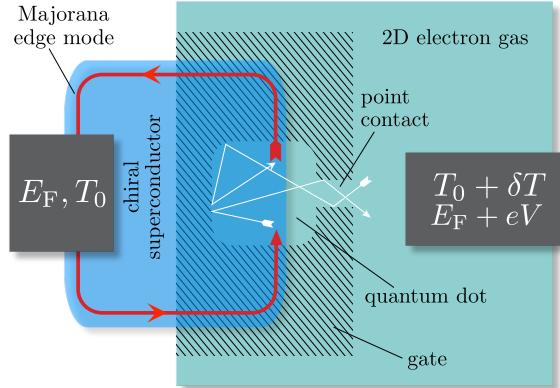
Figure 2.2: Andreev-billiard geometry to measure the thermopower $\mathcal{S}$ of a semiconductor quantum dot coupled to chiral Majorana modes at the edge of a topological superconductor. A temperature difference δT induces a voltage difference $V = -\mathcal{S}\delta T$ under the condition that no electrical current flows between the contacts. For a random-matrix theory we assume that the Majorana modes are uniformly mixed with the modes in the point contact, by chaotic scattering events in the quantum dot.

of states, as well as in the thermopower — but not, we hasten to add, in the Andreev conductance.[18]

The outline of the chapter is as follows. In the next section we present the geometry of an "Andreev billiard",[19] a semiconductor quantum dot with Andreev reflection from a superconductor and a point-contact coupling to a metallic conductor. (Systems of this type have been studied experimentally, for example in Refs. 20–22.) We derive a formula relating the thermopower to the scattering matrix S and time-delay matrix Q, in a form which is suitable for a random-matrix approach. The distribution of the transmission eigenvalues T_n of S was already derived in Ref. 23; what we need additionally is the distribution of the eigenvalues D_n of Q (the delay times), which we present in Sec. 2.3. The distributions of the Fermi-level density of states and thermopower are given in Secs. 2.4 and 2.5, respectively. We conclude in Sec. 4.10.

2.2 Scattering formula for the thermopower

We study the thermopower of a quantum dot connecting a two-dimensional topological superconductor and a semiconductor two-dimensional electron gas (see Fig. 2.2). In equilibrium the normal-metal contact and the superconducting contact have a common temperature T_0 and chemical potential E_F. Application of a temperature difference δT induces a voltage difference V at zero electrical current. The ratio $\mathcal{S} = -V/\delta T$ is the

thermopower or Seebeck coefficient.

In the low-temperature limit $\delta T \ll T_0 \to 0$ the thermopower is given by the Cutler-Mott formula,[24]

$$\mathcal{S}/\mathcal{S}_0 = -\lim_{E \to 0} \frac{1}{G} \frac{dG}{dE}, \quad \mathcal{S}_0 = \frac{\pi^2 k_B^2 T_0}{3e}, \tag{2.2}$$

in terms of the electrical conductance $G(E)$ near the Fermi level ($E = 0$). See Ref. 16 for a demonstration that this relationship, originally derived for normal metals, still holds when one of the contacts is superconducting and G is the Andreev conductance.

Without gapless Majorana modes in the superconductor the Andreev conductance is an even function of E, so the ratio $\mathcal{S}/\mathcal{S}_0$ vanishes in the low-temperature limit. For that reason, with some exceptions,[25,26] most studies of the effect of a superconductor on thermo-electric transport take a three-terminal geometry, where the temperature difference is applied between two normal contacts and the conductance is not so constrained.[27–36] As pointed out by Hou, Shtengel, and Refael,[16] Majorana edge modes break the $\pm E$ symmetry of the conductance allowing for thermo-electricity in a two-terminal geometry — even if they themselves carry only heat and no charge.

In a random-matrix formulation of the problem two matrices enter, the scattering matrix at the Fermi level $S_0 \equiv S(E = 0)$ and the Wigner-Smith time-delay matrix[37–39]

$$Q = -i\hbar \lim_{E \to 0} S^\dagger \frac{dS}{dE}. \tag{2.3}$$

Before proceeding to the random-matrix theory, we first express the thermopower in terms of these two matrices. The existing expressions in the literature[40,41] cannot be directly applied for this purpose, since they do not incorporate Andreev reflection processes.

The Andreev conductance is given by[42]

$$G(E)/G_0 = \tfrac{1}{2} N - \operatorname{Tr} r_{ee}(E) r_{ee}^\dagger(E) + \operatorname{Tr} r_{he}(E) r_{he}^\dagger(E), \tag{2.4}$$

in terms of the matrix of reflection amplitudes

$$r = \begin{pmatrix} r_{ee} & r_{eh} \\ r_{he} & r_{hh} \end{pmatrix} \tag{2.5}$$

for electrons and holes injected via a point contact into the quantum dot. The submatrix r_{ee} describes normal reflection (from electron back to electron), while r_{he} describes Andreev reflection (from electron to hole, induced by the proximity effect of the superconductor that interfaces

with the quantum dot). The conductance quantum is $G_0 = e^2/h$ and N is the total number of modes in the point contact (counting spin and electron-hole degrees of freedom), so r has dimension $N \times N$.

Without edge modes in the superconductor, the reflection matrix r would be unitary at energies E below the superconducting gap. In that case one can simplify Eq. (2.4) as $G/G_0 = 2 \operatorname{Tr} r_{he} r_{he}^\dagger$. Because of the gapless edge modes the more general formula (2.4) is needed, which does not assume unitarity of r.

Equivalently, Eq. (2.4) may be written in terms of the full unitary scattering matrix $S(E)$,

$$G(E)/G_0 = \tfrac{1}{2}N - \tfrac{1}{2}\operatorname{Tr} \mathcal{P}\tau_z S(E)\mathcal{P}(1+\tau_z)S^\dagger(E), \qquad (2.6)$$

where the Pauli matrix τ_z acts on the electron-hole degree of freedom and $\mathcal{P}$ projects onto the modes at the point contact:

$$S = \begin{pmatrix} r & t' \\ t & r' \end{pmatrix}, \quad \mathcal{P}\tau_z = \begin{pmatrix} \tau_z & 0 \\ 0 & 0 \end{pmatrix}. \qquad (2.7)$$

The off-diagonal matrix blocks t, t' couple the N' Majorana edge modes to the N electron-hole modes in the point contact, mediated by the quasibound states in the quantum dot. The incoming and outgoing Majorana edge modes are coupled by the $N' \times N'$ submatrix r'.

Electron-hole symmetry in class D is most easily accounted for by first making a unitary transformation from S to

$$S' = \begin{pmatrix} U & 0 \\ 0 & U \end{pmatrix} S \begin{pmatrix} U^\dagger & 0 \\ 0 & U^\dagger \end{pmatrix}, \quad U = \sqrt{\tfrac{1}{2}}\begin{pmatrix} 1 & 1 \\ i & -i \end{pmatrix}. \qquad (2.8)$$

In this socalled Majorana basis[*] the electron-hole symmetry relation reads

$$S'(E) = S'^*(-E). \qquad (2.9)$$

The Pauli matrix τ_z transforms into τ_y, so the conductance is given in the Majorana basis by

$$G(E)/G_0 = \tfrac{1}{2}N - \tfrac{1}{2}\operatorname{Tr} \mathcal{P}\tau_y S'(E)\mathcal{P}(1+\tau_y)S'^\dagger(E). \qquad (2.10)$$

In what follows we will omit the prime, for ease of notation.

To first order in E the energy dependence of the scattering matrix is given by

$$S(E) = S_0[1 + iE\hbar^{-1}Q + \mathcal{O}(E^2)]. \qquad (2.11)$$

---

[*]The transformation (2.8) from electron-hole basis to Majorana basis assumes that there is an even number of modes at each contact. This number is odd if the superconductor has an unpaired Majorana mode, in which case we have to work in the Majorana basis from the very beginning.

Unitarity and electron-hole symmetry together require that S_0 is real orthogonal and Q is real symmetric, both in the Majorana basis. The conductance, still to first order in E, then takes the form

$$G(E)/G_0 = \tfrac{1}{2}N - \tfrac{1}{2}\operatorname{Tr}\mathcal{P}\tau_y S_0 \mathcal{P}(1+\tau_y)S_0^{\mathrm{T}}$$
$$- \tfrac{1}{2}iE\hbar^{-1}\operatorname{Tr}\mathcal{P}\tau_y S_0\big[Q\mathcal{P}(1+\tau_y) - \mathcal{P}(1+\tau_y)Q\big]S_0^{\mathrm{T}}. \qquad (2.12)$$

Since $\operatorname{Tr}\mathcal{P}\tau_y X$ vanishes for any symmetric matrix X, we can immediately set some of the traces in Eq. (2.12) to zero:

$$G(E)/G_0 = \tfrac{1}{2}N - \tfrac{1}{2}\operatorname{Tr}\mathcal{P}\tau_y S_0 \mathcal{P}\tau_y S_0^{\mathrm{T}}$$
$$- \tfrac{1}{2}iE\hbar^{-1}\operatorname{Tr}\mathcal{P}\tau_y S_0\big(Q\mathcal{P} - \mathcal{P}Q\big)S_0^{\mathrm{T}}. \qquad (2.13)$$

The resulting thermopower is

$$\mathcal{S}/\mathcal{S}_0 = i\hbar^{-1}\frac{\operatorname{Tr}\mathcal{P}\tau_y S_0 (Q\mathcal{P} - \mathcal{P}Q)S_0^{\mathrm{T}}}{N - \operatorname{Tr}\mathcal{P}\tau_y S_0 \mathcal{P}\tau_y S_0^{\mathrm{T}}}, \qquad (2.14)$$

in the Majorana basis. Equivalently, in the electron-hole basis one has

$$\mathcal{S}/\mathcal{S}_0 = i\hbar^{-1}\frac{\operatorname{Tr}\mathcal{P}\tau_z S_0 (Q\mathcal{P} - \mathcal{P}Q)S_0^{\dagger}}{N - \operatorname{Tr}\mathcal{P}\tau_z S_0 \mathcal{P}\tau_z S_0^{\dagger}}. \qquad (2.15)$$

This scattering formula for the thermopower is a convenient starting point for a random-matrix calculation. Notice that the commutator of Q and $\mathcal{P}$ in the numerator ensures a vanishing thermopower in the absence of gapless modes in the superconductor, because then the projector $\mathcal{P}$ is just the identity.

2.3 Delay-time distribution in the Altland-Zirnbauer ensembles

Chaotic scattering in the quantum dot mixes the N' Majorana edge modes with the N electron-hole modes in the point contact. The assumption that the mixing uniformly covers the whole available phase space produces one of the circular ensembles of random-matrix theory, distinguished by fundamental symmetries that restrict the available phase space.[43] Two Altland-Zirnbauer symmetry classes support chiral Majorana modes at the edge of a two-dimensional superconductor,[44–46] corresponding to spin-singlet d-wave pairing (symmetry class C) or spin-triplet p-wave pairing (symmetry class D). Time-reversal symmetry is broken in both, in class C there is electron-hole symmetry as well as spin-rotation symmetry, while in class D only electron-hole symmetry remains. (See Table 2.1.)

symmetry class	C	D
pair potential	spin-singlet d-wave	spin-triplet p-wave
canonical basis	electron-hole	Majorana
S-matrix elements	quaternion	real
S-matrix space	symplectic	orthogonal
circular ensemble	CQE	CRE
d_T	4	1
d_E	2	1
α	2	-1
β	4	1

Table 2.1: The two Altland-Zirnbauer symmetry classes that support chiral Majorana edge modes, with d-wave pairing (class C) or p-wave pairing (class D). The "canonical basis" is the basis in which the scattering matrix elements are quaternion (class C) or real (class D). The degeneracies d_T and d_E refer to transmission eigenvalues and energy eigenvalues, respectively. The α and β parameters determine the exponents in the probability distributions (2.17) and (2.18) of the transmission eigenvalues and inverse delay times.

The uniformity of the circular ensembles is expressed by the invariance

$$P[S(E)] = P[U \cdot S(E) \cdot U'] \tag{2.16}$$

of the distribution functional $P[S(E)]$ upon multiplication of the scattering matrix by a pair of energy-independent matrices U, U', restricted by symmetry to a subset of the full unitary group: In class C they are quaternion symplectic* in the electron-hole basis (circular quaternion ensemble, CQE), while in class D they are real orthogonal in the Majorana basis (circular real ensemble, CRE).

The unitary invariance (2.16) of the Wigner-Dyson scattering matrix ensembles was postulated in Ref. 47 and derived from the corresponding Hamiltonian ensembles in Ref. 48. We extend the derivation to the Altland-Zirnbauer ensembles in App. 2.7.1. The key step in this extension is to ascertain that the class-D unitary invariance applies to U, U' in the full orthogonal group — without any restriction on the sign of the determinant.

For the thermopower statistics we need the joint distribution $P(S_0, Q)$ of Fermi-level scattering matrix and time-delay matrix. The invariance (2.16) implies $P(S_0, Q) = P(-1, Q)$ (take $U = -S_0^\dagger$, $U' = 1$), so Q is statistically independent of S_0 and the two matrices can be considered separately.[17†]

---

*We recall the definition of a quaternion, $q = q_0\tau_0 + iq_1\tau_x + iq_2\tau_y + iq_3\tau_z$, with real coefficients q_n. A symplectic matrix U is unitary, $UU^\dagger = 1$, and satisfies $U^* = \tau_y U \tau_y$. Since $q^* = \tau_y q \tau_y$, a symplectic matrix is a unitary matrix with quaternion elements (just like an orthogonal matrix is a unitary matrix with real elements).

†Ref. 17 uses a modified definition of the time-delay matrix, with a symmetrized

The uniform distribution of S_0 in the symplectic group (CQE, class C) or orthogonal group (CRE, class D) directly gives the probability distribution of the transmission eigenvalues $T_n \in [0,1]$ of quasiparticles from the normal metal into the superconductor. [These are the quantities that determine the thermal conductance $\propto \sum_n T_n$, not the electrical conductance (2.4).] For a transmission matrix of dimension $N' \times N$ there are $N_{\min} = \min(N, N')$ nonzero transmission eigenvalues, fourfold degenerate ($d_T = 4$) in class C and nondegenerate ($d_T = 1$) in class D. The $N_{\min}/d_T$ distinct T_n's have probability distribution[23]

$$P(\{T_n\}) \propto \prod_k T_k^{\beta|\delta N|/2} T_k^{-1+\beta/2} (1 - T_k)^{\alpha/2}$$
$$\times \prod_{i<j} |T_i - T_j|^{\beta}, \qquad (2.17)$$

with $\delta N = (N - N')/d_T$ and parameters α, β listed in Table 2.1.[49]

The Hermitian positive-definite matrix Q has dimension $\mathcal{M} \times \mathcal{M}$ with $\mathcal{M} = N + N'$. Its eigenvalues $D_n > 0$ are the delay times, and $\gamma_n \equiv 1/D_n$ are the corresponding rates. The degeneracy d_T of the D_n's is the same as that of the T_n's. The derivation of the distribution $P(\gamma_1, \gamma_2, \ldots \gamma_M)$ of the $M = \mathcal{M}/d_T$ distinct delay rates is given in App. 2.7, for all four Altland-Zirnbauer symmetry classes: C, D without time-reversal symmetry and CI, DIII with time-reversal symmetry. The result is

$$P(\{\gamma_n\}) \propto \prod_k \Theta(\gamma_k) \gamma_k^{\alpha + M\beta/2} \exp\left(-\tfrac{1}{2}\beta t_0 \gamma_k\right)$$
$$\times \prod_{i<j} |\gamma_i - \gamma_j|^{\beta}. \qquad (2.18)$$

The unit step function $\Theta(\gamma)$ ensures that the probability vanishes if any γ_n is negative. The characteristic time t_0 is defined by

$$t_0 = \frac{d_E}{d_T} \frac{2\pi\hbar}{\delta_0}, \qquad (2.19)$$

in terms of the average spacing δ_0 of d_E-fold degenerate energy levels in the isolated quantum dotThe mean level spacing δ_0 includes the electron-hole degree of freedom, so the single-electron Hamiltonian has mean level spacing $2\delta_0$. Since δ_0 is the mean spacing of *distinct* levels, the mean spacing of all levels is δ_0/d_E.. For $\alpha = 0$ and $d_E = d_T$ we recover the result of Ref. 17 for the Wigner-Dyson ensembles.

energy derivative, to ensure the independence of S_0 and Q also in the presence of time-reversal symmetry. This modification is not needed for the class C and D ensembles considered in the main text, so we can stay with the usual unsymmetrized definition (4.8). The more general case is considered in App. 2.7.3.

The difference between the Altland-Zirnbauer and Wigner-Dyson ensembles manifests itself in a nonzero value of α and in a difference in the degeneracies d_E and d_T of energy and transmission eigenvalues (see Table 2.1). One has $d_T = d_E$ in the absence of particle-hole symmetry or when the particle-hole conjugation operator $\mathcal{C}$ squares to $+1$; when $\mathcal{C}^2 = -1$ one has $d_T = 2d_E$.[*]

Already at this stage we can conclude that the thermopower distribution in the circular ensemble does not depend on the presence or absence of Majorana zero-modes inside the quantum dot, for example, bound to the vortex core in a chiral p-wave superconductor.[3,4] The parity of the number n_M of Majorana zero-modes fixes the sign of the determinant of the orthogonal class-D scattering matrix,

$$\text{Det } S_0 = (-1)^{n_M}. \tag{2.20}$$

The unitary invariance (2.16) of the CRE implies, on the one hand, that $P(S_0, Q)$ is unchanged under the transformation $S_0 \mapsto U S_0$, $U = \text{diag}(-1, 1, 1, \ldots 1)$, that inverts the sign of $\text{Det } S_0$. (Here we make essential use of the fact that Eq. (2.16) in class D applies to the full orthogonal group.) On the other hand, the same transformation leaves the thermopower (2.14) unaffected, provided we assign the first matrix element to a superconducting edge mode (so $\mathcal{P}\tau_y$ commutes with U).

2.4 Fermi-level anomaly in the density of states

2.4.1 Analytical calculation

A striking difference between the Wigner-Dyson and Altland-Zirnbauer ensembles appears when one considers the density of states at the Fermi level ρ_0, related to the time-delay matrix by

$$\rho_0 = \frac{1}{2\pi\hbar} \frac{d_T}{d_E} \sum_{n=1}^{M} D_n. \tag{2.21}$$

(The factor d_T/d_E is needed because delay times and energy levels may have a different degeneracy. The density of states counts degenerate

---

[*]To understand why the degeneracies d_E and d_T of energy and transmission eigenvalues may differ in the presence of particle-hole symmetry, we recall that Kramers degeneracy applies to Hermitian operators that commute with an anti-unitary operator squaring to -1. The Hamiltonian H anti-commutes with the particle-hole conjugation operator $\mathcal{C}$, so Kramers theorem does not apply. In contrast, the transmission matrix product $tt^\dagger$ commutes with $\mathcal{C}$, so when $\mathcal{C}^2 = -1$ its eigenvalues have a Kramers degeneracy.

levels once.) In the Wigner-Dyson ensembles the average density of states equals exactly $1/\delta_0$, independent of the symmetry index β and of the number of channels M that couple the discrete spectrum inside the quantum dot to the continuum outside.[17,51]

In the Altland-Zirnbauer ensembles, instead, we find from Eq. (2.18) thatThe result (2.22) for the average density of states in the Altland-Zirnbauer ensembles follows upon integration of the probability distribution (2.18). This can be achieved with the help of the general integral formulas of F. Mezzadri and N. J. Simm, J. Math. Phys. **52**, 103511 (2011), but it's easier to start from the zero-α equation $(Mt_0)^{-1}\langle\sum_n D_n\rangle = 1/M$ and note that a nonzero α amounts to the substitution $M \mapsto M + 2\alpha/\beta$ on the right-hand-side.

$$\delta_0\langle\rho_0\rangle = \frac{1}{t_0}\left\langle\sum_{n=1}^{M} D_n\right\rangle = \frac{M}{\max(0, M + 2\alpha/\beta)}$$

$$= \begin{cases} M/(M+1) & \text{in class C for any } M \geq 1, \\ M/(M-2) & \text{in class D for } M \geq 3, \\ \infty & \text{in class D for } M = 1, 2. \end{cases} \qquad (2.22)$$

It is known[1,6,8–15] that the tunneling density of states of a superconducting quantum dot with broken time-reversal symmetry, weakly coupled to the outside, has a Fermi-level anomaly consisting of a narrow dip in symmetry class C and a narrow peak in class D. Eq. (2.22) shows the effect of level broadening upon coupling via M channels to the continuum. For $M \to \infty$ the normal-state result $1/\delta_0$ is recovered, but for small M the Fermi-level anomaly persists.

For $M = 1, 2$ the average density of states in class D diverges, because of a long tail in the probability distribution of $\kappa \equiv \delta_0\rho_0$:

$$P_{\mathrm{D}}(\kappa) = \begin{cases} (2\pi)^{-1/2}\kappa^{-3/2}e^{-(2\kappa)^{-1}} & \text{for } M = 1, \\ \kappa^{-3}(2 + \kappa)e^{-2/\kappa} & \text{for } M = 2. \end{cases} \qquad (2.23)$$

See Fig. 2.3 for a plot and a comparison with the class-C distribution, that has a finite average for alle M.

The result (2.23) holds irrespective of the sign of Det S_0, in other words, the statistics of the Fermi-level anomaly in the CRE does not depend on the presence or absence of an unpaired Majorana zero-mode in the quantum dot. As we remarked at the end of the previous section, in connection with the thermopower, this is a direct consequence of the unitary invariance (2.16) of the circular ensemble.
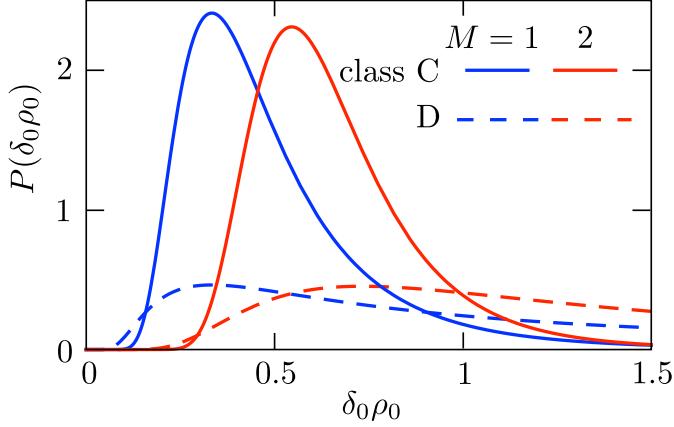
Figure 2.3: Probability distributions of the Fermi-level density of states, for $M = 1$ and $M = 2$ modes coupling the quantum dot to the continuum, in symmetry classes C and D. The ensemble average diverges for class D, see Eq. (2.22).

2.4.2 Numerical check

As check on our analytical result we have calculated $P(\rho_0)$ numerically from the Gaussian ensemble of random Hamiltonians. We focus on symmetry class D, where we can test in particular for the effect of a Majorana zero-mode.

The Hamiltonian H is related to the scattering matrix $S(E)$ by the Weidenmüller formula,[52,53]

$$S(E) = \frac{1 + i\pi W^\dagger (H - E)^{-1} W}{1 - i\pi W^\dagger (H - E)^{-1} W}$$
$$= 1 + 2\pi i W^\dagger (H_{\text{eff}} - E)^{-1} W, \quad H_{\text{eff}} = H - i\pi W W^\dagger. \qquad (2.24)$$

The $M_0 \times M$ matrix W couples the M_0 energy levels in the quantum dot to $M \ll M_0$ scattering channels. Ballistic coupling corresponds to

$$W_{nm} = \delta_{nm} \sqrt{M_0 \delta_0}/\pi. \qquad (2.25)$$

The density of states is determined by the scattering matrix via[54]

$$\rho(E) = -\frac{i}{2\pi} \frac{d}{dE} \ln \text{Det}\, S(E). \qquad (2.26)$$

From Eqs. (4.4) and (2.26) we obtain an expression for the Fermi-level density of states in terms of the Hamiltonian,

$$\rho_0 = \text{Tr}\left(\left[1 - 2\pi i W^\dagger (H_{\text{eff}}^\dagger)^{-1} W \right] W^\dagger H_{\text{eff}}^{-2} W \right). \qquad (2.27)$$
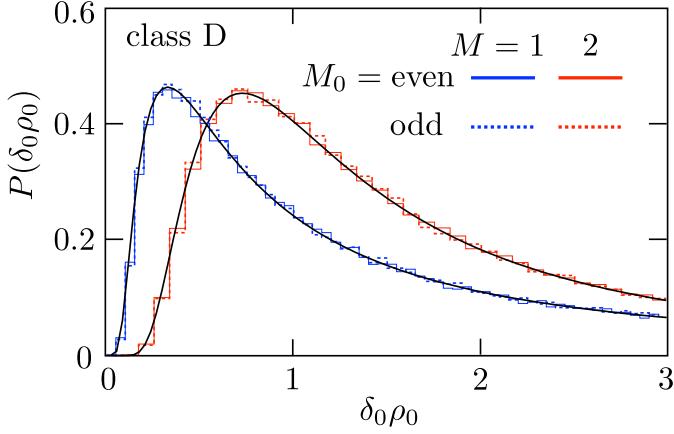
Figure 2.4: Histograms: Probability distributions of the Fermi-level density of states in symmetry class D for $M = 1$, $M_0 = 140, 141$ and $M = 2$, $M_0 = 200, 201$, calculated numerically from Eq. (2.27) by averaging the Hamiltonian over the Gaussian ensemble. For each dimensionality M of the scattering matrix we compare an even-dimensional Hamiltonian, without a Majorana zero-mode, to an odd-dimensional Hamiltonian with a zero-mode. The black curve is the analytical result (2.23) for the circular scattering matrix ensemble, predicting no effect from the Majorana zero-mode for this case of ballistic coupling. Notice that there is no fit parameter in this comparison between numerics and analytics.

In the Majorana basis the class-D Hamiltonian is purely imaginary, $H = iA$, with A a real antisymmetric matrix. The Gaussian ensemble has probability distribution[6,50]

$$P(A) \propto \prod_{n>m} \exp\left(-\frac{\pi^2 A_{nm}^2}{2M_0 \delta_0^2}\right).$$ (2.28)

The dimensionality of A is odd if the quantum dot contains an unpaired Majorana zero-mode, otherwise it is even.

Numerical results for the probability distribution of ρ_0 for $M = 1, 2$ scattering channels are shown in Fig. 2.4. The agreement with the analytical distribution (2.23) is excellent, including the absence of any effect from the Majorana zero-mode.

2.5 Thermopower distribution

We apply the general thermopower formulas (2.14) and (2.15) to a single-channel point contact, with transmission probability T into the edge mode of the superconductor. There are two independent delay times D_1, D_2 in class C, each with a twofold spin degeneracy and a twofold electron-hole degeneracy ($d_T = 4$). Because of this degeneracy the class-C

edge mode contains Kramers pairs of Majorana fermions. In class D the Majorana edge mode is unpaired and all delay times are nondegenerate ($d_T = 1$). The point contact contributes two and the edge mode one more, so class D has a total of three independent delay times D_1, D_2, D_3.

Eqs. (2.14) and (2.15) can be expressed in terms of these quantities, see App. 2.8. We denote the dimensionless thermopower by $p = (\hbar/t_0)\mathcal{S}/\mathcal{S}_0$ and add a subscript C,D to indicate the symmetry class. For class C we have

$$p_{\mathrm{C}} = \frac{(D_2/t_0 - D_1/t_0)\xi\sqrt{T(1-T)}}{1 - (1-T)\cos 2\beta}. \tag{2.29}$$

The independent variables β, ξ enter via the eigenvectors of S_0 and Q, with distribution

$$P(\beta,\xi) = \tfrac{3}{4}(1 - \xi^2)\sin 2\beta, \ \ |\xi| < 1, \ \ 0 < \beta < \pi/2. \tag{2.30}$$

The class-D distribution p_{D} has a more lengthy expression, involving three delay times, see App. 2.8. These are all averages in the grand-canonical ensemble, without including effects from the charging energy of the quantum dot (which could force a transition into the canonical ensemble).[55]

The resulting distributions, shown in Fig. 2.5, are qualitatively different, with a quadratic maximum in class C and a cusp in class D. The variance diverges in class D, while in class C

$$\langle p_{\mathrm{C}}^2 \rangle = \frac{2}{15}(3\ln 2 - 2) = 0.011. \tag{2.31}$$

2.6 Conclusion

Perhaps the most remarkable conclusion of our analysis is that the density of states of a Majorana zero-mode is not topologically protected in an open system.

Take a superconducting quantum dot with an unpaired Majorana zero-mode and bring it into contact with a metallic contact, as in Fig. 4.6 — is something left of the spectral peak? The answer is "yes" for tunnel coupling,[8–15] as it should be if the level broadening is less than the level spacing in the quantum dot. What we have found is that the answer is "no" for ballistic coupling, with level broadening comparable to level spacing.

As an intuitive explanation, one might argue that this is the ultimate consequence of the fact that the two average densities of states $\rho_+(E)$ and $\rho_-(E) + \delta(E)$ of a closed quantum dot without and with a Majorana zero-mode are markedly different,[5,6] see Eq. (2.1), and yet have the same
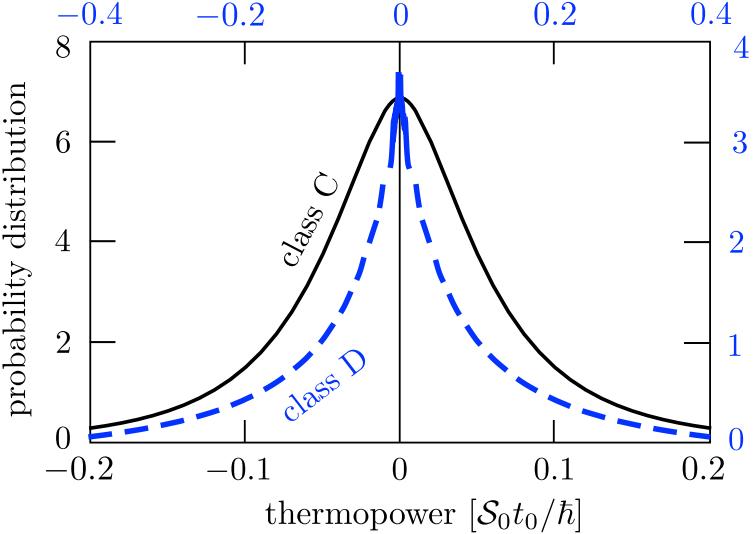
Figure 2.5: Probability distribution of the dimensionless thermopower $p = \mathcal{S} \times \hbar/t_0 \mathcal{S}_0$ in symmetry class C (black solid curve, bottom and left axes), and in class D (blue dashed curve, top and right axes). These are results for the quantum dot of Fig. 2.2 connecting a single-channel point contact to the unpaired Majorana edge mode of a chiral p-wave superconductor (class D), or to the paired Majorana mode of a chiral d-wave superconductor (class C).

integrated spectral weight of half a fermion. Still, we had not expected to find that the entire probability distribution of the Fermi-level density of states becomes identical in the topologically trivial and nontrivial system, once the quantum dot is coupled ballistically to $M \geq 1$ conducting modes.

It would be a mistake to conclude that the whole notion of a topologically nontrivial superconductor applies only to a closed system. Indeed, the Andreev conductance remains sensitive to the presence or absence of a Majorana zero-mode, even for ballistic coupling, when no trace is left in the density of states. [18] This can be seen most directly for the case $M = 2$ of a superconducting quantum dot coupled to a normal metal by a pair of spin-resolved electron-hole modes. The Andreev conductance is then given simply by

$$G = \frac{e^2}{h}(1 - \mathrm{Det}\, S_0), \qquad (2.32)$$

and so is in one-to-one relationship with the topological quantum number $\mathrm{Det}\, S_0 = \pm 1$. In contrast, the Fermi-level density of states has the same probability distribution (2.23) regardless of the sign of $\mathrm{Det}\, S_0$.

We have applied our results for the probability distribution of the time-delay matrix to a calculation of the thermopower induced by edge modes
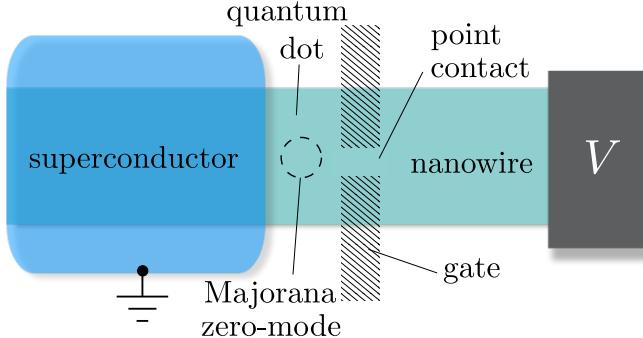
Figure 2.6: Geometry to detect a Majorana zero-mode by a measurement of the Andreev conductance of a ballistic point contact to a superconducting quantum dot. The probability distribution of the conductance depends on the presence or absence of the Majorana zero-mode, while the distribution of the density of states does not.

of a chiral p-wave or chiral d-wave superconductor.[16] The search for electrical edge conduction in such topological superconductors, notably Sr_2RuO_4,[56] has remained inconclusive,[57] in part because of the charge-neutrality of an unpaired Majorana mode at the Fermi level.[58–61] Fig. 2.5 shows that both unpaired and paired Majorana edge modes can produce a nonzero thermopower — of random sign, with a magnitude of order $\mathcal{S}_0/\delta_0 = (0.3\,\mathrm{mV/K}) \times k_B T_0/\delta_0$. This is a small signal, but it has the attractive feature that it directly probes for the existence of propagating edge modes — irrespective of their charge neutrality.

2.7 Appendix A. Derivation of the delay-time distribution for the Altland-Zirnbauer ensembles

Repeating the steps of Refs. 17 and 48 we extend the calculation of the joint distribution $P(S_0, Q)$ from the nonsuperconducting Wigner-Dyson ensembles to the superconducting Altland-Zirnbauer ensembles. We treat the two symmetry classes C, D without time-reversal symmetry, of relevance for the main text (see Table 2.1), and for completeness also consider the time-reversally symmetric classes CI and DIII (see Table 2.2).

symmetry class	CI	DIII
S-matrix space	symplectic & symmetric	orthogonal & selfdual
d_T	4	2
d_E	2	2
α	1	-1
β	2	2

Table 2.2: The two Altland-Zirnbauer classes with time-reversal symmetry.

2.7.1 Unitary invariance

Since the entire calculation relies on the unitary invariance (2.16) of the Altland-Zirnbauer circular ensembles, we demonstrate that first. Following Ref. 48 we construct the $\mathcal{M} \times \mathcal{M}$ energy-dependent unitary scattering matrix $S(E)$ in terms of an $\mathcal{M}_0 \times \mathcal{M}_0$ energy-independent unitary matrix U,

$$S(E) = \mathcal{P}U(e^{-2\pi iE/M_0\delta_0} + \mathcal{R}U)^{-1}\mathcal{P}^{\mathrm{T}}. \tag{2.33}$$

The rectangular $\mathcal{M} \times \mathcal{M}_0$ matrix $\mathcal{P}$ has elements $\mathcal{P}_{nm} = \delta_{nm}$ and $\mathcal{R} = 1 - \mathcal{P}^{\mathrm{T}}\mathcal{P}$. The eigenvalues $e^{i\phi_n}$ of U have the same degeneracy d_E as the energy eigenvalues, so there are $M_0 = \mathcal{M}_0/d_E$ distinct eigenvalues on the unit circle, arranged symmetrically around the real axis.

The $\mathcal{M}_0 \times \mathcal{M}_0$ Hermitian matrix H is related to U via a Cayley transform,

$$
\begin{aligned}
U &= e^{2\pi i\epsilon/M_0\delta_0} \frac{\pi H/M_0\delta_0 + i}{\pi H/M_0\delta_0 - i} \\
\Leftrightarrow H &= \frac{iM_0\delta_0}{\pi} \frac{U + e^{2\pi i\epsilon/M_0\delta_0}}{U - e^{2\pi i\epsilon/M_0\delta_0}}.
\end{aligned}
\tag{2.34}
$$

The factor $e^{2\pi i\epsilon/M_0\delta_0}$ with $\epsilon \to 0$ is introduced to regularize the singular inverse when U has an eigenvalue pinned at $+1$, as we will discuss in just a moment.

We can immediately observe that if we take a circular ensemble for U, with distribution function $P(U) = P(U'U) = P(UU')$, then the unitary invariance (2.16) of the distribution functional $P[S(E)]$ is manifestly true. So what we have to verify is that the construction (2.33)–(2.34) with U in the circular ensemble is, firstly, equivalent to the Weidenmüller formula (4.4), and secondly, produces a Gaussian ensemble for H. It is sufficient if the equivalence holds in the low-energy range $|E| \lesssim M\delta_0 \ll M_0\delta_0$.

Firstly, substitution of Eq. (2.34) into Eq. (2.33) gives

$$S(E) = \frac{1 + i\mathcal{P}\frac{M_0\delta_0 - i\pi H \tan(\pi E^+/M_0\delta_0)}{\pi H - M_0\delta_0 \tan(\pi E^+/M_0\delta_0)}\mathcal{P}^{\mathrm{T}}}{1 - i\mathcal{P}\frac{M_0\delta_0 - i\pi H \tan(\pi E^+/M_0\delta_0)}{\pi H - M_0\delta_0 \tan(\pi E^+/M_0\delta_0)}\mathcal{P}^{\mathrm{T}}}$$

$$= \frac{1 + i\mathcal{P}\frac{M_0\delta_0}{\pi(H - E^+)}\mathcal{P}^{\mathrm{T}}}{1 - i\mathcal{P}\frac{M_0\delta_0}{\pi(H - E^+)}\mathcal{P}^{\mathrm{T}}} + \mathcal{O}(M/M_0), \qquad (2.35)$$

with $E^+ = E + \epsilon$. This is the Weidenmüller formula (4.4), with the ballistic coupling matrix $W = \mathcal{P}^{\mathrm{T}}(M_0\delta_0/\pi^2)^{1/2}$ from Eq. (4.5).

Secondly, the Cayley transform (2.34) produces a Lorentzian instead of a Gaussian distribution for H, but in the low-energy range the two ensembles are equivalent.[62] One also readily checks that a uniform distribution with spacing $2\pi/M_0$ of the distinct eigenphases ϕ_n of U produces a mean spacing δ_0 of the distinct eigenvalues E_n of H, through the relation $(\pi/M_0\delta_0)E_n = \cot(\phi_n/2) \approx (\pi - \phi_n)/2$ in the low-energy range.

The finite-ϵ regularization is irrelevant in the class C and CI circular ensembles, because there the U's with an eigenvalue $+1$ are of measure zero. In the class D and DIII circular ensembles, in contrast, an eigenvalue may be pinned at unity and the regularization is essential. Let us analyze this for class D (the discussion in class DIII is similar). The matrix U in class D is real orthogonal, with determinant $\mathrm{Det}\, U = (-1)^{n_{\mathrm{M}}}$ fixed by the parity of the number of Majorana zero-modes [cf. Eq. (2.20)]. This implies that U has an eigenvalue pinned at $+1$ if M_0 is even and n_{M} is odd, or if M_0 is odd and n_{M} is even. The Cayley transform (2.34) then maps to an eigenvalue of H at infinity. This eigenvalue does not contribute to the low-energy scattering matrix (2.35), so that it can be removed from the spectrum of H. Hence, whereas the dimension M_0 of the unitary matrix U can be arbitrary, the dimension of H is always even for even n_{M} and odd for odd n_{M}.

2.7.2 Broken time-reversal symmetry, class C and D

We now proceed with the calculation of the distribution of the time-delay matrix, first in symmetry classes C and D. Starting point is the Weidenmüller formula (4.4) or (2.35) for the energy-dependent scattering matrix. Differentiation gives the time-delay matrix defined in Eq. (4.8),

$$Q^{-1} = \frac{1}{2\pi\hbar} \lim_{\epsilon \to 0} [1 - i\pi W^\dagger (H - \epsilon)^{-1} W]$$

$$\times \frac{1}{W^\dagger (H - \epsilon)^{-2} W} [1 + i\pi W^\dagger (H - \epsilon)^{-1} W], \qquad (2.36)$$

in terms of the Hamiltonian H of the closed quantum dot and the coupling matrix W to the scattering channels. The dimensionality of H is $d_E M_0 \times d_E M_0$ while the dimensionality of Q and S is $d_T M \times d_T M$ (and W has dimension $d_E M_0 \times d_T M$). The unitary invariance (2.16) implies $P(S_0, Q) = P(-1, Q)$, so we may restrict ourselves to the case that H has a zero-eigenvalue with multiplicity $d_T M$ — since then $S_0 = \lim_{E \to 0} S(E) = -1$.

Restricting H to its $d_T M$-dimensional nullspace we have, using the ballistic coupling matrix (4.5),

$$W^\dagger (H - \epsilon)^{-p} W \to (M_0 \delta_0 / \pi^2)(-\epsilon)^{-p} \tilde{\Omega}^\dagger \tilde{\Omega}, \qquad (2.37)$$

$$Q^{-1} \to (\delta_0 / 2\pi\hbar) \Omega^\dagger \Omega, \ \ \Omega = M_0^{1/2} \tilde{\Omega}. \qquad (2.38)$$

The matrix Ω is a $d_T M \times d_T M$ submatrix of a $d_E M_0 \times d_E M_0$ unitary matrix, rescaled by a factor $\sqrt{M_0}$. In the relevant limit $M_0 / M \to \infty$ this matrix has independent Gaussian elements,

$$\begin{aligned} P(\Omega) &\propto \exp\left[-\tfrac{1}{2}\beta(d_E/d_T)\operatorname{Tr}' \Omega^\dagger \Omega\right] \\ &= \exp\left(-\tfrac{1}{2}\beta t_0 \operatorname{Tr}' Q^{-1}\right), \end{aligned} \qquad (2.39)$$

with $t_0 = (2\pi\hbar/\delta_0)(d_E/d_T)$. The prime in the trace, and in the determinants appearing below, indicates that the d_T-fold degenerate eigenvalues are only counted once. The symmetry index β counts the number of independent degrees of freedom of the matrix elements of Ω, real in class D ($\beta = 1$) and quaternion in class C ($\beta = 4$). The positive-definite matrix Q^{-1} of the form (2.38) is called a Wishart matrix in random-matrix theory.[63]

Using Eq. (4.4), an infinitesimal deviation of S_0 from -1 can be expressed as

$$V\Omega(S_0 + 1)\Omega^\dagger V^\dagger = A, \qquad (2.40)$$

with A a $d_T M \times d_T M$ anti-Hermitian matrix, $A = -A^\dagger$. The matrix A is a submatrix of iH, so its matrix elements are real in class D and quaternion in class C. The unitary matrix V has been inserted so that $P(A) = \text{constant}$ near $A = 0$. Since the transformation $\Omega \mapsto V\Omega$ has no effect on $P(\Omega)$ and leaves Q unaffected, we may in what follows omit V.

The joint distribution $P(S_0, Q^{-1})$ follows from $P(\Omega)P(A)$ upon multiplication by two Jacobian determinants,

$$P(S_0, Q^{-1}) = P(\Omega)P(A) \left\| \frac{\partial \Omega}{\partial Q^{-1}} \right\| \times \left\| \frac{\partial A}{\partial S_0} \right\|$$

$$\propto \exp\left(-\tfrac{1}{2}\beta t_0 \operatorname{Tr}' Q^{-1}\right) \left\| \frac{\partial \Omega^\dagger \Omega}{\partial \Omega} \right\|^{-1} \left\| \frac{\partial \Omega^{-1} A \Omega^{\dagger -1}}{\partial A} \right\|^{-1}. \qquad (2.41)$$

The Jacobians can be evaluated using textbook methods, [63,64]

$$\left\| \left| \frac{\partial \Omega^\dagger \Omega}{\partial \Omega} \right| \right\|^{-1} \propto (\mathrm{Det}' \, \Omega^\dagger \Omega)^{-1+\beta/2}, \tag{2.42}$$

$$\left\| \left| \frac{\partial \Omega^{-1} A \Omega^{\dagger -1}}{\partial A} \right| \right\|^{-1} \propto (\mathrm{Det}' \, \Omega^\dagger \Omega)^{\alpha+1+(M-1)\beta/2}. \tag{2.43}$$

Here $\alpha + 1$ equals the number of degrees of freedom of a diagonal element of A, while an off-diagonal element has β degrees of freedom. So $\alpha + 1 = 0$, $\beta = 1$ for a real antisymmetric matrix A (class D), while $\alpha + 1 = 3$, $\beta = 4$ for a quaternion anti-Hermitian A (class C).

Collecting results, we arrive at the distribution

$$P(S_0, Q^{-1}) \propto \exp(-\tfrac{1}{2}\beta t_0 \, \mathrm{Tr}' \, Q^{-1}) \, (\mathrm{Det}' \, Q^{-1})^{\alpha+M\beta/2}. \tag{2.44}$$

The distribution (2.18) of the eigenvalues γ_n of Q^{-1} follows upon multiplication by one more Jacobian, from matrix elements to eigenvalues.

2.7.3 Preserved time-reversal symmetry, class CI and DIII

The time-reversal operator acts in a different way in class CI and DIII. In class CI the action is the transpose, so that $S = S^{\mathrm{T}}$, $H = H^{\mathrm{T}}$ are symmetric matrices. In class DIII these matrices are selfdual, $S = \sigma_y S^{\mathrm{T}} \sigma_y \equiv S^{\mathrm{D}}$, where the Pauli matrix σ_y acts on the spin-degree of freedom. It is convenient to use a unified notation $\tilde{U}$ to denote the transpose U^{T} of a matrix in class CI and the dual U^{D} in class DIII. Unitary invariance of the circular ensemble then amounts to

$$P[S(E)] = P[\tilde{U} \cdot S(E) \cdot U], \tag{2.45}$$

for energy-independent unitary matrices U.

Time-reversal symmetry allows to "take the square root" of the Fermi-level scattering matrix (Takagi factorization [65]),

$$S_0 = \tilde{S}_{1/2} S_{1/2}. \tag{2.46}$$

In class DIII the sign of the determinant of $S_{1/2}$ is a topological quantum number, [66]

$$\mathrm{Det} \, S_{1/2} = \mathrm{Pf} \, (i\sigma_y S_0) = \pm 1, \tag{2.47}$$

equal to -1 when the quantum dot contains a Kramers pair of Majorana zero-modes. The symmetrized time-delay matrix is defined in terms of this square root,

$$Q = -i\hbar \lim_{E \to 0} \tilde{S}_{1/2}^\dagger \frac{dS}{dE} S_{1/2}^\dagger. \tag{2.48}$$

	C	D	CI	DIII
H_{nm}	$iq_0 + \boldsymbol{q} \cdot \boldsymbol{\tau}$	iq_0	$a\tau_x + b\tau_z$	$ia\sigma_x + ib\sigma_z$
$(n \neq m)$	$\beta = 4$	$\beta = 1$	$\beta = 2$	$\beta = 2$
H_{nn}	$\boldsymbol{q} \cdot \boldsymbol{\tau}$	0	$a\tau_x + b\tau_z$	0
	$\alpha + 1 = 3$	$\alpha + 1 = 0$	$\alpha + 1 = 2$	$\alpha + 1 = 0$

	A	AI	AII
H_{nm}	$a + ib$	a	$q_0 + i\boldsymbol{q} \cdot \boldsymbol{\sigma}$
$(n \neq m)$	$\beta = 2$	$\beta = 1$	$\beta = 4$
H_{nn}	a	a	q_0
	$\alpha + 1 = 1$	$\alpha + 1 = 1$	$\alpha + 1 = 1$

Table 2.3: Upper table: Representation of the Hamiltonian H in the four Altland-Zirnbauer symmetry classes. All coefficients q_n, a, b are real. The Pauli matrices $\boldsymbol{\tau} = (\tau_x, \tau_y, \tau_z)$ act on the electron-hole degree of freedom, while the $\boldsymbol{\sigma}$'s act on the spin degree of freedom. The symmetry indices β and $\alpha + 1$ from Tables 2.1 and 2.2 count, respectively, the number of degrees of freedom of the off-diagonal and diagonal components of the Hermitian matrix H, in the Majorana basis for class D, DIII and in the electron-hole basis for class C, CI . For completeness and comparison, we show in the lower table the corresponding listing for the three Wigner-Dyson symmetry classes.

The definition (4.8) of the matrix Q used in class C and D, without time-reversal symmetry, gives the same eigenvalues as definition (2.48), but would introduce a spurious correlation between S and Q. With the definition (2.48) the unitary invariance (2.45) allows to equate $P(S_0, Q) = P(-1, Q)$, by taking $U = S_{1/2}^\dagger i\sigma_x$ in class CI and $U = S_{1/2}^\dagger \sigma_x$ in class DIII.

Comparing to the derivation of the previous subsection, what changes is that the matrix elements of Ω and A are equivalent to complex numbers $a + ib$, rather than being real or quaternion. Specifically, Ω has matrix elements of the form $a\sigma_0 + ib\sigma_y$ in both class CI and DIII (to ensure that $\Omega^\dagger = \tilde{\Omega}$), while the matrix elements of A are of the form $ia\sigma_x + ib\sigma_z$ in class CI and of the form $a\sigma_x + b\sigma_z$ in class DIII (to ensure that $A^\dagger = -\tilde{A}$). The Jacobian (2.42) still applies, now with $\beta = 2$, while the Jacobian (2.43) evaluates to

$$\left\| \left| \frac{\partial \Omega^{-1} A \Omega^{\dagger -1}}{\partial A} \right| \right\|^{-1} \propto \begin{cases} (\mathrm{Det}'\, \Omega^\dagger \Omega)^{M+1} & \text{in class CI,} \\ (\mathrm{Det}'\, \Omega^\dagger \Omega)^{M-1} & \text{in class DIII.} \end{cases} \qquad (2.49)$$

Collecting results, we arrive at

$$P(S_0, Q^{-1}) \propto \exp(-t_0 \,\mathrm{Tr}'\, Q^{-1}) \, (\mathrm{Det}'\, Q^{-1})^{M \pm 1}, \qquad (2.50)$$

with exponent $M + 1$ in class CI and $M - 1$ in class DIII. As before, the primed trace and determinant count degenerate eigenvalues only once.

The distribution (2.18) of the eigenvalues γ_n of Q^{-1} follows with $\beta = 2$ and $\alpha = \pm 1$.

2.8 Appendix B. Details of the calculation of the thermopower distribution

2.8.1 Invariant measure on the unitary, orthogonal, or symplectic groups

For later reference, we record explicit expressions for the invariant measure $dU = P(\{\alpha_n\}) \prod_n d\alpha_n$ (the Haar measure) in parameterizations $U(\{\alpha_n\})$ of the unitary group $\mathrm{SU}(N)$, as well as the orthogonal or unitary symplectic subgroups $\mathrm{SO}(N)$, $\mathrm{Sp}(2N)$. (We will only need results for small N.)

The invariant measure is determined by the metric tensor

$$g_{mn} = -\mathrm{Tr}\, U^\dagger(\partial U/\partial \alpha_m) U^\dagger(\partial U/\partial \alpha_n), \qquad (2.51)$$

via $P(\{\alpha_n\}) \propto \sqrt{\det g}$. The function P represents the probability distribution of the α_n's when the matrix U is drawn randomly and uniformly from the unitary group (circular unitary ensemble, CUE), or from the orthogonal and symplectic subgroups (circular real and quaternion ensembles, CRE and CQE).

For $\mathrm{SO}(2)$ we have trivially

$$R(\theta) = \begin{pmatrix} \cos\theta & -\sin\theta \\ \sin\theta & \cos\theta \end{pmatrix} \Rightarrow P(\theta) = \text{constant}. \qquad (2.52)$$

For $\mathrm{SU}(2) = \mathrm{Sp}(2)$ we can choose different parameterizations:

$$U = \exp\big[i\beta(\tau_z \cos\theta + \tau_x \sin\theta\cos\phi + \tau_y \sin\theta\sin\phi)\big]$$
$$\Rightarrow P(\beta, \theta, \phi) \propto \sin^2\beta \sin\theta, \qquad (2.53a)$$
$$U = e^{i\alpha\tau_z} \exp\big[i\beta(\tau_x \cos\phi + \tau_y \sin\phi)\big]$$
$$\Rightarrow P(\alpha, \beta, \phi) \propto \sin 2\beta, \qquad (2.53b)$$
$$U = e^{i\alpha\tau_z} R(\theta) e^{i\alpha'\tau_z} \Rightarrow P(\alpha, \alpha', \theta) \propto \sin 2\theta. \qquad (2.53c)$$

For the group of 3×3 orthogonal matrices we will use the Euler angle parameterization

$$O_\pm = \begin{pmatrix} R(\alpha) & 0 \\ 0 & 1 \end{pmatrix} \begin{pmatrix} \pm 1 & 0 \\ 0 & R(\theta) \end{pmatrix} \begin{pmatrix} R(\alpha') & 0 \\ 0 & 1 \end{pmatrix}$$
$$\Rightarrow P(\alpha, \alpha', \theta) \propto \sin\theta. \qquad (2.54)$$

The $\pm$ sign distinguishes the sign of the determinant $\text{Det}\,O_\pm = \pm 1$, with SO(3) corresponding to O_+.

Finally, for Sp(4) we use the polar decomposition

$$U = \begin{pmatrix} U_1 & 0 \\ 0 & U_2 \end{pmatrix} \begin{pmatrix} \tau_0 \cos\theta & -\tau_0 \sin\theta \\ \tau_0 \sin\theta & \tau_0 \cos\theta \end{pmatrix} \begin{pmatrix} \tau_0 & 0 \\ 0 & U_3 \end{pmatrix}$$

$$\Rightarrow P(\theta) = \sin^3 2\theta. \tag{2.55}$$

The matrices U_p are independently and uniformly distributed in SU(2), see Eq. (2.53). There are only three independent U_p's, with 3 free parameters each, because one of the four blocks can be absorbed in the three others, so we have set it to the unit τ_0 without loss of generality. (One can check that the total number $N(2N+1) \mapsto 10$ of free parameters of Sp($2N$) agrees: $3+3+3$ from the U_p's plus θ makes 10.)

2.8.2 Elimination of eigenvector components

The thermopower expressions (2.14) and (2.15) depend on the transmission eigenvalues T_n and delay times D_n, but in addition there is a dependence on eigenvectors. Many of the eigenvector degrees of freedom can be eliminated by using the invariance of the distribution of the time-delay matrix under the unitary transformation $Q \mapsto U^\dagger Q U$, following from Eq. (2.16).

Class C

In class C we proceed as follows. The 4×4 unitary symplectic scattering matrix S_0 has the polar decomposition (2.55), which we write in the form

$$S_0 = \begin{pmatrix} U_1 & 0 \\ 0 & U_2 \end{pmatrix} \begin{pmatrix} \tau_0\sqrt{1-T} & -\tau_0\sqrt{T} \\ \tau_0\sqrt{T} & \tau_0\sqrt{1-T} \end{pmatrix} \begin{pmatrix} \tau_0 & 0 \\ 0 & U_3 \end{pmatrix}, \tag{2.56}$$

$$U_n = e^{i\alpha_n \tau_z} \exp\left[i\beta_n (\tau_x \cos\phi_n + \tau_y \sin\phi_n) \right]. \tag{2.57}$$

We ignore the spin degree of freedom, which plays no role in the calculation. The remaining two-fold degeneracy of the transmission eigenvalue T comes from the electron-hole degree of freedom.

The time-delay matrix is Hermitian with quaternion elements,

$$Q = \begin{pmatrix} a\tau_0 & q \\ q^\dagger & b\tau_0 \end{pmatrix}, \quad q = q_0\tau_0 + iq_1\tau_x + iq_2\tau_y + iq_3\tau_z. \tag{2.58}$$

With some trial and error, we found the unitary symplectic transformation

$$Q \mapsto U^\dagger Q U, \;\; U = (U_0)^2 \begin{pmatrix} \tau_0 & 0 \\ 0 & e^{-i\alpha_3\tau_z} U_3^\dagger e^{i\alpha_3\tau_z} \end{pmatrix}, \tag{2.59}$$

$$U_0 = \begin{pmatrix} U_1 & 0 \\ 0 & \tau_0 \end{pmatrix} \begin{pmatrix} \tau_0\sqrt{1-T} & -\tau_0\sqrt{T} \\ \tau_0\sqrt{T} & \tau_0\sqrt{1-T} \end{pmatrix}, \tag{2.60}$$

that eliminates most of the eigenvector components from the class-C thermopower expression (2.15). We are left with

$$\mathcal{S}/\mathcal{S}_0 = -\hbar^{-1} \frac{2q_3\sqrt{T(1-T)}}{1-(1-T)\cos 2\beta_1}. \tag{2.61}$$

The probability distribution of the eigenvector parameter β_1 follows from Eq. (2.53b),

$$P(\beta_1) = \sin 2\beta_1, \;\; 0 < \beta_1 < \pi/2. \tag{2.62}$$

Class D

The algebra is simpler in class D, where the matrix elements are real rather than quaternion. We use the Euler angle parameterization (2.54) of the 3×3 orthogonal matrix S_0 with determinant $\text{Det}\, S_0 = \pm 1$. Substitution of the orthogonal transformation

$$Q \mapsto \begin{pmatrix} R(-\alpha') & 0 \\ 0 & 1 \end{pmatrix} Q \begin{pmatrix} R(\alpha') & 0 \\ 0 & 1 \end{pmatrix} \tag{2.63}$$

into the class-D thermopower expression (2.14) leads directly to

$$\frac{\mathcal{S}}{\mathcal{S}_0} = \frac{Q_{13}}{\hbar} \times \begin{cases} -\cotan(\theta/2) & \text{if } \text{Det}\, S_0 = +1, \\ \tan(\theta/2) & \text{if } \text{Det}\, S_0 = -1, \end{cases} \tag{2.64a}$$

$$P(\theta) = \tfrac{1}{2}\sin\theta, \;\; 0 < \theta < \pi. \tag{2.64b}$$

The transmission eigenvalue is $T = \sin^2\theta$. Since $P(\theta) = P(\pi-\theta)$ the probability distribution of the thermopower does not depend on the sign of $\text{Det}\, S_0$.

2.8.3 Marginal distribution of an element of the time-delay matrix

The two expressions (2.61) and (2.64a) for the thermopower contain a single off-diagonal element of the time-delay matrix Q. We can calculate its marginal distribution, using the eigenvalue distribution of Sec. 2.3 and the fact that the eigenvectors of Q are uniformly distributed with the invariant measure of the symplectic group (class C) or the orthogonal group (class D).

Class C

In class C the 4×4 time-delay matrix Q is diagonalized by a unitary symplectic matrix U,

$$Q = U \begin{pmatrix} D_1 \tau_0 & 0 \\ 0 & D_2 \tau_0 \end{pmatrix} U^\dagger. \qquad (2.65)$$

Each of the eigenvalues D_1 and D_2 of Q has a two-fold degeneracy from the electron-hole degree of freedom. (As before, we can ignore the spin degree of freedom.) The matrix U has the polar decomposition (2.55).

The quaternion Q_{12} is given in this parameterization by

$$Q_{12} = \tfrac{1}{2}(D_1 - D_2)(\sin 2\theta) U_1 U_2^\dagger, \qquad (2.66)$$

and since q_3 from Eq. (2.58) equals $-\tfrac{1}{2} i \operatorname{Tr} \tau_z Q_{12}$, we have

$$q_3 = \tfrac{1}{4}(D_1 - D_2)(\sin 2\theta) \operatorname{Tr} U_0. \qquad (2.67)$$

The matrix $U_0 = -i\tau_z U_1 U_2^\dagger$ is uniformly distributed in SU(2). Using the invariant measures (2.53a) and (2.55) we arrive at

$$\begin{aligned} q_3 &= \tfrac{1}{2}(D_1 - D_2)\cos\beta \sin 2\theta, \\ P(\beta, \theta) &= (6/\pi)\sin^2\beta \sin^3 2\theta, \;\; 0 < \beta, \theta < \pi/2. \end{aligned} \qquad (2.68)$$

The two angular variables β, θ can be combined into a single variable ξ:

$$\begin{aligned} q_3 &= \tfrac{1}{2}(D_1 - D_2)\xi, \\ P(\xi) &= \tfrac{3}{4}(1 - \xi^2), \;\; -1 < \xi < 1. \end{aligned} \qquad (2.69)$$

The marginal distribution of q_3 then follows upon integration.

Collecting results, we have the following probability distributions for the variables appearing in the class-C thermopower:

$$\mathcal{S}/\mathcal{S}_0 = t_0 \hbar^{-1} \frac{(D_2 - D_1)\xi \sqrt{T(1-T)}}{1 - (1-T)\cos 2\beta}, \qquad (2.70)$$

$$P(\beta) = \sin 2\beta, \;\; 0 < \beta < \pi/2, \qquad (2.71)$$

$$P(\xi) = \tfrac{3}{4}(1 - \xi^2), \;\; -1 < \xi < 1, \qquad (2.72)$$

$$P(T) = 6\, T(1 - T), \;\; 0 < T < 1, \qquad (2.73)$$

$$\begin{aligned} P(D_1, D_2) = \;&\frac{32}{42525}(D_1 - D_2)^4 (D_1 D_2)^{-12} \\ &\times \exp[-2/D_1 - 2/D_2], \;\; D_1, D_2 > 0, \end{aligned} \qquad (2.74)$$

where for notational convenience we measure the delay times in units of t_0.

2.8 Appendix B. Details of the calculation of the thermopower distribution

Class D

The 3×3 time-delay matrix in class D is diagonalized by $Q = O_+ \operatorname{diag}(D_1, D_2, D_3) O_+^{\mathrm{T}}$, with $O_+ \in \mathrm{SO}(3)$ parameterized as in Eq. (2.54). In terms of these parameters, the matrix element Q_{13} is given by

$$
\begin{aligned}
Q_{13} &= X \cos \alpha + Y \sin \alpha, \\
X &= \tfrac{1}{2}(D_1 - D_2) \sin \theta' \sin 2\alpha', \\
Y &= \tfrac{1}{2}\left[(D_3 - D_2) \cos^2 \alpha' + (D_3 - D_1) \sin^2 \alpha'\right] \sin 2\theta', \\
P(\alpha, \alpha', \theta') &= (8\pi^2)^{-1} \sin \theta', \quad 0 < \alpha, \alpha' < 2\pi, \quad 0 < \theta < \pi.
\end{aligned}
\tag{2.75}
$$

The thermopower distribution follows upon integration, using Eqs. (2.18), (2.64), and (2.75).

Bibliography of chapter 2

[1] A. Altland and M. R. Zirnbauer, Phys. Rev. B **55**, 1142 (1997).

[2] *Handbook on Random Matrix Theory*, edited by G. Akemann, J. Baik, and P. Di Francesco (Oxford University Press, Oxford, 2011).

[3] G. Volovik, JETP Lett. **70**, 609 (1999).

[4] N. Read and D. Green, Phys. Rev. B **61**, 10267 (2000).

[5] M. Bocquet, D. Serban, and M. R. Zirnbauer, Nucl. Phys. B **578**, 628 (2000).

[6] D. A. Ivanov, J. Math. Phys. **43**, 126 (2002); arXiv:cond-mat/0103089.

[7] R. Jackiw and C. Rebbi, Phys. Rev. D **13**, 3398 (1976).

[8] D. Bagrets and A. Altland, Phys. Rev. Lett. **109**, 227005 (2012).

[9] J. Liu, A. C. Potter, K. T. Law, and P. A. Lee, Phys. Rev. Lett. **109**, 267002 (2012).

[10] M. A. Skvortsov, P. M. Ostrovsky, D. A. Ivanov, and Ya. V. Fominov, Phys. Rev. B **87**, 104502 (2013).

[11] T. D. Stanescu and S. Tewari, Phys. Rev. B **87**, 140504(R) (2013).

[12] J. D. Sau and S. Das Sarma, Phys. Rev. B **88**, 064506 (2013).

[13] P. A. Ioselevich and M. V. Feigel'man, New J. Phys. **15**, 055011 (2013).

[14] P. Neven, D. Bagrets, and A. Altland, New J. Phys. **15**, 055019 (2013).

[15] D. A. Ivanov, P. M. Ostrovsky, and M. A. Skvortsov, Europhys. Lett. **106**, 37006 (2014).

[16] C.-Y. Hou, K. Shtengel, and G. Refael, Phys. Rev. B **88**, 075304 (2013).

Bibliography of chapter 2

[17] P. W. Brouwer, K. M. Frahm, and C. W. J. Beenakker, Phys. Rev. Lett. **78**, 4737 (1997).

[18] C. W. J. Beenakker, J. P. Dahlhaus, M. Wimmer, and A. R. Akhmerov, Phys. Rev. B **83**, 085413 (2011).

[19] C. W. J. Beenakker, Lect. Notes Phys. **667**, 131 (2005).

[20] T. Dirks, T. L. Hughes, S. Lal, B. Uchoa, Y.-F. Chen, C. Chialvo, P. M. Goldbart, and N. Mason, Nature Phys. **7**, 386 (2011).

[21] E. J. H. Lee, X. Jiang, R. Aguado, G. Katsaros, C. M. Lieber, and S. De Franceschi, Phys. Rev. Lett. **109**, 186802 (2012).

[22] W. Chang, V. E. Manucharyan, T. S. Jespersen, J. Nygard, and C. M. Marcus, Phys. Rev. Lett. **110**, 217005 (2013).

[23] J. P. Dahlhaus, B. Béri, and C. W. J. Beenakker, Phys. Rev. B **82**, 014536 (2010).

[24] M. Cutler and N. F. Mott, Phys. Rev. **181**, 1336 (1969).

[25] M. S. Kalenkov, A. D. Zaikin, and L. S. Kuzmin, Phys. Rev. Lett. **109**, 147004 (2012).

[26] A. Ozaeta, P. Virtanen, F. S. Bergeret, and T. T. Heikkilä, Phys. Rev. Lett. **112**, 057001 (2014).

[27] N. R. Claughton and C. J. Lambert, Phys. Rev. B **53**, 6605 (1996).

[28] J. Eom, C.-J. Chien, and V. Chandrasekhar, Phys. Rev. Lett. **81**, 437 (1998).

[29] R. Seviour and A. F. Volkov, Phys. Rev. B **62**, 6116 (2000).

[30] D. A. Dikin, S. Jung, and V. Chandrasekhar, Phys. Rev. B **65**, 12511 (2001).

[31] A. Parsons, I. A. Sosnin, and V. T. Petrashov, Phys. Rev. B **67**, 140502 (2003).

[32] A. F. Volkov and V. V. Pavlovskii, Phys. Rev. B **72**, 14529 (2005).

[33] P. Virtanen and T. T. Heikkilä, Phys. Rev. Lett. **92**, 177004 (2004); Appl. Phys. A **89**, 625 (2007).

[34] G. Srivastava, I. Sosnin, and V. T. Petrashov, Phys. Rev. B **72**, 012514 (2005).

[35] Ph. Jacquod and R. S. Whitney, EPL **91**, 67009 (2010).

[36] P. Machon, M. Eschrig, and W. Belzig, Phys. Rev. Lett. **110**, 047002 (2013); New J. Phys. **16**, 073002 (2014).

[37] E. P. Wigner, Phys. Rev. **98**, 145 (1955).

[38] F. T. Smith, Phys. Rev. **118**, 349 (1960).

[39] Y. V. Fyodorov and D. V. Savin, in Ref. 2 [arXiv:1003.0702].

[40] S. A. van Langen, P. G. Silvestrov, and C. W. J. Beenakker, Superlatt. Microstruct. **23**, 691 (1998).

[41] S. F. Godijn, S. Möller, H. Buhmann, L. W. Molenkamp, and S. A. van Langen, Phys. Rev. Lett. **82**, 2927 (1999).

[42] Y. Takane and H. Ebisawa, J. Phys. Soc. Japan **61**, 2858 (1992).

[43] M. R. Zirnbauer, in Ref. 2 [arXiv:1001.0722].

[44] S. Ryu, A. P. Schnyder, A. Furusaki, and A. W. W. Ludwig, New J. Phys. **12**, 065010 (2010).

[45] M. Z. Hasan and C. L. Kane, Rev. Mod. Phys. **82**, 3045 (2010).

[46] X.-L. Qi and S.-C. Zhang, Rev. Mod. Phys. **83**, 1057 (2011).

[47] E. P. Wigner, Ann. Math. **53**, 36 (1951); **55**, 7 (1952).

[48] P. W. Brouwer, K. M. Frahm, and C. W. J. Beenakker, Waves in Random Media **9**, 91 (1999) [arXiv:cond-mat/9809022].

[49] In differential geometry, $\alpha + 1$ and β from Table 2.1 appear as the root multiplicities m_ℓ and m_o of the symmetric space of transfer matrices, see P. W. Brouwer, A. Furusaki, C. Mudry, and S. Ryu, BUTSURI **60**, 935 (2005) [arXiv:cond-mat/0511622]. An alternative algebraic interpretation, in terms of the number of degrees of freedom of matrix elements of the Hamiltonian, is given in Table 2.3 of the Appendix.

[50] M. L. Mehta, *Random Matrices* (Elsevier, Amsterdam, 2004).

[51] V. L. Lyuboshits, Phys. Lett. B **72**, 41 (1977).

[52] T. Guhr, A. Müller-Groeling, and H. A. Weidenmüller, Phys. Rep. **299**, 189 (1998).

[53] C. W. J. Beenakker, Rev. Mod. Phys. **69**, 731 (1997); arXiv:0904.1432.

[54] E. Akkermans, A. Auerbach, J. E. Avron, and B. Shapiro, Phys. Rev. Lett. **66**, 76 (1991).

[55] P. W. Brouwer, S. A. van Langen, K. M. Frahm, M. Büttiker, and C. W. J. Beenakker, Phys. Rev. Lett. **79**, 913 (1997). In this study of charging effects on normal quantum dots the canonical and grand-canonical averages are simply related by $\langle \cdots \rangle_{\mathrm{canon}} = t_0^{-1} \langle \cdots \times \mathrm{Tr}\, Q \rangle_{\mathrm{grand\text{-}canon}}$. To include charging effects in the superconducting quantum dot considered here, the quasiparticle density of states $\mathrm{Tr}\, Q$ should be replaced by the charge density $\mathrm{Tr}\, \tau_z Q$.

[56] A. Mackenzie and Y. Maeno, Rev. Mod. Phys. **75**, 657 (2003).

[57] S. Lederer, W. Huang, E. Taylor, S. Raghu, and C. Kallin, Phys. Rev. B **90**, 134521 (2014).

[58] A. Furusaki, M. Matsumoto, and M. Sigrist, Phys. Rev. B **64**, 054514 (2001).

[59] M. Stone and R. Roy, Phys. Rev. B **69**, 184511 (2004).

[60] I. Serban, B. Béri, A. R. Akhmerov, and C. W. J. Beenakker, Phys. Rev. Lett. **104**, 147001 (2010).

[61] J. A. Sauls, Phys. Rev. B **84**, 214509 (2011).

[62] P. W. Brouwer, Phys. Rev. B **51**, 16878 (1995).

[63] P. J. Forrester, *Log-Gases and Random Matrices* (Princeton University Press, 2010).

[64] A. M. Mathai, *Jacobians of Matrix Transformations and Functions of Matrix Argument* (World Scientific Publishing, 1997).

[65] R. A. Horn and J. R. Johnson, *Matrix Analysis* (Cambridge University Press, 1985).

[66] I. C. Fulga, F. Hassler, A. R. Akhmerov, and C. W. J. Beenakker, Phys. Rev. B **83**, 155429 (2011).

3 Effect of chiral symmetry on chaotic scattering from Majorana zero-modes

3.1 Introduction

In classical mechanics the duration τ of a scattering process can be defined without ambiguity, for example as the energy derivative of the action. The absence of a quantum mechanical operator of time complicates the simple question "by how much is an electron delayed?"[1,2]. Since the action, in units of $\hbar$, corresponds to the quantum mechanical phase shift ϕ, the quantum analogue of the classical definition is $\tau = \hbar d\phi/dE$. In a multi-channel scattering process, described by an $N \times N$ unitary scattering matrix $S(E)$, one then has a set of delay times $\tau_1, \tau_2, \ldots \tau_N$, defined as the eigenvalues of the socalled Wigner-Smith matrix

$$Q = -i\hbar S^\dagger (dS/dE). \tag{3.1}$$

(For a scalar $S = e^{i\phi}$ the single-channel definition is recovered.)

This dynamical characterization of quantum scattering processes goes back to work by Wigner and others[3–5] in the 1950's. Developments in the random-matrix theory of chaotic scattering from the 1990's[6,7] allowed for a universal description of the statistics of the delay times τ_n in an ensemble of chaotic scatterers. The inverse delay matrix Q^{-1} turns out to be statistically equivalent to a socalled Wishart matrix[8]: the Hermitian positive-definite matrix product $WW^\dagger$, with W a rectangular matrix having independent Gaussian matrix elements. The corresponding probability distribution of the inverse delay times $\gamma_n \equiv 1/\tau_n > 0$ (measured in units of the Heisenberg time $\tau_{\mathrm{H}} = 2\pi\hbar/\delta_0$, with mean level spacing δ_0), takes the form[9]*

$$P(\{\gamma_n\}) \propto \prod_{j>i=1}^{N} |\gamma_i - \gamma_j|^\beta \prod_{k=1}^{N} \gamma_k^{\beta N/2} e^{-\beta \tau_{\mathrm{H}} \gamma_k/2}. \tag{3.2}$$

---

*The distribution (3.2) is known as a Laguerre distribution in random-matrix theory. It represents the eigenvalue distribution of a Wishart matrix $WW^\dagger$ for $\beta = 1$ (when W is a real Gaussian $N \times (2N+1)$-dimensional matrix) and for $\beta = 2$ (complex Gaussian $N \times 2N$ matrix W). For $\beta = 4$ there is no corresponding Wishart ensemble.

The symmetry index $\beta \in \{1, 2, 4\}$ distinguishes real, complex, and quaternion Hamiltonians. This connection between delay-time statistics and the Wishart ensemble is the dynamical counterpart of the connection between spectral statistics and the Wigner-Dyson ensemble[10,11] — discovered several decades later although the Wishart ensemble[12] is several decades older than the Wigner-Dyson ensemble.

The delay-time distribution (3.2) assumes ballistic coupling of the N scattering channels to the outside world. It has been generalized to coupling via a tunnel barrier[13,14], and has been applied to a variety of transport properties (such as thermopower, low-frequency admittance, charge relaxation resistance) of disordered electronic quantum dots and chaotic microwave cavities[15–28]. Because the density of states $\rho(E)$ is directly related to the Wigner-Smith matrix,

$$\rho(E) = (2\pi\hbar)^{-1} \operatorname{Tr} Q(E) = \sum_n (2\pi\hbar\gamma_n)^{-1}, \qquad (3.3)$$

the delay-time distribution also provides information on the degree to which levels are broadened by coupling to a continuum.

The discovery of topological insulators and superconductors[29,30] has opened up a new arena of applications of random-matrix theory[31,32]. Topologically nontrivial chaotic scatterers are distinguished by a topological invariant ν that is either a parity index, $\nu \in \mathbb{Z}_2$, or a winding number $\nu \in \mathbb{Z}$. In the spectral statistics, topologically distinct systems are immediately identified through the number of zero-modes, a total of $|\nu|$ levels pinned to the middle of the excitation gap[33,34]. If the gap is induced by a superconductor, the zero-modes are Majorana, of equal electron and hole character[35–37].

These developments raise the question how topological invariants connect to the Wishart ensemble: How do Majorana zero-modes affect the dynamics of chaotic scattering? That is the problem adressed and solved in this chapter, building on two earlier works[38,39]. In Ref. 38 it was found that a $\mathbb{Z}_2$ invariant (only particle-hole symmetry, symmetry class D in the Altland-Zirnbauer classification[40]) has no effect on the delay-time distribution for ideal (ballistic) coupling to the scatterer: The distribution is the same with or without an unpaired Majorana zero-mode in the spectrum. Here we show that the $\mathbb{Z}$ invariant of $|\nu|$-fold degenerate Majorana zero-modes does significantly affect the delay-time distribution. This is symmetry class BDI, with particle-hole symmetry as well as chiral symmetry[41,42]. Chiral symmetry without particle-hole symmetry, symmetry class AIII, was considered in Ref. 39 for a scalar $S = e^{i\phi}$, with a single delay time $\tau = \hbar d\phi/dE$. While our interest here is in Majorana modes, for which particle-hole symmetry is essential, our general results include a multi-channel generalization of Ref. 39.

Majorana zero-modes are being pursued in either two-dimensional (2D) or one-dimensional (1D) systems[35,36,43,44]. In the former geometry the zero-modes are bound to a magnetic vortex core, in the latter geometry they appear at the end point of a nanowire. Particle-hole symmetry by itself can only protect a single zero-mode, so even though the Majoranas always come in pairs, they have to be widely separated. The significance of chiral symmetry is that it provides additional protection for multiple overlapping Majorana zero-modes[45–48]. The origin of the chiral symmetry is different in the 1D and 2D geometries.

3.2 Chiral symmetry and time-delay matrix

By definition, chiral symmetry means that the Hamiltonian H anticommutes with a unitary operator. The 1D realization of chiral symmetry relies on the fact that the Rashba Hamiltonian of a nanowire in a parallel magnetic field is real — if its width W is well below the spin-orbit scattering length. Particle-hole symmetry $H = -\tau_x H^* \tau_x$ then implies that H anticommutes with the Pauli matrix τ_x that switches electrons and holes. It follows that a nanowire with $W \lesssim l_{so}$ (the typical regime of operation) is in the BDI symmetry class and supports multiple degenerate Majorana zero-modes at its end[49–51].

The Andreev billiard of Fig. 4.1 illustrates a 2D realization on the surface of a topological insulator. The massless Dirac fermions on the surface have a chiral symmetry at the charge-neutrality point (the Dirac point), because the 2D Dirac Hamiltonian

$$H_0 = v(p_x - eA_x)\sigma_x + v(p_y - eA_y)\sigma_y \tag{3.4}$$

anticommutes with the Pauli spin-matrix σ_z. The coupling to a superconducting pair potential Δ introduces particle-hole symmetry without breaking the chiral symmetry, since the Bogoliubov-De Gennes Hamiltonian

$$H = \begin{pmatrix} H_0 - \mu & -i\sigma_y \Delta \\ i\sigma_y \Delta^* & \mu - H_0^* \end{pmatrix} \tag{3.5}$$

still anticommutes with σ_z for $\mu = 0$.

Therefore, overlapping Majorana zero-modes in a superconductor/topological insulator heterostructure (the Fu-Kane model[52]) will not split when the chemical potential is tuned to within a Thouless energy $N\delta_0$ from the Dirac point[53–55]. In this 2D geometry one needs random scattering by disorder to produce a finite density of states at $E = 0$, but in order to preserve the chiral symmetry the disorder cannot be electrostatic (V must remain zero). Scattering by a random vector potential is one possibility[56,57], or alternatively scattering by random surface deformations[58–60].
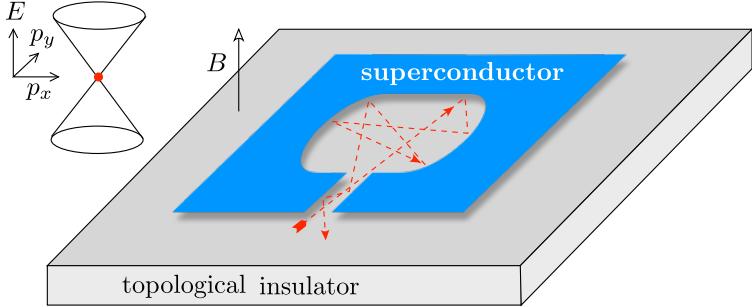
Figure 3.1: Andreev billiard on the conducting surface of a three-dimensional topological insulator in a magnetic field. The winding number ν of the superconducting order parameter around the billiard is associated with $|\nu|$ Majorana zero-modes, that affect the quantum delay time when the Fermi level lines up with the Dirac point (red dot) of the conical band structure.

To be definite, we will refer to the 2D Andreev billiard geometry in the following, but our results apply as well to 1D nanowires[*].

The unitary scattering matrix $S(E)$ of the Andreev billiard is obtained from the Green's function $\mathcal{G}(E) = K(E - H)^{-1} K^\dagger$ via

$$S(E) = [1 - i\pi\mathcal{G}(E)][1 + i\pi\mathcal{G}(E)]^{-1}. \tag{3.6}$$

The matrix K describes the coupling of the quasibound states inside the billiard to the continuum outside via $2N$ scattering channels[61]. We assume that K commutes with σ_z so as not to spoil the chiral symmetry of the Green's function and scattering matrix,

$$\sigma_z\mathcal{G}(E) = -\mathcal{G}(-E)\sigma_z \Rightarrow \sigma_z S(E) = S^\dagger(-E)\sigma_z. \tag{3.7}$$

It follows that the matrix product $S_0 = \sigma_z S(0)$ is both Hermitian and unitary, so its eigenvalues can only be $+1$ or -1. There are $N \pm \nu_0$ eigenvalues equal to ± 1, where the socalled matrix signature ν_0 is determined by the number of Majorana zero-modes[62]:

$$\nu_0 = \tfrac{1}{2}\operatorname{Tr} S_0 = \begin{cases} \nu & \text{if } |\nu| \leq N, \\ N\,(\operatorname{sign}\nu) & \text{if } |\nu| \geq N. \end{cases} \tag{3.8}$$

---

[*]According to the "ten-fold way" classification of topological states of matter[29–31,40], class BDI is nontrivial in 1D but not in 2D. To reconcile this with the 2D realization of Fig. 4.1, we refer to the analysis of Teo and Kane[54], who showed that the effective dimensionality for a topological defect is $d - d'$, where $d = 2$, $d' = 1$ for a vortex on the surface of a topological insulator. More generally, d is the dimensionality of the Brillouin zone and d' is the dimensionality of a contour that encloses the defect.

At the Fermi level, the time-delay matrix (4.8) depends on S_0 and on the first-order energy variation, $\sigma_z S(E) = S_0 \cdot [1 + iES_1 + \mathcal{O}(E^2)]$. Unitarity requires that S_1 is Hermitian and the chiral symmetry (3.7) then implies that S_1 commutes with S_0. Since $Q(0) \equiv Q_0 = \hbar S_1$, the same applies to the time-delay matrix at the Fermi level: $S_0 Q_0 = Q_0 S_0$. This implies the block structure

$$S_0 = U_0 \begin{pmatrix} \mathbb{1}_{N_+} & 0 \\ 0 & -\mathbb{1}_{N_-} \end{pmatrix} U_0^\dagger, \quad Q_0 = U_0 \begin{pmatrix} Q_+ & 0 \\ 0 & Q_- \end{pmatrix} U_0^\dagger, \qquad (3.9)$$

with $\mathbb{1}_n$ the $n \times n$ unit matrix, U_0 a $2N \times 2N$ unitary matrix, and $Q_\pm$ a pair of $N_\pm \times N_\pm$ Hermitian matrices. There are therefore two sets of delay times $\tau_n^\pm$, $n = 1, 2, \dots N_\pm$, corresponding to an eigenvalue ± 1 of S_0.

After these preparations we can now state our central result: For ballistic coupling the two matrices Q_+^{-1} and Q_-^{-1} are statistically independent, each described by its own Wishart ensemble[63] and eigenvalue distribution $P_\pm$ of $\gamma_n^\pm = 1/\tau_n^\pm$ given by

$$P_\pm(\{\gamma_n^\pm\}) \propto \prod_{j>i=1}^{N_\pm} |\gamma_i^\pm - \gamma_j^\pm|^\beta \prod_{k=1}^{N_\pm} (\gamma_k^\pm)^{\beta/2-1} e^{-\beta\tau_\mathrm{H}\gamma_k^\pm/4}$$
$$\times (\gamma_k^\pm)^{(\beta/2)|\pm\nu-N|}, \qquad (3.10)$$

with symmetry index $\beta = 1$ for the class BDI Hamiltonian (3.5). The distribution (3.10) holds also for $|\nu| \geq N$, when the scattering matrix signature (3.8) is saturated. In that case a single Wishart ensemble remains for all $2N$ delay times, with distribution

$$P(\{\gamma_n\}) \propto \prod_{j>i=1}^{2N} |\gamma_i - \gamma_j|^\beta \prod_{k=1}^{2N} \gamma_k^{\beta/2-1} e^{-\beta\tau_\mathrm{H}\gamma_k/4}$$
$$\times \gamma_k^{(\beta/2)(|\nu|-N)}, \quad |\nu| \geq N. \qquad (3.11)$$

The derivation of Eq. (3.10) starts from the Gaussian ensemble for Hamiltonians with chiral symmetry[8,42],

$$H = \begin{pmatrix} 0 & \mathcal{A} \\ \mathcal{A}^\dagger & 0 \end{pmatrix}, \quad P(\mathcal{A}) \propto \exp\left(-\frac{\beta\pi^2}{8\delta_0^2 \mathcal{N}} \mathrm{Tr}\,\mathcal{A}\mathcal{A}^\dagger\right). \qquad (3.12)$$

The rectangular matrix $\mathcal{A}$ has dimensions $\mathcal{N} \times (\mathcal{N} + \nu)$, so H has $|\nu|$ eigenvalues pinned to zero. The matrix elements of $\mathcal{A}$ are real ($\beta = 1$, symmetry class BDI, chiral orthogonal ensemble), complex ($\beta = 2$, class AIII, chiral unitary ensemble) or quaternion ($\beta = 4$, class CII, chiral symplectic ensemble).

The coupling matrix $K = K_1 \oplus K_2$ is composed of two rectangular blocks of dimensions $N \times \mathcal{N}$ and $N \times (\mathcal{N} + \nu)$, having nonzero matrix elements

$$(K_1)_{nn} = (K_2)_{nn} = \kappa_n, \quad n = 1, 2, \ldots N, \tag{3.13}$$

with $\kappa_n = \sqrt{2\mathcal{N}\delta_0/\pi^2} \equiv \kappa_0$ for ballistic coupling. These matrices determine the time-delay matrix (4.8) via Eq. (3.6). At the Fermi level one has

$$Q_0 = 2\pi\hbar\Omega\Omega^\dagger, \quad \Omega = K(H + i\pi K^\dagger K)^{-1}. \tag{3.14}$$

We seek the distribution of Q_0 given the Gaussian distribution of H, in the limit $\mathcal{N} \to \infty$ at fixed ν.

The corresponding problem in the absence of chiral symmetry was solved[9,38] by using the unitary invariance of the distribution to perform the calculation in the limit $S \to -1$, when a major simplification occurs. Here this would only work in the topologically trivial case* $\nu_0 = 0$, so a different approach is needed. We would like to exploit the block decomposition (3.12) of the Hamiltonian, but this decomposition is lost in Eq. (3.14).

Unitary invariance does allow us to directly obtain the distribution of the eigenvectors of $Q_\pm = U_\pm \operatorname{diag}(\tau_1^\pm, \tau_2^\pm, \ldots)U_\pm^\dagger$. From the invariance $P(S_0, Q_0) = P(VS_0V^\dagger, VQ_0V^\dagger)$ under joint unitary transformations of S_0 and Q_0 we conclude that the matrices of eigenvectors U_0, U_+, U_- are all independent and uniformly distributed in the unitary group (for $\beta = 2$, and in the orthogonal or symplectic subgroups for $\beta = 1$ or $\beta = 4$).

The "trick" that allows us to obtain the eigenvalue distribution is to note that $\tilde{Q}_0 = 2\pi\hbar\Omega^\dagger\Omega$ has the same nonzero eigenvalues as Q_0 — but unlike Q_0 it is block-diagonal:

$$\tilde{Q}_0 = 2\pi\hbar \begin{pmatrix} \Lambda_-^{-1} & 0 \\ 0 & \Lambda_+^{-1} \end{pmatrix}, \tag{3.15a}$$

$$\Lambda_- = \pi^2 K_1^\dagger K_1 + \mathcal{A}(K_2^\dagger K_2 + \epsilon)^{-1}\mathcal{A}^\dagger, \tag{3.15b}$$

$$\Lambda_+ = \pi^2 K_2^\dagger K_2 + \mathcal{A}^\dagger(K_1^\dagger K_1 + \epsilon)^{-1}\mathcal{A}. \tag{3.15c}$$

The infinitesimal ϵ is introduced to regularize the inversion of the singular matrices $K_n^\dagger K_n = \kappa_0^2 \mathcal{P}_n$, where $(\mathcal{P}_n)_{ij} = 1$ if $1 \leq i = j \leq N$ and zero otherwise. In the limit $\epsilon \to 0$ some eigenvalues of $\Lambda_\pm$ diverge, while the others converge to the inverse delay times $\gamma_n^\pm$.

The calculation of the eigenvalues of $\Lambda_\pm$ in the $\epsilon \to 0$ limit is now a matter of perturbation theory[64]. This is a degenerate perturbation expansion in the null space of $\mathcal{A}(\mathbb{1}_{\mathcal{N}+\nu}-\mathcal{P}_2)\mathcal{A}^\dagger$ for Λ_+ and in the null space of $\mathcal{A}^\dagger(\mathbb{1}_{\mathcal{N}}-\mathcal{P}_1)\mathcal{A}$ for Λ_-. The small perturbation (an order ϵ smaller than

---

*This complication was explained to us by P. W. Brouwer.
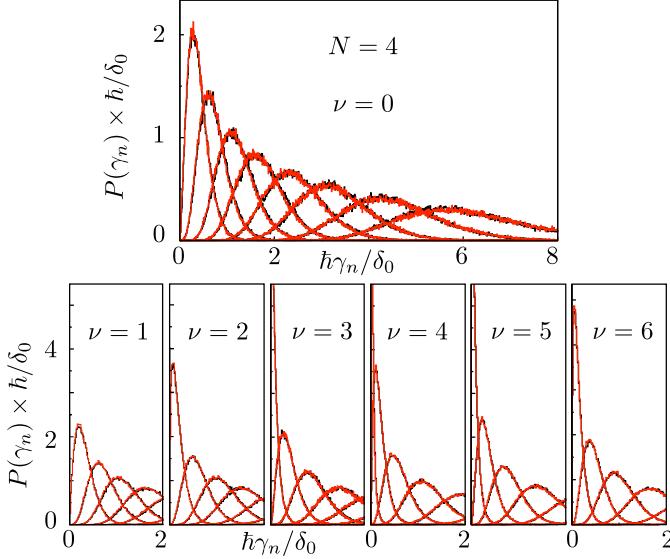
Figure 3.2: Probability distributions in symmetry class BDI ($\beta = 1$) of the n-th inverse delay time γ_n, ordered from small to large: $0 < \gamma_1 < \gamma_2 \cdots < \gamma_{2N}$, with $N = 4$. The various plots are for different numbers $\nu = 0, 1, 2, \ldots 6$ of Majorana zero-modes. The black histograms of the chiral Gaussian ensemble (3.12) (calculated for $\mathcal{N} = 80$) are almost indistinguishable from the the red histograms of the Wishart ensemble, validating our theory. The divergent peak of $P(\gamma_1)$ for $\nu = 3, 4, 5$ is responsible for the divergence of the average density of states (3.3) when the number of zero-modes differs by less than two units from the number of channels.

the leading order term) is $\pi^2 \kappa_0^2 \mathcal{P}_1 + \kappa_0^{-2} \mathcal{A} \mathcal{P}_2 \mathcal{A}^\dagger$ and $\pi^2 \kappa_0^2 \mathcal{P}_2 + \kappa_0^{-2} \mathcal{A}^\dagger \mathcal{P}_1 \mathcal{A}$, for Λ_+ and Λ_- respectively. The Gaussian distribution (3.12) of the matrix elements of $\mathcal{A}$ results in the eigenvalue distributions $P(\{\gamma_n\}) = P_+(\{\gamma_n^+\}) P_-(\{\gamma_n^-\})$ given by Eq. (3.10).

To test our analysis, we have numerically generated random matrices from the chiral Gaussian ensemble, on the one hand, and from the Wishart ensemble, on the other hand, and compared the resulting time delay matrices. We find excellent agreement of the delay-time statistics for all three values of the symmetry index $\beta \in \{1, 2, 4\}$, representative plots for $\beta = 1$ are shown in Fig. 3.2.

In view of Eq. (3.3) we can directly apply the delay-time distribution to determine the density $\rho(E)$ of quasi-bound states in the Andreev billiard. This is the density of states in the continuous spectrum. For $|\nu| > N$ the full density of states contains additionally a contribution $(|\nu| - N)\delta(E)$ from the discrete spectrum of zero-modes that are not coupled to the continuum*.

---

*The $|\nu| - N$ uncoupled zero-modes in the Andreev billiard, not broadened by
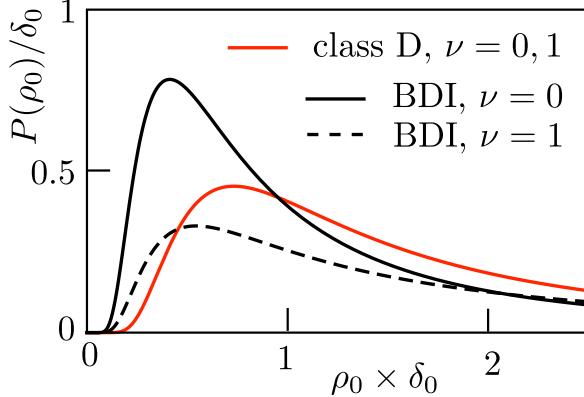
Figure 3.3: Probability distribution of the Fermi-level density of states, calculated from Eqs. (3.17) and (3.18) in symmetry class D (only particle-hole symmetry) and class BDI (particle-hole with chiral symmetry). In class D there is no dependence on the presence or absence of Majorana zero-modes[38], while in class BDI there is.

The probability distribution of the Fermi-level density of states $\rho_0 = \rho(0)$ follows upon integration of Eq. (3.10). The ensemble average $\langle \rho_0 \rangle$ has a closed-form expression[64],

$$\delta_0 \langle \rho_0 \rangle = \begin{cases} \frac{N(N+1-2/\beta)+\nu^2}{(N+1-2/\beta)^2-\nu^2}, & \text{if } |\nu| < N+1-2/\beta, \\ \frac{N}{|\nu|-N+1-2/\beta}, & \text{if } |\nu| > N-1+2/\beta. \end{cases} \quad (3.16)$$

For $\beta = 1$, $|\nu| \in \{N, N \pm 1\}$ and for $\beta = 2$, $|\nu| = N$ the average of ρ_0 diverges. (There is no divergency for $\beta = 4$.) Notice that the $|\nu| - N$ uncoupled zero-modes still affect the density of states coupled to the continuum, because they repel the quasi-bound states away from the Fermi level.

As a concrete example we return to the Andreev billiard at the surface of a topological insulator of Fig. 4.1, and contrast the delay-time distribution at the Dirac point [chemical potential $\mu = 0$ in the Hamiltonian (3.5)] and away from the Dirac point ($\mu \gg N\delta_0$). Away from the Dirac point the symmetry class is D (only particle-hole symmetry), while at the Dirac point the additional chiral symmetry promotes the system to class BDI. To simplify the comparison between these two cases we take a point contact with one electron and one hole mode ($N = 1$). The scattering matrix has dimension 2×2 and there are two delay times τ_1, τ_2.

The class-D distribution is independent of the presence or absence of

---

the $2N$ scattering channels into the continuum, span the null-space of $\mathcal{H} + i\pi K^\dagger K$. For $|\nu| \le N$ all zero-modes are broadened by coupling to the continuum.

Majorana zero-modes[38],

$$P_{\mathrm{D}}(\tau_1, \tau_2) \propto (\tau_1 \tau_2)^{-3} |\tau_1 - \tau_2| e^{-(\tau_{\mathrm{H}}/2)(1/\tau_1 + 1/\tau_2)}. \qquad (3.17)$$

In contrast, the class-BDI distribution (3.10) is sensitive to the number $|\nu|$ of Majorana zero-modes,

$$P_{\mathrm{BDI}}(\tau_1, \tau_2) \propto e^{-(\tau_{\mathrm{H}}/4)(1/\tau_1 + 1/\tau_2)}$$
$$\times \begin{cases} (\tau_1 \tau_2)^{-2} & \text{for } \nu = 0, \\ (\tau_1 \tau_2)^{-2-|\nu|/2} |\tau_1 - \tau_2| & \text{for } |\nu| \geq 1. \end{cases} \qquad (3.18)$$

The corresponding probability distributions of the Fermi-level density of states $\rho_0 = \tau_1/\delta_0 + \tau_2/\delta_0$ are plotted in Fig. 3.3. Chiral symmetry has a strong effect even for unpaired Majorana zero-modes: While away from the Dirac point (class D) the distribution $P(\rho_0)$ is the same for $\nu = 0, 1$, at the Dirac point (class BDI) these two distributions are significantly different.

3.3 Conclusions

This chapter presents the solution to a long-standing problem in the theory of chaotic scattering: the effect of chiral symmetry on the statistics of the Wigner-Smith time-delay matrix Q. The solution completes a line of investigation in random-matrix theory started six decades ago[10,11], by establishing the connection between Q and Wishart matrices for the chiral counterparts of the Wigner-Dyson ensembles[41,42]. The solution predicts an effect of Majorana zero-modes on the quantum delay-times for chaotic scattering, with significant consequences for the density of states (Fig. 3.3). Because the experimental search for Majorana zero-modes operates on 1D and 2D systems with chiral symmetry, the general and exact results obtained here are likely to provide a reliable starting point for more detailed investigations.

3.4 Appendix A. Details of the calculation of the Wigner-Smith time-delay distribution in the chiral ensembles

3.4.1 Wishart matrix preliminaries

Wishart matrices originate from multivariate statistics[12]. We collect some formulas we need[8].

The Hermitian positive definite matrix $WW^\dagger$ is called a Wishart matrix if the $n \times m$ ($m \geq n$) rectangular matrix W has real ($\beta = 1$), complex ($\beta = 2$), or quaternion ($\beta = 4$) matrix elements with a Gaussian distribution. For unit covariance matrix, $\langle W_{ij} W^*_{i'j'} \rangle = \delta_{ii'} \delta_{jj'}$, the distribution reads

$$P(W) \propto \exp\left(-\tfrac{1}{2}\beta \operatorname{Tr} WW^\dagger\right). \tag{3.19}$$

The eigenvalues of $WW^\dagger$ have the probability distribution

$$P(\lambda_1, \lambda_2, \dots \lambda_n) \propto \prod_{j>i=1}^{n} |\lambda_i - \lambda_j|^\beta$$

$$\times \prod_{k=1}^{n} \lambda_k^{\beta/2-1} \lambda_k^{\beta(m-n)/2} e^{-\beta\lambda_k/2}, \quad \lambda_k > 0. \tag{3.20}$$

The distribution (3.20) is called Wishart distribution, or Laguerre distribution because of its connection with Laguerre polynomials.

3.4.2 Degenerate perturbation theory

We seek the eigenvalue distribution of the $2N \times 2N$-dimensional Wigner-Smith time-delay matrix

$$Q_0 = -i\hbar S^\dagger \frac{dS}{dE} = 2\pi\hbar\,\Omega\Omega^\dagger, \quad \Omega = K(H + i\pi K^\dagger K)^{-1}. \tag{3.21}$$

As explained in the main text, the key step that allows us to make progress is to invert the order of Ω and $\Omega^\dagger$, and to consider a larger matrix that is block-diagonal:

$$\tilde{Q}_0 = 2\pi\hbar\,\Omega^\dagger\Omega = 2\pi\hbar(\Lambda_-^{-1} \oplus \Lambda_+^{-1}), \tag{3.22a}$$

$$\Lambda_- = \pi^2 K_1^\dagger K_1 + \mathcal{A}(K_2^\dagger K_2 + \epsilon)^{-1}\mathcal{A}^\dagger, \tag{3.22b}$$

$$\Lambda_+ = \pi^2 K_2^\dagger K_2 + \mathcal{A}^\dagger(K_1^\dagger K_1 + \epsilon)^{-1}\mathcal{A}. \tag{3.22c}$$

In this way we can separate the chirality sectors from the very beginning, which is a major simplification.

The two matrices Q_0 and $\tilde{Q}_0$ have the same set of nonzero eigenvalues, and $\tilde{Q}_0$ has an additional set of eigenvalues that are identically zero. The corresponding diverging eigenvalues of $\Lambda_\pm$ need to be separated from the finite eigenvalues that determine the inverse delay times $\gamma_n^\pm$. We assume $|\nu| \leq N$ and handle the case $|\nu| > N$ at the end.

To simplify the notation we scale the chiral blocks in the Hamiltonian (3.12) as $\mathcal{A} = (2\mathcal{N}\delta_0/\pi)a$, where a has the Gaussian distribution

$$P(a) \propto \exp\left(-\tfrac{1}{2}\beta\mathcal{N} \operatorname{Tr} aa^\dagger\right). \tag{3.23}$$

3.4 Appendix A. Details of the calculation of the time-delay distribution

We scale the coupling matrix as $K_i = (2\mathcal{N}\delta_0/\pi^2)^{1/2}P_i$. The rank-$N$ projector onto the open channels in chirality sector $i = 1, 2$ is $P_i^{\mathrm{T}}P_i$, with $P_i P_i^{\mathrm{T}} = \mathbb{1}_N$.

To access the finite eigenvalues of $\Lambda_\pm$, we need to perform degenerate perturbation theory in the null spaces of

$$\Lambda_-^{(0)} = a(\mathbb{1}_{\mathcal{N}+\nu} - P_2^{\mathrm{T}}P_2)a^\dagger, \;\; \Lambda_+^{(0)} = a^\dagger(\mathbb{1}_{\mathcal{N}} - P_1^{\mathrm{T}}P_1)a, \qquad (3.24)$$

with perturbation

$$\begin{aligned}
\delta\Lambda_- &= 2\mathcal{N}\delta_0(P_1^{\mathrm{T}}P_1 + aP_2^{\mathrm{T}}P_2 a^\dagger), \\
\delta\Lambda_+ &= 2\mathcal{N}\delta_0(P_2^{\mathrm{T}}P_2 + a^\dagger P_1^{\mathrm{T}}P_1 a).
\end{aligned} \qquad (3.25)$$

The null space of $\Lambda_\pm^{(0)}$ has rank $N_\pm = N \pm \nu \geq 0$. To project onto this null space we make an eigenvalue decomposition,

$$\Lambda_-^{(0)} = u_- s_- u_-^\dagger, \;\; \Lambda_+^{(0)} = u_+ s_+ u_+^\dagger. \qquad (3.26)$$

The matrix $u_\pm$ is unitary and $s_\pm$ is a diagonal matrix with nonnegative entries in descending order. The last $N_\pm = N \pm \nu$ entries on the diagonal of $s_\pm$ vanish, so the projector $p_\pm$ onto the null space consists of the last $N_\pm$ columns of $u_\pm$. The dimensionalities of p_+ and p_- are $(\mathcal{N} + \nu) \times N_+$ and $\mathcal{N} \times N_-$, respectively. For later use we note that the null space condition $p_\pm^\dagger \Lambda_\pm^{(0)} = 0 = \Lambda_\pm^{(0)} p_\pm$ requires that

$$P_2^{\mathrm{T}}P_2 a^\dagger p_- = a^\dagger p_-, \;\; P_1^{\mathrm{T}}P_1 a p_+ = a p_+. \qquad (3.27)$$

The $N_\pm$ finite eigenvalues of $\Lambda_\pm$ are the eigenvalues of the projected perturbation $p_\pm^\dagger \delta\Lambda_\pm p_\pm$, which we decompose as

$$p_\pm^\dagger \delta\Lambda_\pm p_\pm = 2\mathcal{N}\delta_0(X_\pm X_\pm^\dagger + Y_\pm Y_\pm^\dagger), \qquad (3.28)$$

$$\begin{aligned}
X_- &= p_-^\dagger P_1^{\mathrm{T}}, \;\; X_+ = p_+^\dagger P_2^{\mathrm{T}}, \\
Y_- &= p_-^\dagger a P_2^{\mathrm{T}}, \;\; Y_+ = p_+^\dagger a^\dagger P_1^{\mathrm{T}}.
\end{aligned} \qquad (3.29)$$

The dimensionality of $X_\pm$ and $Y_\pm$ is $N_\pm \times N$. The null space condition (3.27) implies the constraint

$$X_- Y_+^\dagger = Y_- X_+^\dagger. \qquad (3.30)$$

It is helpful to rescale and combine $X_\pm, Y_\pm$ into a single matrix $W_\pm$ of dimension $N_\pm \times 2N$,

$$W_+ = \sqrt{\frac{\mathcal{N}\delta_0}{\pi\hbar}}\left(X_+, \, Y_+\right), \;\; W_- = \sqrt{\frac{\mathcal{N}\delta_0}{\pi\hbar}}\left(-Y_-, \, X_-\right). \qquad (3.31)$$

The eigenvalues of $W_\pm W_\pm^\dagger$ equal the inverse delay times $\gamma_n^\pm$ and the constraint (3.30) now reads

$$W_- W_+^\dagger = 0. \tag{3.32}$$

Considering first the marginal distributions $P_\pm(W_\pm)$ of W_+ and W_- separately, we see that these matrices are constructed from rank-N sub-blocks taken from rank-$\mathcal{N}$ random unitary matrices $u_\pm$ and Gaussian matrices a. In the limit $\mathcal{N} \to \infty$ at fixed N the marginal distributions of $W_\pm$ tend to a Gaussian,

$$P_\pm(W_\pm) \propto \exp\left(-\frac{\beta\pi\hbar}{2\delta_0} \operatorname{Tr} W_\pm W_\pm^\dagger\right). \tag{3.33}$$

In view of Eq. (3.20), the eigenvalues of $W_\pm W_\pm^\dagger$ then have marginal distributions $P_\pm(\{\gamma_n^\pm\})$ of the Wishart form (3.10).

It remains to show that the two sets of eigenvalues γ_n^+ and γ_n^- have independent distributions, so that

$$P(\{\gamma_n^\pm\}) = P_+(\{\gamma_n^+\})P_-(\{\gamma_n^-\}). \tag{3.34}$$

The two matrices W_+ and W_- are not independent, because of the constraint (3.32). To see that this constraint has no effect on the eigenvalue distributions, we make the singular value decomposition

$$W_\pm = \omega_\pm \left(\operatorname{diag}\left(\sqrt{\gamma_n^\pm}\right), \emptyset_{N_\pm,(2N-N_\pm)}\right) \Omega_\pm^\dagger. \tag{3.35}$$

The unitary matrices $\omega_\pm$ and $\Omega_\pm$ have dimension $N_\pm \times N_\pm$ and $2N \times 2N$, respectively, and $\emptyset_{n,m}$ is the $n \times m$ null matrix. The constraint (3.32) is now expressed exclusively in terms of the matrices $\Omega_\pm$ — the first N_- columns of Ω_- have to be orthogonal to the first N_+ columns of Ω_+. The matrix products

$$W_\pm W_\pm^\dagger = \omega_\pm \operatorname{diag}(\gamma_n^\pm)\omega_\pm^\dagger \tag{3.36}$$

thus have independent Wishart distributions.

All of this is for $|\nu| \le N$. The extension to $|\nu| > N$ goes as follows. For $\nu > N$ one has $N_- = 0$, so we deal only with a single set of delay times, obtained as the $N_+ = 2N$ eigenvalues of the Wishart matrix $W_+^\dagger W_+$. (We have inverted the order, because $W_+ W_+^\dagger$ has a spurious set of ν vanishing eigenvalues, representing zero-modes that are uncoupled to the continuum.) Similarly, for $\nu < -N$ one has $N_+ = 0$ and the delay times are the $N_- = 2N$ eigenvalues of the Wishart matrix $W_-^\dagger W_-$. The resulting eigenvalue distribution is Eq. (3.11).

3.4.3 Numerical test

We have performed extensive numerical simulations to test our analytical result of two independent Wishart distributions for the inverse delay times, comparing with a direct calculation using the Gaussian ensemble of random Hamiltonians. Some results for $\beta = 1$, symmetry class BDI are show in the main text (Fig. 3.2), some more results for all three chiral symmetry classes are shown in Fig. 3.4. The quality of the agreement (the two sets of histograms are almost indistinguishable) convinces us of the validity of our analysis.

3.4.4 Generalization to unbalanced coupling

The results in Appendix 3.4.2 pertain to the case of an equal number $N_1 = N_2 = N$ of channels coupling to each chiral sector. This is the appropriate case in the context of superconductivity, where the chirality refers to the electron and hole degrees of freedom — which are balanced under most circumstances. In other contexts, in particular when the chirality refers to a sublattice degree of freedom, the coupling may be unbalanced. We generalize our results to that case.

When $N_1 = N_2 + \delta N$ Eq. (3.8) for the topological invariant should be replaced by

$$\nu_0 = \tfrac{1}{2} \operatorname{Tr} S_0 = \max \left[-\tfrac{1}{2} N_{\text{tot}}, \min \left(\nu + \tfrac{1}{2} \delta N, \tfrac{1}{2} N_{\text{tot}} \right) \right]. \qquad (3.37)$$

The unitary and Hermitian matrix S_0 has dimension $2N_{\text{tot}} \times 2N_{\text{tot}}$, with $N_{\text{tot}} = N_1 + N_2$. When N_{tot} is odd the number ν_0 is half-integer. The winding number ν is always an integer.

Because S_0 stills commutes with the time-delay matrix Q_0 we still have two sets of inverse delay times $\gamma_n^\pm$, associated to the $N_\pm = N_{\text{tot}}/2 \pm \nu_0$ eigenvalues of S_0 equal to ± 1. The two sets again have independent Wishart distributions,

$$P_\pm(\{\gamma_n^\pm\}) \propto \prod_{j>i=1}^{N_\pm} |\gamma_i^\pm - \gamma_j^\pm|^\beta \prod_{k=1}^{N_\pm} (\gamma_k^\pm)^{\beta/2-1} e^{-\beta \tau_{\text{H}} \gamma_k^\pm /4}$$
$$\times (\gamma_k^\pm)^{(\beta/4)|N_{\text{tot}} \mp \delta N \mp 2\nu|}. \qquad (3.38)$$

This formula also applies to the saturation regime $|2\nu + \delta N| > N_{\text{tot}}$, where either N_+ or N_- vanishes and only one set of delay times remains. In this regime the system has an additional $|\nu + \delta N/2| - N_{\text{tot}}/2$ zero-modes that are not coupled to the continuum.

We can use Eq. (3.38) to make contact with the "single-site limit" $N_1 = 1$, $N_2 = 0$ studied by Fyodorov and Ossipov[39]. We distinguish
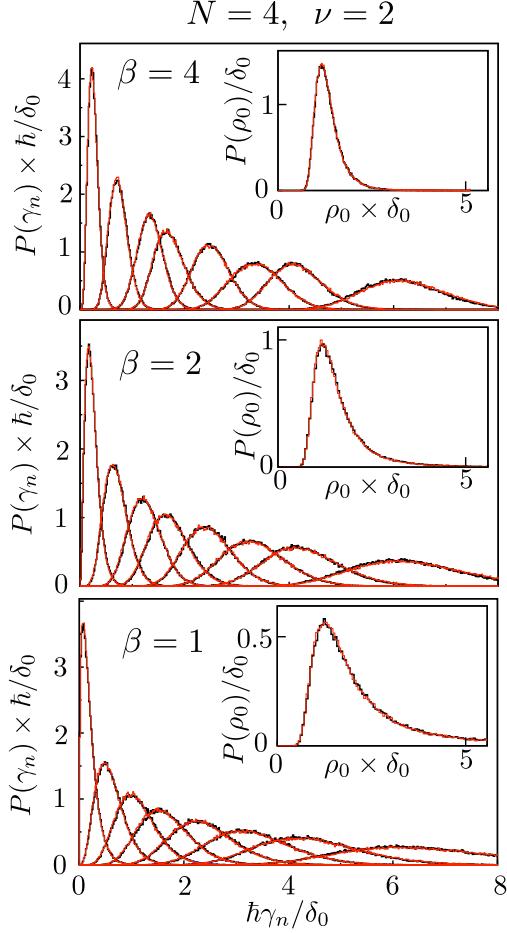
Figure 3.4: Probability distributions in symmetry class BDI ($\beta = 1$), class AIII ($\beta = 2$), and class CII ($\beta = 4$) of the n-th inverse delay time γ_n, ordered from small to large: $0 < \gamma_1 < \gamma_2 \cdots < \gamma_{2N}$, with $N = 4$. All plots are for $\nu = 2$ Majorana zero-modes. The black histograms of the chiral Gaussian ensemble (3.12) (calculated with $\mathcal{N} = 80$ for $\beta = 1, 2$ and $\mathcal{N} = 120$ for $\beta = 4$) are almost indistinguishable from the red histograms of the Wishart ensemble. In each panel the inset shows the corresponding probability distribution of the density of states $\rho_0 = \sum_n (2\pi\hbar\gamma_n)^{-1}$.

positive and negative winding number ν. For $\nu \geq 0$ one has $\nu_0 = 1/2$, $N_+ = 1$, $N_- = 0$. The single delay time $\tau \equiv 1/\gamma_1^+$ has distribution

$$P(\tau) \propto \tau^{-(\beta/2)(1+\nu)-1} e^{-\beta \tau_{\mathrm{H}}/4\tau}, \quad \nu \geq 0, \qquad (3.39)$$

in agreement with Ref. [39] for $\beta = 2$. There are then ν zero-modes not coupled to the continuum.

For negative ν (or equivalently, positive ν with $N_1 = 0$, $N_2 = 1$) Ref. [39] argues that all delay times diverge, but instead we do find one finite $\tau \equiv 1/\gamma_1^-$ with distribution

$$P(\tau) \propto \tau^{(\beta/2)\nu-1} e^{-\beta \tau_{\mathrm{H}}/4\tau}, \quad \nu \leq -1, \qquad (3.40)$$

accompanied by $|\nu| - 1$ zero-modes not coupled to the continuum.

3.4.5 Calculation of the average density of states

The formula (3.16) for the ensemble averaged density of states results upon integration of

$$2\pi\hbar\delta_0 \langle \rho_0 \rangle = \int_0^\infty d\gamma_1^+ \cdots \int_0^\infty d\gamma_{N_+}^+ P_+(\{\gamma_n^+\}) \sum_{n=1}^{N_+} \frac{1}{\gamma_n^+}$$

$$+ \int_0^\infty d\gamma_1^- \cdots \int_0^\infty d\gamma_{N_-}^- P_-(\{\gamma_n^-\}) \sum_{n=1}^{N_-} \frac{1}{\gamma_n^-}, \qquad (3.41)$$

with probability distributions $P_\pm$ given by Eq. (3.10). These integrals can be carried out in closed form, as follows.

We need to evaluate an expression of the form

$$I = \frac{1}{C} \prod_{k=1}^N \int_0^\infty d\gamma_k \, \gamma_k^p e^{-\beta \tau_{\mathrm{H}} \gamma_k/4} \prod_{j>i=1}^N |\gamma_i - \gamma_j|^\beta \left(\sum_{n=1}^N \frac{1}{\gamma_n} \right), \qquad (3.42)$$

with normalization integral

$$C = \prod_{k=1}^N \int_0^\infty d\gamma_k \, \gamma_k^p e^{-\beta \tau_{\mathrm{H}} \gamma_k/4} \prod_{j>i=1}^N |\gamma_i - \gamma_j|^\beta. \qquad (3.43)$$

For a finite answer we need an exponent $p > 0$.

We substitute $\gamma_k^{p-1} = p^{-1} d\gamma_k^p / d\gamma_k$ and perform a partial integration,

$$
\begin{aligned}
I &= \frac{1}{pC} \prod_{k=1}^{N} \int_0^\infty d\gamma_k \, e^{-\beta \tau_\mathrm{H} \gamma_k / 4} \prod_{j>i=1}^{N} |\gamma_i - \gamma_j|^\beta \\
&\quad \times \left(\sum_{n=1}^{N} \frac{d}{d\gamma_n} \right) \prod_{k'=1}^{N} \gamma_{k'}^p \quad\quad\quad\quad (3.44) \\
&= \frac{\beta N \tau_\mathrm{H}}{4p} - \frac{1}{pC} \prod_{k=1}^{N} \int_0^\infty d\gamma_k \, \gamma_k^p e^{-\beta \tau_\mathrm{H} \gamma_k / 4} \\
&\quad \times \left(\sum_{n=1}^{N} \frac{d}{d\gamma_n} \right) \prod_{j>i=1}^{N} |\gamma_i - \gamma_j|^\beta \\
&= \frac{\beta N \tau_\mathrm{H}}{4p}, \quad\quad\quad\quad (3.45)
\end{aligned}
$$

because

$$
\left(\sum_{n=1}^{N} \frac{d}{d\gamma_n} \right) \prod_{j>i=1}^{N} |\gamma_i - \gamma_j|^\beta = 0. \quad\quad\quad\quad (3.46)
$$

Bibliography of chapter 3

[1] M. Büttiker, in *Time in Quantum Mechanics*, edited by J. G. Muga, R. Sala Mayato, and I. L. Egusquiza (Springer, Berlin, 2002).

[2] C. A. A. de Carvalho and H. M. Nussenzveig, Phys. Rep. **364**, 83 (2002).

[3] L. Eisenbud, Ph.D. thesis (Princeton University, 1948).

[4] E. P. Wigner, Phys. Rev. **98**, 145 (1955).

[5] F. T. Smith, Phys. Rev. **118**, 349 (1960).

[6] R. Blümel and U. Smilansky, Phys. Rev. Lett. **64**, 241 (1990).

[7] U. Smilansky, in *Chaos and Quantum Physics*, edited by M.-J. Giannoni, A. Voros, and J. Zinn-Justin (North- Holland, Amsterdam, 1991).

[8] P. J. Forrester, *Log-gases and Random Matrices* (Princeton University Press, 2010).

[9] P. W. Brouwer, K. M. Frahm, and C. W. J. Beenakker, Phys. Rev. Lett. **78**, 4737 (1997); Waves in Random Media **9**, 91 (1999).

[10] E. P. Wigner, SIAM Review **9**, 1 (1967).

[11] F. J. Dyson, J. Math. Phys. **3**, 1199 (1962).

[12] J. Wishart, Biometrika A **20**, 32 (1928).

[13] H.-J. Sommers, D. V. Savin, and V. V. Sokolov, Phys. Rev. Lett. **87**, 094101 (2001).

[14] D. V. Savin, Y. V. Fyodorov, and H.-J. Sommers, Phys. Rev. E **63**, 035202(R) (2001).

[15] V. A. Gopar, P. A. Mello, and M. Büttiker, Phys. Rev. Lett. **77**, 4974 (1996).

[16] P. W. Brouwer, S. A. van Langen, K. M. Frahm, M. Büttiker, and C. W. J. Beenakker, Phys. Rev. Lett. **79**, 913 (1997).

Bibliography of chapter 3

[17] S. F. Godijn, S. Möller, H. Buhmann, L. W. Molenkamp, and S. A. van Langen, Phys. Rev. Lett. **82**, 2927 (1999).

[18] T. Kottos and M. Weiss, Phys. Rev. Lett. **89**, 056401 (2002).

[19] M. G. A. Crawford and P. W. Brouwer, Phys. Rev. E **65**, 026221 (2002).

[20] D. V. Savin and H.-J. Sommers, Phys. Rev. E **68**, 036211 (2003).

[21] M. Büttiker and M. L. Polianski, J. Phys. A **38**, 10559 (2005).

[22] S. E. Nigg and M. Büttiker, Phys. Rev. B **77**, 085312 (2008)

[23] C. Texier and S. N. Majumdar, Phys. Rev. Lett. **110**, 250602 (2013).

[24] A. Abbout, G. Fleury, J.-L. Pichard, and K. Muttalib, Phys. Rev. B **87**, 115147 (2013).

[25] F. Mezzadri and N. J. Simm, Comm. Math. Phys **324**, 465 (2013).

[26] J. Kuipers, D. V. Savin, and M. Sieber, New J. Phys. **16**, 123018 (2014).

[27] A. Grabsch and C. Texier, Europhys. Lett. **109**, 50004 (2015).

[28] F. D. Cunden, Phys. Rev. E **91**, 060102(R) (2015).

[29] M. Z. Hasan and C. L. Kane, Rev. Mod. Phys. **82**, 3045 (2010).

[30] X.-L. Qi and S.-C. Zhang, Rev. Mod. Phys. **83**, 1057 (2011).

[31] S. Ryu, A. P. Schnyder, A. Furusaki, and A. W. W. Ludwig, New J. Phys. **12**, 065010 (2010).

[32] C. W. J. Beenakker, Rev.Mod.Phys. **87**, 1037 (2015).

[33] M. Bocquet, D. Serban, and M. R. Zirnbauer, Nucl. Phys. B **578**, 628 (2000).

[34] D. A. Ivanov, J. Math. Phys. **43**, 126 (2002); arXiv:cond-mat/0103089.

[35] J. Alicea, Rep. Progr. Phys. **75**, 076501 (2012).

[36] C. W. J. Beenakker, Annu. Rev. Con. Mat. Phys. **4**, 113 (2013).

[37] S. R. Elliott and M. Franz, Rev. Mod. Phys. **87**, 137 (2015).

[38] M. Marciani, P. W. Brouwer, and C. W. J. Beenakker, Phys. Rev. B **90**, 045403 (2014).

[39] Y. V. Fyodorov and A. Ossipov, Phys. Rev. Lett. **92**, 084103 (2004).

[40] A. Altland and M. R. Zirnbauer, Phys. Rev. B **55**, 1142 (1997).

[41] J. J. M. Verbaarschot and I. Zahed, Phys. Rev. Lett. **70**, 3852 (1993).

[42] J. J. M. Verbaarschot and T. Wettig, Ann. Rev. Nucl. Part. Sci. **50**, 343 (2000).

[43] M. Leijnse and K. Flensberg, Semicond. Science Techn. **27**, 124003 (2012).

[44] T. D. Stanescu and S. Tewari, J. Phys. Cond. Matt. **25**, 233201 (2013).

[45] L. Fidkowski and A. Kitaev, Phys. Rev. B **81**, 134509 (2010); **83**, 075103 (2011).

[46] A. M. Turner, F. Pollmann, and E. Berg, Phys. Rev. B **83**, 075102 (2011).

[47] S. R. Manmana, A. M. Essin, R. M. Noack, and V. Gurarie, Phys. Rev. B **86**, 205119 (2012).

[48] D. Meidan, A. Romito, and P. W. Brouwer, Phys. Rev. Lett. **113**, 057003 (2014).

[49] S. Tewari and J. D. Sau, Phys. Rev. Lett. **109**, 150408 (2012).

[50] M. Diez, J. P. Dahlhaus, M. Wimmer, and C. W. J. Beenakker, Phys. Rev. B **86**, 094501 (2012).

[51] H.-Y. Hui, P. M. R. Brydon, J. D. Sau, S. Tewari, and S. Das Sarma, Sci. Rep. **5**, 8880 (2015).

[52] L. Fu and C. L. Kane, Phys. Rev. Lett. **100**, 096407 (2008).

[53] M. Cheng, R. M. Lutchyn, V. Galitski, and S. Das Sarma, Phys. Rev. B **82**, 094504 (2010).

[54] J. C. Y. Teo and C. L. Kane, Phys. Rev. B **82**, 115120 (2010).

[55] C.-K. Chiu, D. I. Pikulin, and M. Franz, Phys. Rev. B **91**, 165402 (2015).

[56] A. W. W. Ludwig, M. P. A. Fisher, R. Shankar, and G. Grinstein, Phys. Rev. B **50**, 7526 (1994).

[57] O. Motrunich, K. Damle, and D. A. Huse, Phys. Rev. B **65**, 064206 (2002).

Bibliography of chapter 3

[58] D.-H. Lee, Phys. Rev. Lett. **103**, 196804 (2009).

[59] J. P. Dahlhaus, C.-Y. Hou, A. R. Akhmerov, and C. W. J. Beenakker, Phys. Rev. B **82**, 085312 (2010).

[60] V. Parente, P. Lucignano, P. Vitale, A. Tagliacozzo, and F. Guinea, Phys. Rev. B **83**, 075424 (2011).

[61] The number $2N$ of scattering channels includes a factor of 2 from the electron-hole degree of freedom. For $\beta = 4$ each scattering channel (and hence each delay time τ_n) has a twofold Kramers degeneracy from the spin degree of freedom, while for $\beta = 1, 2$ the spin degree of freedom is counted separately in N. The mean level spacing δ_0 refers to distinct levels in the bulk of the spectrum (away from $E = 0$), including electron-hole and spin degrees of freedom but not counting degeneracies.

[62] I. C. Fulga, F. Hassler, A. R. Akhmerov, and C. W. J. Beenakker, Phys. Rev. B **83**, 155429 (2011).

[63] The Laguerre distributions (3.10) and (3.11) are the eigenvalue distributions of a Wishart matrix $WW^\dagger$ when W has dimension $(N \pm \nu) \times 2N$ for $|\nu| < N$ and dimension $2N \times (N + |\nu|)$ for $|\nu| \geq N$.

[64] For details of the calculation, see the Appendix.

4 Effect of a tunnel barrier on the scattering from a Majorana bound state in an Andreev billiard

4.1 Introduction

The quantum states of particle and anti-particle excitations in a superconductor (Bogoliubov quasiparticles) are related by a unitary transformation, which means that they can be represented by a *real* wave function. In this so-called Majorana representation the $N \times N$ scattering matrix S at the Fermi level is real orthogonal rather than complex unitary[1]. Since the orthogonal group $O(N)$ is doubly connected, this immediately implies a twofold distinction of scattering problems in a superconductor: The subgroup $O_+(N) \equiv SO(N)$ of scattering matrices with determinant $+1$, connected to the unit matrix, is called *topologically trivial*, while the disconnected set $O_-(N)$ of scattering matrices with determinant -1 is called *topologically nontrivial*. In mathematical terms, the experimental search for Majorana bound states can be called a search for systems that have $\text{Det } S = -1$. This search has been reviewed, from different perspectives, in Refs. [2–6].

If the scattering is chaotic the scattering matrix becomes very sensitive to microscopic details, and it is useful to develop a statistical description: Rather than studying a particular S, one studies the probability distribution $P(S)$ in an ensemble of chaotic scatterers. This is the framework of random-matrix theory (RMT)[7–9]. The ensemble generated by drawing S uniformly from the unitary group $U(N)$, introduced by Dyson in the context of nuclear scattering[10], is called the circular unitary ensemble (CUE). Superconductors need a new ensemble. A natural name would have been the circular orthogonal ensemble (COE), but since that name is already taken for the coset $U(N)/O(N)$, the alternative name circular real ensemble (CRE) is used when S is drawn uniformly from $O(N)$. The RMT of the CRE, and the physical applications to Majorana fermions and topological superconductors, have been reviewed recently[11].
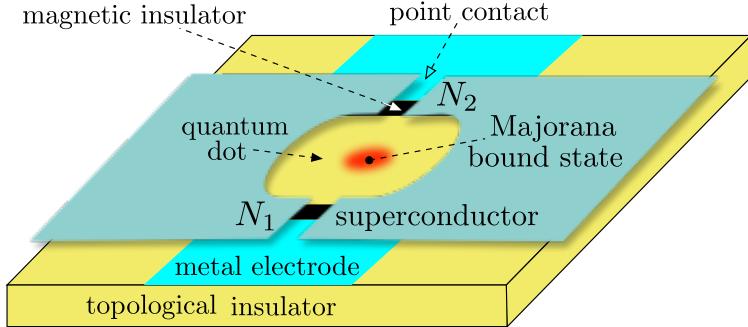
Figure 4.1: Andreev billiard on the conducting surface of a three-dimensional topological insulator. The billiard consists of a confined region (quantum dot, mean level spacing δ_0) with superconducting boundaries, connected to metal electrodes by a pair of point contacts (supporting a total of $N = N_1 + N_2$ propagating modes). A magnetic insulator introduces a tunnel barrier in each point contact (transmission probability Γ per mode). A magnetic vortex may introduce a Majorana bound state in the quantum dot.

The uniformity of the distribution requires ideal coupling of the scattering channels to the continuum, which physically means that the discrete spectrum of a quantum dot is coupled to metal electrodes by ballistic point contacts. If the point contact contains a tunnel barrier, then $P(S)$ is no longer uniform but biased towards the reflection matrix r_{B} of the barrier. The modified distribution $P_{\mathrm{Poisson}}(S)$ is known[12–16], it goes by the name "Poisson kernel" and equals

$$P_{\mathrm{Poisson}}(S) \propto \mathrm{Det}\,(1 - r_{\mathrm{B}}^{\dagger}S)^{1-N} \qquad (4.1)$$

in the CRE[16].

In the present work we apply this result to the scattering (Andreev reflection) in a superconducting quantum dot (Andreev billiard), see Fig. 4.1. We focus in particular on the effect of a bound state at the Fermi level ($E = 0$) in the quantum dot, a so-called Majorana zero-mode or Majorana bound state. In addition to the scattering matrix, which determines the thermal and electrical conductance, we consider also the time-delay matrix $Q = -i\hbar S^{\dagger}dS/dE$. The eigenvalues of Q are positive numbers with the dimension of time, that govern the low-frequency dynamics of the system (admittance and charge relaxation[17–19]). Moreover, the trace of Q gives the density of states and Q and S together determine the thermopower[20,21].

The joint distribution of S and Q is known for ballistic coupling[22–24], here we generalize that to tunnel coupling. The effect of a tunnel barrier on the time-delay matrix has been studied for complex scattering matrices[25,26], but not yet for real matrices. One essential distinction is that

the tunnel barrier has no effect on the density of states in the CUE and COE, but it does in the CRE.

The outline of the chapter is as follows. The next two sections formulate the scattering theory of the Andreev billiard and the appropriate random-matrix theory. Our key technical result, the joint distribution $P(S, Q)$, is given in Sec. 4.4. We apply this to the simplest single-channel case ($N = 1$) in Sec. 4.5, where obtain a remarkable scaling relation: For a high tunnel barrier (transmission probability $\Gamma \ll 1$) the distribution $P(\rho|\Gamma)$ of the density of states at the Fermi level is described by a one-parameter scaling function $F(x)$:

$$P(\rho|\Gamma) \propto \begin{cases} F(\Gamma\rho/4) & \text{with a Majorana bound state,} \\ F(4\rho/\Gamma) & \text{without a Majorana.} \end{cases} \qquad (4.2)$$

The average density of states in the multi-channel case is calculated in Sec. 4.6. By relating the ensemble averages of Q and S we derive the relation

$$\langle\rho\rangle = \langle\rho\rangle_{\text{ballistic}} \left(1 - \frac{2}{N\Gamma}\text{Tr}\, r_{\text{B}}^{\dagger}[\langle S\rangle - r_{\text{B}}]\right), \qquad (4.3)$$

for a mode-independent tunnel probability Γ. In the CUE and COE the average scattering matrix $\langle S\rangle$ is just equal to r_{B}, so $\langle\rho\rangle$ remains equal to its ballistic value $\langle\rho\rangle_{\text{ballistic}}$, but the CRE is not so constrained.

Applications to the thermal conductance g and the electrical (Andreev) conductance g_{A} follow in Secs. 4.7 and 4.8. For ballistic coupling it is known that $P(g)$ is the same with or without the Majorana bound state[27]. (This also holds for $P(\rho)$[23].) In the presence of a tunnel barrier this is no longer the case, but we find that the Majorana bound state remains hidden if even a single scattering channel has $\Gamma = 1$. The distribution of g_{A}, in contrast, is sensitive to the presence or absence of the Majorana bound state even for ballistic coupling[28]. The way in which $P(g_{\text{A}})$ changes as we tune the system through a topological phase transition, at which a Majorana bound state emerges, is calculated in Sec. 4.9. We conclude in Sec. 4.10.

In the main text we focus on the results and applications. Details of the calculations are moved to the Appendices. These also contain more general results for other RMT ensembles, with or without time-reversal and/or spin-rotation symmetry. (Both symmetries are broken in the CRE.)

4.2 Scattering formulation

Fig. 4.1 shows the scattering geometry, consisting of a superconducting quantum dot (Andreev billiard) on the surface of a topological insulator,

connected to normal metal electrodes by point contacts. The Hamiltonian H of the quantum dot is related to the energy-dependent scattering matrix $S(E)$ by the Mahaux-Weidenmüller formula[29],

$$
\begin{aligned}
S(E) &= \frac{1 - i\pi W^\dagger (E - H)^{-1} W}{1 + i\pi W^\dagger (E - H)^{-1} W} \\
&= 1 - 2\pi i W^\dagger (E - H + i\pi W W^\dagger)^{-1} W.
\end{aligned}
\tag{4.4}
$$

The $M \times N$ matrix W couples the M energy levels in the quantum dot (mean level spacing δ_0) to a total of $N \ll M$ propagating modes in the point contact.

We assume that degeneracies are broken by spin-orbit coupling in the topological insulator in combination with a magnetic field (perpendicular to the surface). All degrees of freedom are therefore counted separately in N and M, as well as in δ_0. The electron-hole degree of freedom is also included in the count, but we leave open the possibility of an unpaired Majorana fermion — a coherent superposition of electron and hole quasiparticles that does not come with a distinct antiparticle. An odd level number M indicates the presence of a Majorana bound state in the quantum dot, produced when a magnetic vortex enters[30]. An odd mode number N signals a propagating Majorana mode in the point contact, allowed by a π-phase difference between the superconducting boundaries[31].

The N modes have an energy-independent transmission probability $\Gamma_n \in [0,1]$ per mode. If we choose a basis such that the coupling matrix W has only nonzero elements on the diagonal, it has the explicit form[32]

$$
\begin{aligned}
&W_{mn} = w_n \delta_{mn}, \;\; 1 \le m \le M, \;\; 1 \le n \le N, \\
&|w_n|^2 = \frac{M \delta_0 \kappa_n}{\pi^2}, \;\; \kappa_n = \frac{1 - r_n}{1 + r_n}, \;\; r_n^2 = 1 - \Gamma_n.
\end{aligned}
\tag{4.5}
$$

Notice that the tunnel probability Γ_n determines the reflection amplitude $r_n \in [-1, 1]$ up to a sign. The conventional choice is to take $r_n \ge 0$, when $\kappa_n = \kappa_n^+$ can be written as

$$
\kappa_n^+ = \frac{1}{\Gamma_n}(2 - \Gamma_n - 2\sqrt{1 - \Gamma_n}).
\tag{4.6}
$$

Alternatively, if $r_n \le 0$ one has $\kappa_n = \kappa_n^-$ given by

$$
\kappa_n^- = \frac{1}{\Gamma_n}(2 - \Gamma_n + 2\sqrt{1 - \Gamma_n}) = 1/\kappa_n^+.
\tag{4.7}
$$

The two choices are equivalent for ballistic coupling, $\Gamma_n = 1 = \kappa_n^\pm$, but for a high tunnel barrier $\Gamma_n \ll 1$ one has $\kappa_n^+ \to 0$ while $\kappa_n^- \to \infty$. The sign

change of r_n is a topological phase transition[33], which we will analyze in Section 4.9. For now we take $r_n \geq 0$ for all n, so $\kappa_n = \kappa_n^+$.

From the scattering matrix we can obtain transport properties, such as the electrical and thermal conductance, and thermodynamic properties, such as the density of states. If we restrict ourselves to properties at the Fermi level, $E = 0$, we need the matrix $S(0) \equiv S$ and the derivative

$$Q = -i\hbar \lim_{E \to 0} S^\dagger(E) \frac{dS(E)}{dE}. \tag{4.8}$$

The unitarity of $S(E)$ implies that Q is Hermitian, so it has real eigenvalues τ_n with the dimension of time. The τ_n's are called (proper) delay times and Q is called the Wigner-Smith time-delay matrix[34–36]. The Fermi-level density of states ρ is obtained from Q via the Birman-Krein formula[37–39],

$$\rho = \frac{1}{2\pi i} \lim_{E \to 0} \frac{d}{dE} \ln \mathrm{Det}\, S(E) = \frac{1}{2\pi\hbar} \mathrm{Tr}\, Q. \tag{4.9}$$

For the thermal conductance we partition the modes into two sets, $N = N_1 + N_2$, each set connected to a different terminal, and decompose the scattering matrix into reflection and transmission subblocks,

$$S = \begin{pmatrix} r & t' \\ t & r' \end{pmatrix}. \tag{4.10}$$

A small temperature difference δT between the two terminals, at average temperature T_0, drives a heat current $J = G_{\mathrm{thermal}} \delta T$. The thermal conductance G_{thermal} in the low-temperature linear-response limit $T_0, \delta T/T_0 \to 0$ is given by

$$g = G_{\mathrm{thermal}}/G_0 = \mathrm{Tr}\, tt^\dagger, \quad G_0 = \frac{\pi^2 k_{\mathrm{B}}^2 T_0}{6h}. \tag{4.11}$$

The quantum G_0 is a factor-of-two smaller than in systems without superconductivity[41], due to our separate counting of electron and hole degrees of freedom that allows to account for the possibility of propagation via an unpaired Majorana mode.

If we keep the two terminals at the same temperature but instead apply a voltage difference, we can drive an electrical current. We consider a situation where both terminal 2 and the superconductor are grounded, while terminal 1 is biased at voltage V. The current I from terminal 1 to ground is then given by the Andreev conductance

$$\begin{aligned} g_{\mathrm{A}} = \frac{h}{e^2} \frac{dI}{dV} &= \mathrm{Tr}\,(1 - r_{ee} r_{ee}^\dagger + r_{he} r_{he}^\dagger) \\ &= \tfrac{1}{2} \mathrm{Tr}\,(1 - r\tau_z r^\dagger \tau_z), \end{aligned} \tag{4.12}$$

in the zero-temperature, zero-voltage limit. In the last equality we used the particle-hole symmetry relation $t = \tau_x t^* \tau_x$ at $E = 0$, where the τ_i Pauli matrices act on the electron (e) and hole (h) degree of freedom.

4.3 Random-matrix formulation

For a statistical description we consider an ensemble of quantum dots, each with its own random Hamiltonian H. The mean level spacing δ_0 and coupling matrix W are kept fixed. If the wave dynamics in the quantum dot is chaotic, the ensemble is fully characterized by the presence or absence of certain fundamental symmetries. This is the universal framework of random-matrix theory.

Superconducting systems are characterized by particle-hole symmetry,

$$
\begin{aligned}
H = -\tau_x H^* \tau_x, \;\; & W = \tau_x W^* \tau_x, \\
\Rightarrow S = \tau_x S^* \tau_x, \;\; & Q = \tau_x Q^* \tau_x.
\end{aligned}
\tag{4.13}
$$

The Pauli matrices τ_x can be removed from the symmetry relation by a unitary transformation

$$
H \mapsto \Omega H \Omega^\dagger, \;\; \Omega = \sqrt{\tfrac{1}{2}} \begin{pmatrix} 1 & 1 \\ i & -i \end{pmatrix},
\tag{4.14}
$$

after which we simply have

$$
H = -H^*, \;\; W = W^*, \;\; S = S^*, \;\; Q = Q^*.
\tag{4.15}
$$

In this so-called Majorana basis the Hamiltonian is real antisymmetric, $H = iA$ with $A_{nm} = A_{nm}^* = -A_{mn}$.

If no other symmetries are imposed on the Hamiltonian we have the class-D ensemble of random-matrix theory [1,11], with Gaussian probability distribution

$$
P(\{A_{nm}\}) \propto \prod_{n>m} \exp\left(-\frac{\pi^2 A_{nm}^2}{2M \delta_0^2} \right).
\tag{4.16}
$$

The eigenvalues of the antisymmetric $M \times M$ matrix H come in $\pm E$ pairs, hence if M is odd there must be a nondegenerate eigenvalue $E = 0$ at the Fermi level, in the middle of the superconducting gap. This so-called Majorana bound state is the hallmark of a topologically nontrivial superconductor [42,43]. If M is even there is no level pinned to $E = 0$, and the superconductor is called topologically trivial. It is helpful to encode the distinction in a topological quantum number ν that counts the number of Majorana bound states, so ν equals 0 or 1 if the superconductor is topologically trivial or non-trivial, respectively.

In the scattering matrix the presence of a Majorana bound state is signaled by the sign of the determinant,

$$\text{Det}\, S = (-1)^{\nu}, \ \ \nu \in \{0, 1\}. \tag{4.17}$$

This can be seen directly from the definition (4.4) in the Majorana basis: For M even the matrix $H = iA$ is invertible, so we have

$$S = \frac{1 + \pi W^{\text{T}} A^{-1} W}{1 - \pi W^{\text{T}} A^{-1} W} \Rightarrow \text{Det}\, S = +1, \tag{4.18}$$

since $\text{Det}\,(1 + \mathcal{A}) = \text{Det}\,(1 - \mathcal{A})$ if $\mathcal{A} = -\mathcal{A}^{\text{T}}$. For M odd the bound state contributes to the determinant a factor

$$\lim_{\epsilon \to 0} \frac{\text{Det}\,(1 + \epsilon^{-1} v v^{\text{T}})}{\text{Det}\,(1 - \epsilon^{-1} v v^{\text{T}})} = -1,$$

for some vector v, so $\text{Det}\, S = -1$.

The class-D ensemble of scattering matrices thus consists of two disjunct sets: The special orthogonal group $\text{SO}(N) \equiv \text{O}_{+}(N)$ of orthogonal matrices with determinant $+1$ in the topologically trivial case, and the complement $\text{O}_{-}(N)$ of orthogonal matrices with determinant -1 in the topologically nontrivial case.

4.4 Joint distribution of scattering matrix and time-delay matrix

For ballistic coupling ($\Gamma_n = 1$ for all n) the matrices S and Q are statistically independent[22], so they can be considered separately. The class-D ballistic scattering matrix is uniformly distributed in $\text{O}_{\pm}(N)$ — uniformity being defined with respect to the Haar measure[1,11]. This is the Circular Real Ensemble (CRE), the analogue for real orthogonal matrices of the Circular Unitary Ensemble (CUE) for complex unitary matrices[8–10].

The class-D ballistic time-delay matrix has probability distribution[23],

$$P_{\text{ballistic}}(Q) \propto (\text{Det}\, Q)^{-3N/2} \Theta(Q) \exp(-\tfrac{1}{2} \tau_{\text{H}} \text{Tr}\, Q^{-1}), \tag{4.19}$$

where $t_{\text{H}} = 2\pi\hbar/\delta_0$ is the Heisenberg time and $\Theta(Q)$ restricts Q to positive definite real symmetric matrices. This constraint can be implemented more directly by defining

$$Q^{-1} = t_{\text{H}}^{-1} K K^{\text{T}}, \ \ K \in \mathbb{R}_{N, 2N-1}, \tag{4.20}$$

with $\mathbb{R}_{n,m}$ the set of $n \times m$ matrices with real elements. The distribution (4.19) is then equivalent[*] to the Wishart distribution[9]

$$P_{\text{Wishart}}(K) \propto \exp(-\tfrac{1}{2} \operatorname{Tr} KK^{\mathrm{T}}). \qquad (4.21)$$

Remarkably, there is no dependence on the topological quantum number for ballistic coupling: Q has the same distribution irrespective of the presence or absence of a Majorana bound state.

Tunnel coupling is described by a reflection matrix r_{B} (from outside to outside) and transmission matrix t_{B} (from outside to inside). In the Majorana basis these are real matrices, parameterized by

$$\begin{aligned}
r_{\mathrm{B}} &= O_1 \operatorname{diag}(r_1, r_2, \dots r_N) O_2, \\
t_{\mathrm{B}} &= O_3 \operatorname{diag}(\Gamma_1^{1/2}, \Gamma_2^{1/2}, \dots \Gamma_N^{1/2}) O_2, \\
O_1, O_2, O_3 &\in \mathrm{SO}(N), \ \Gamma_n = 1 - r_n^2 \in (0,1].
\end{aligned} \qquad (4.22)$$

As we derive in App. 4.11, the matrix product

$$\Sigma = (1 - S^{\mathrm{T}} r_{\mathrm{B}}) t_{\mathrm{B}}^{-1} \qquad (4.23)$$

determines the joint distribution

$$\begin{aligned}
P(S, Q) &\propto (\operatorname{Det} \Sigma)^N (\operatorname{Det} Q)^{-3N/2} \Theta(Q) \\
&\qquad \times \exp(-\tfrac{1}{2} \tau_{\mathrm{H}} \operatorname{Tr} \Sigma^{\mathrm{T}} Q^{-1} \Sigma),
\end{aligned} \qquad (4.24\mathrm{a})$$

$$\Leftrightarrow P(S, K) \propto (\operatorname{Det} \Sigma)^N \exp(-\tfrac{1}{2} \operatorname{Tr} \Sigma^{\mathrm{T}} KK^{\mathrm{T}} \Sigma). \qquad (4.24\mathrm{b})$$

As a check, we can integrate out the time-delay matrix to obtain the marginal distribution of the scattering matrix,

$$P(S) = \int dK \, P(S, K) \propto (\operatorname{Det} \Sigma)^N \left\| \frac{\partial \Sigma^{\mathrm{T}} K}{\partial K} \right\|^{-1}. \qquad (4.25)$$

The Jacobian evaluates to[44]

$$\left\| \frac{\partial \Sigma^{\mathrm{T}} K}{\partial K} \right\| = (\operatorname{Det} \Sigma)^{2N-1} \ \text{ for } \ K \in \mathbb{R}_{N, 2N-1}, \qquad (4.26)$$

and we recover the class-D Poisson kernel[† 16],

$$P_{\text{Poisson}}(S) = (\operatorname{Det} \Sigma)^{1-N} = \left(\frac{\prod_n \sqrt{\Gamma_n}}{\operatorname{Det}(1 - r_{\mathrm{B}}^{\mathrm{T}} S)} \right)^{N-1}. \qquad (4.27)$$

---

[*]To transform from $P(Q)$ to $P(K)$ multiply by the Jacobians $\|\partial Q/\partial Q^{-1}\| \times \|\partial KK^{\mathrm{T}}/\partial K\| = (\operatorname{Det} Q)^{N+1} \times (\operatorname{Det} K)^{2-N} \propto (\operatorname{Det} Q)^{3N/2}$, for $Q = Q^{\mathrm{T}} \in \mathbb{R}_{N,N}$ and $K \in \mathbb{R}_{N, 2N-1}$.

[†]In most expressions for the probability distribution we write $\propto$ to indicate an unspecified normalization constant. The Poisson kernel (4.27) is normalized, $\int P_{\text{Poisson}}(S) \, dS = \int dS \equiv 1$ with dS the Haar measure on $\mathrm{O}_\pm(N)$, so we use $=$ instead of $\propto$.

The joint distribution (4.24) tells us that S and Q become correlated in the presence of a tunnel barrier. However, S remains independent of the matrix product

$$Q_0 = \frac{1}{\Sigma} Q \frac{1}{\Sigma^{\mathrm{T}}}, \tag{4.28}$$

so that the joint distribution of S and Q_0 factorizes,

$$P(S, Q_0) = P_{\mathrm{Poisson}}(S) \times P_{\mathrm{ballistic}}(Q_0). \tag{4.29}$$

The transformation from Q to Q_0 removes the effect of the tunnel barrier on the time-delay matrix (see App. 4.11).

4.5 Single-channel delay-time statistics

For ballistic coupling the distribution (4.19) implies that the eigenvalues $\gamma_n \equiv 1/\tau_n$ of Q^{-1} have the ν-independent distibution[23]

$$P_{\mathrm{ballistic}}(\{\gamma_n\}) \propto \prod_{k=1}^{N} \gamma_k^{-1+N/2} \exp(-\tfrac{1}{2} t_{\mathrm{H}} \gamma_k) \theta(\gamma_k)$$
$$\times \prod_{i<j} |\gamma_i - \gamma_j|, \quad \nu \in \{0, 1\}. \tag{4.30}$$

The unit step function $\theta(x)$ ensures that $\gamma_n > 0$ for all $n = 1, 2, \ldots N$.

In the single-channel case $N = 1$ we can use the joint distribution (4.24) to immediately extend this result to arbitrary tunnel probability $\Gamma = 1 - r_{\mathrm{B}}^2$. The scalar S is pinned to $(-1)^\nu$, hence

$$\Sigma = \frac{(1 - (-1)^\nu r_{\mathrm{B}})}{\sqrt{1 - r_{\mathrm{B}}^2}} = \begin{cases} \sqrt{\kappa} & \text{for } \nu = 0, \\ 1/\sqrt{\kappa} & \text{for } \nu = 1, \end{cases} \tag{4.31}$$

$$\kappa = \frac{1}{\Gamma}(2 - \Gamma - 2\sqrt{1 - \Gamma}). \tag{4.32}$$

[This definition of κ corresponds to κ^+ from Eq. (4.6).]

Since κ then appears only as a scale factor, we conclude that the single eigenvalue $\gamma_1 \equiv \gamma$ of Q^{-1} for $N = 1$ and any $\kappa \in (0, 1]$ has distribution

$$P(\gamma) = \frac{\theta(\gamma) t_{\mathrm{H}}}{\sqrt{2\pi t_{\mathrm{H}} \gamma}} \times \begin{cases} \kappa^{1/2} \exp(-\tfrac{1}{2}\kappa\, t_{\mathrm{H}}\gamma) & \text{for } \nu = 0, \\ \kappa^{-1/2} \exp(-\tfrac{1}{2}\kappa^{-1} t_{\mathrm{H}}\gamma) & \text{for } \nu = 1. \end{cases} \tag{4.33}$$

The single-parameter scaling $P(\gamma|\kappa, \nu) = \kappa^{1-2\nu} F(\kappa^{1-2\nu}\gamma)$ is tested numerically in Fig. 4.2, by drawing random Hamiltonians from the Gaussian
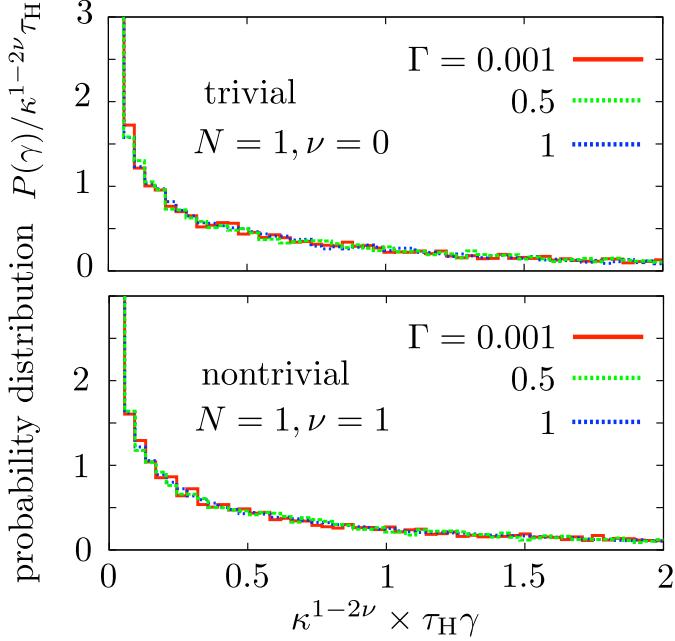
Figure 4.2: Probability distribution of the inverse delay time γ for a single-channel chaotic scatterer, without ($\nu = 0$) or with ($\nu = 1$) a Majorana bound state. The histograms are numerical results obtained by generating random Hamiltonians (of size $M = 40 + \nu$) with distribution (4.16). The scattering matrix, and hence the delay time, then follows from Eqs. (4.4) and (4.5). The different curves correspond to different transmission probability Γ of the tunnel barrier. Rescaling with a factor $\kappa^{1-2\nu}$, with κ defined in Eq. (4.32), makes all histograms collapse onto a single curve, in agreement with the analytical result (4.33).

class-D ensemble (4.16). The excellent agreement serves as a check on our analytics.

With $\rho = (2\pi\hbar\gamma)^{-1}$ the distribution (4.33) gives the scaling form (4.2) of the density of states distribution $P(\rho|\Gamma)$ from the introduction, in the tunneling regime $\Gamma \ll 1$ when $\kappa = \Gamma/4$.

4.6 Average density of states

For ballistic coupling, integration of $\rho = (2\pi\hbar)^{-1} \sum_n \gamma_n^{-1}$ with distribution (4.30) gives the average density of states at the Fermi level [23],

$$\langle\rho\rangle_{\text{ballistic}} = \delta_0^{-1} \frac{N}{N-2}, \quad \delta_0 = 2\pi\hbar/\tau_{\text{H}}, \tag{4.34}$$

for $N \geq 3$. The ensemble average diverges for $N = 1, 2$.

To calculate the effect of a tunnel barrier we write

$$\rho = (2\pi\hbar)^{-1} \operatorname{Tr}(\Sigma Q_0 \Sigma^{\mathrm{T}}), \tag{4.35}$$

see Eq. (4.28), and then use the fact that Q_0 is independent of S and hence independent of Σ. The average of Q_0 with distribution $P_{\mathrm{ballistic}}(Q_0)$ is proportional to the unit matrix,

$$\langle Q_0 \rangle = \mathbb{1}\, \frac{2\pi\hbar}{N} \langle \rho \rangle_{\mathrm{ballistic}} = \mathbb{1}\, \frac{\tau_{\mathrm{H}}}{N-2}, \tag{4.36}$$

so the average density of states (still for $N \geq 3$) is given by

$$\delta_0 \langle \rho \rangle = \frac{1}{N-2} \operatorname{Tr} \langle \Sigma \Sigma^{\mathrm{T}} \rangle$$
$$= \frac{1}{N-2} \left(\sum_n \frac{2 - \Gamma_n}{\Gamma_n} - 2 \operatorname{Tr}\left[(t_{\mathrm{B}}^{\mathrm{T}} t_{\mathrm{B}})^{-1} r_{\mathrm{B}}^{\mathrm{T}} \langle S \rangle \right] \right). \tag{4.37}$$

(This is Eq. (4.3) from the introduction.)

It remains to calculate the average of S with the Poisson kernel (4.27). In the Wigner-Dyson symmetry classes this average is just r_{B}, but as pointed out in Ref. 16 this no longer holds in the Altland-Zirnbauer class D. A simple result for $\langle S \rangle$ is possible for mode-independent tunnel probabilities, $\Gamma_n = \Gamma$ for all n, see App. 4.12:

$$\langle S \rangle_{\pm} = r_{\mathrm{B}} \left(1 - N^{-1} \pm N^{-1}(1-\Gamma)^{N/2-1} \right), \tag{4.38}$$

where again the $+$ sign corresponds to $\nu = 0$ (without a Majorana bound state) and the $-$ sign to $\nu = 1$ (with a Majorana bound state).

We thus arrive at the average density of states,

$$\delta_0 \langle \rho \rangle_{\pm} = \frac{N}{N-2} \left(1 - \frac{2}{N\Gamma} \left[\Gamma - 1 \pm (1-\Gamma)^{N/2} \right] \right), \tag{4.39}$$

plotted in Fig. 4.3. In the ballistic limit $\Gamma \to 1$ the dependence on the Majorana bound state drops out, while in the tunneling limit $\Gamma \to 0$ we obtain

$$\delta_0 \langle \rho \rangle = \frac{2}{N-2} \times \begin{cases} N - 1 + \mathcal{O}(\Gamma) & \text{for } \nu = 0, \\ 2/\Gamma - 1 + \mathcal{O}(\Gamma) & \text{for } \nu = 1. \end{cases} \tag{4.40}$$

The $1/\Gamma$ divergence of the density of states for $\nu = 1$ corresponds to the delta-function contribution from the Majorana bound state in the closed system. Without the Majorana bound state ($\nu = 0$) the density of states at the Fermi level remains finite in the $\Gamma \to 0$ limit, but it does remain above the normal-state value of $1/\delta_0$. This midgap spectral
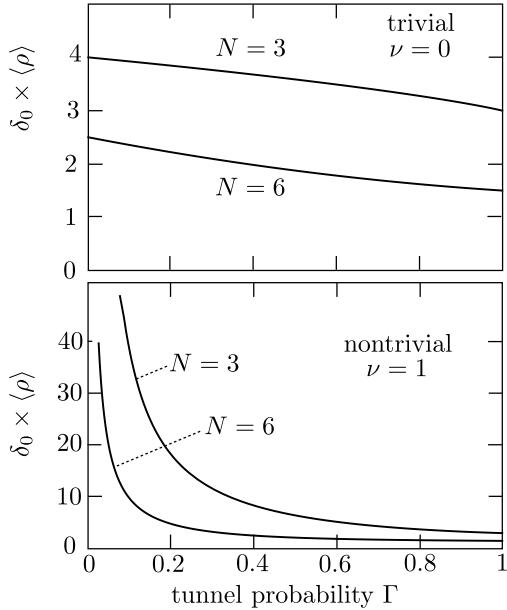
Figure 4.3: Ensemble averaged density of states as a function of mode-independent transmission probability through the barrier, in the absence ($\nu = 0$) or in the presence ($\nu = 1$) of a Majorana bound state. The curves are calculated from the analytical expression (4.39).

peak is characteristic for a class-D superconductor [1,11,42,43,45]. While in a closed system the peak is simply a factor of two, in the weakly coupled open system it is a larger factor $2(N-1)/(N-2)$, which only tends to 2 in the large-N limit. The fact that the ensemble of open systems does not reduce to an ensemble of closed systems in the limit $\Gamma \to 0$ is due to statistical fluctuations that remain important for small N.

4.7 Thermal conductance

We consider the thermal conductance in the simplest case $N_1 = N_2 = 1$ of a quantum dot with single-mode point contacts. These are Majorana modes, carrying heat but no charge.

The scattering matrix $S \in \mathrm{O}_\pm(2)$ is parameterized by

$$S_\pm = \begin{pmatrix} \cos\theta & \mp\sin\theta \\ \sin\theta & \pm\cos\theta \end{pmatrix}, \quad S = \begin{cases} S_+ & \text{if } \nu = 0, \\ S_- & \text{if } \nu = 1. \end{cases} \tag{4.41}$$

The Haar measure equals

$$d\mu = \pi^{-1}d\theta, \quad 0 < \theta < \pi, \tag{4.42}$$

the same for both O_+ and O_-.

For the tunnel barrier we take the reflection matrix $r_{\mathrm{B}} = \mathrm{diag}\,(r_1, r_2)$, with $r_n = \sqrt{1 - \Gamma_n} \geq 0$. The Poisson kernel (4.27) then has the explicit form

$$P_\pm(\theta) = \frac{\sqrt{\Gamma_1 \Gamma_2}}{1 \pm r_1 r_2 - (r_1 \pm r_2)\cos\theta}. \tag{4.43}$$

The dimensionless thermal conductance (4.11) has distribution

$$P_\pm(g) = \frac{1}{\pi} \int_0^\pi d\theta\, \delta(g - \sin^2\theta) P_\pm(\theta)$$

$$= P_{\mathrm{ballistic}}(g) \frac{(1 \pm r_1 r_2)\sqrt{\Gamma_1 \Gamma_2}}{(1 \pm r_1 r_2)^2 - (1 - g)(r_1 \pm r_2)^2}, \tag{4.44}$$

where as before, P_+ applies to $\nu = 0$ and P_- to $\nu = 1$. The distribution

$$P_{\mathrm{ballistic}}(g) = \frac{1}{\pi\sqrt{g(1-g)}}, \;\; 0 < g < 1, \tag{4.45}$$

is the result [27] for ballistic coupling ($\Gamma_n = 1$, $r_n = 0$).

For identical tunnel barriers, $\Gamma_1 = \Gamma_2 = \Gamma$, this reduces to

$$P(g) = P_{\mathrm{ballistic}}(g) \times \begin{cases} \frac{\Gamma(2-\Gamma)}{\Gamma^2 + 4g(1-\Gamma)} & \text{if } \nu = 0, \\ 1 & \text{if } \nu = 1. \end{cases} \tag{4.46}$$

Quite remarkably, the distribution of the thermal conductance for two identical single-mode point contacts is unaffected by the presence of a tunnel barrier in the topologically nontrivial case. Fig. 4.4 is a numerical check of this analytical result.

Notice that the distribution (4.11) becomes independent of ν if $r_1 r_2 = 0$. This is a special case of a more general result, valid for any N_1, N_2:

$$P_+(g) = P_-(g) \;\; \text{if} \;\; \mathrm{Det}\, r_{\mathrm{B}} = 0, \tag{4.47}$$

in words: The probability distribution of the thermal conductance becomes independent of the presence or absence of a Majorana bound state if the quantum dot is coupled ballistically to at least one of the scattering channels. In other words, *ballistic coupling to a propagating Majorana mode hides the Majorana bound state.*

The proof is straightforward: If $\Gamma_{n_0} = 1$ for one of the indices $n_0 \in \{1, 2, \ldots N\}$, then the Poisson kernel (4.27) is unchanged if we multiply $S \mapsto O_1 \Lambda O_1^{\mathrm{T}} S$, with $\Lambda_{nm} = \delta_{nm}(1 - 2\delta_{nn_0})$. [The orthogonal matrix O_1 is defined in Eq. (4.22).] The Haar measure remains unchanged as well, and so does the thermal conductance (4.11). Since $\mathrm{Det}\, S = -\mathrm{Det}\,(\Lambda S)$, so O_+ is mapped onto O_-, we conclude that $P_+(g) = P_-(g)$.
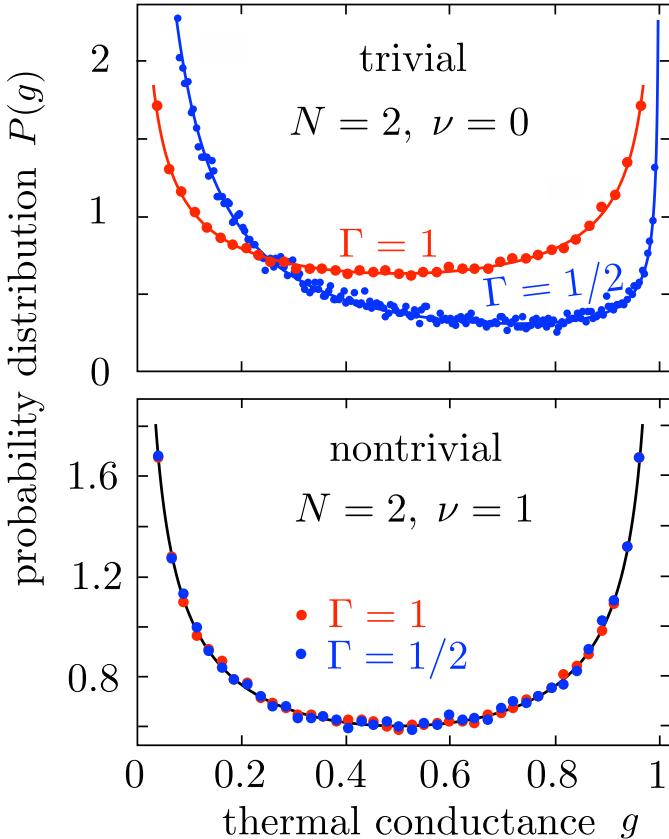
Figure 4.4: Probability distribution of the thermal conductance $g = G_{\mathrm{thermal}}/G_0$, see Eq. (4.11), for a chaotic scatterer having two single-mode point contacts with identical tunnel probabilities Γ. The data points are numerical results for a random Hamiltonian ($M = 46 + \nu$), the curves are the analytical result (4.46). In the presence of a Majorana zero-mode ($\nu = 1$) the distribution is independent of Γ.

This proof for the Poisson kernel extends to the entire joint distribution (4.24) of S and Q: The transformation $S \mapsto O_1 \Lambda O_1^{\mathrm{T}} S$ has no effect on the matrices Q and Σ, so $P(S, Q)$ remains unchanged. It follows that the probability distribution of the density of states is the same with or without a Majorana bound state if $\Gamma_n = 1$ for at least one of the scattering channels.

4.8 Electrical conductance

Because a Majorana mode is charge-neutral, no electrical current can be driven for $N_1 = N_2 = 1$. A nonzero current I is possible for $N_1 = 2$, when terminal 1 biased at voltage V has a distinct electron and hole mode. We investigate the effect of a tunnel barrier for $N_1 = 2$, $N_2 = 1$. In the Majorana basis the expression (4.12) for the Andreev conductance reads

$$g_A = \tfrac{1}{2} \operatorname{Tr} (1 - r\tau_y r^T \tau_y), \tag{4.48}$$

with r a 2×2 real matrix.

The scattering matrix $S_\pm \in O_\pm(3)$ can be conveniently parameterized using three Euler angles [46],

$$S_+ = \begin{pmatrix} R(\alpha) & 0 \\ 0 & 1 \end{pmatrix} \begin{pmatrix} 1 & 0 \\ 0 & R(\theta) \end{pmatrix} \begin{pmatrix} R(\alpha') & 0 \\ 0 & 1 \end{pmatrix},$$
$$S_- = \operatorname{diag}(1, 1, -1) S_+, \tag{4.49}$$

where we have defined

$$R(\alpha) = \begin{pmatrix} \cos\alpha & -\sin\alpha \\ \sin\alpha & \cos\alpha \end{pmatrix}. \tag{4.50}$$

The Haar measure on $O_\pm(3)$ is given by [23]

$$d\mu = \frac{\sin\theta}{8\pi^2} d\theta d\alpha d\alpha', \quad \alpha, \alpha' \in (0, 2\pi), \quad \theta \in (0, \pi). \tag{4.51}$$

Because $R(\alpha)$ commutes with τ_y, the dimensionless conductance (4.48) depends only on the Euler angle θ,

$$g_A = 1 - \cos\theta. \tag{4.52}$$

In point contact 1 we take a tunnel probability Γ_1, the same for the electron and hole mode, while in point contact 2 we have tunnel probability Γ_2 for the unpaired Majorana mode. Evaluation of the Poisson kernel (4.27) with $r_B = \operatorname{diag}(r_1, r_1, r_2)$ gives the conductance distribution

$$P_\pm(g_A) = \frac{\tfrac{1}{2}\Gamma_1^{1/2}\Gamma_2[(\Gamma_1 - 2)(\pm r_2 - 1) + (\pm r_2 - 1 + \Gamma_1)g_A]}{[(1 \pm r_2(g_A - 1))^2 - (g_A - 1 \pm r_2)^2(1 - \Gamma_1)]^{3/2}},$$
$$0 < g_A < 2, \quad r_2 = \sqrt{1 - \Gamma_2}, \tag{4.53}$$

plotted in Fig. 4.5 for $\nu = 0$ (P_+), $\nu = 1$ (P_-) and two values of $\Gamma_1 = \Gamma_2 \equiv \Gamma$.
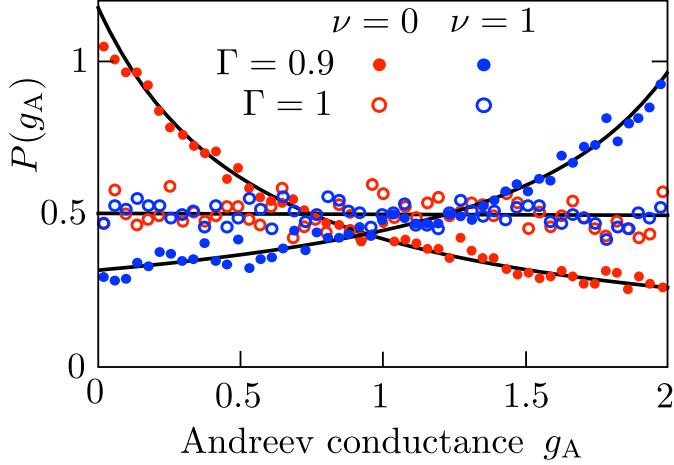
Figure 4.5: Probability distribution of the Andreev conductance g_A, see Eq. (4.12), for $N_1 = 2$, $N_2 = 1$, $\Gamma_1 = \Gamma_2 \equiv \Gamma$. The data points are numerical results for a random Hamiltonian ($M = 46 + \nu$), the curves are the analytical result (4.53). For ballistic coupling ($\Gamma = 1$) the distribution is the same with or without a Majorana bound state. In the limit $\Gamma \to 0$ the distribution becomes sharply peaked at $g_A = 2\nu$.

In the limit $r_2 \to 1$, when terminal 2 is decoupled from the quantum dot, we recover the result [47]

$$P(g_A) = \begin{cases} \delta(g_A) & \text{if } \nu = 0, \\ \delta(2 - g_A) & \text{if } \nu = 1, \end{cases} \qquad (4.54)$$

independent of Γ_1. The conductance in this case is uniquely determined by the topological quantum number.

In the opposite limit $r_2 \to 0$ the distribution (4.53) becomes independent of ν,

$$P(g_A) = \frac{\frac{1}{2}\Gamma_1^{1/2}[2 - \Gamma_1 - (1 - \Gamma_1)g_A]}{[1 - (1 - \Gamma_1)(g_A - 1)^2]^{3/2}}, \quad \text{if } r_2 = 0. \qquad (4.55)$$

This is a special case of a more general result, for any N_1, N_2,

$$P_+(g_A) = P_-(g_A) \text{ if } \text{Det}\,\mathcal{P}_2 r_B = 0, \qquad (4.56)$$

where $\mathcal{P}_2$ projects onto the modes coupled to terminal 2. Ballistic coupling, even for a single mode, to terminal 2 therefore removes the dependence on the topological quantum number.

The proof of Eq. (4.56) proceeds along the lines of the proof of Eq. (4.47), with the difference that the transformation $S \mapsto O_1 \Lambda O_1^{\mathrm{T}} S$ should
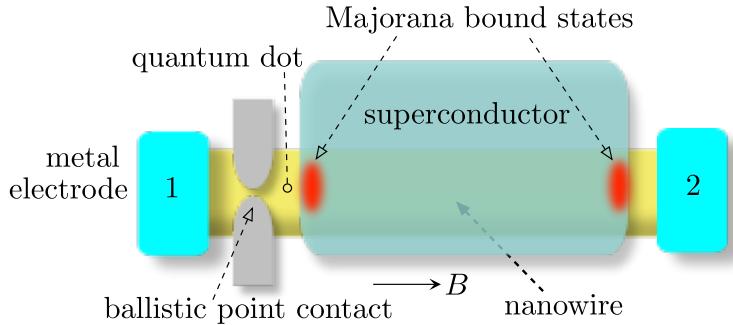
Figure 4.6: Device to study the topological phase transition in a semiconductor nanowire covered by a superconductor. When the Zeeman energy of a parallel magnetic field exceeds the induced superconducting gap in the nanowire, a pair of Majorana bound states emerges at the end points. One of these is coupled directly to electrode 2, while the other is coupled to electrode 1 via a point contact.

leave the upper-left block r of S unaffected — otherwise the Andreev conductance (4.48) would change. This also explains why the ν-dependence of $P(g_{\mathrm{A}})$ remains for ballistic coupling to terminal 1 [28].

4.9 Majorana phase transition

The appearance of a Majorana bound state is a topological phase transition. There is a search for this transition in a nanowire geometry, see Fig. 4.6, where it has been predicted to occur when the Zeeman energy of a magnetic field (parallel to the wire axis) exceeds the gap induced by the proximity to a superconductor [48,49].

Because the Majorana bound states emerge pairwise at the two ends of the nanowire, the topological quantum number ν of the entire structure remains 0 and the determinant $\mathrm{Det}\, S$ of the full scattering matrix remains $+1$ through the transition. What changes is the sign of the determinant $\mathrm{Det}\, r$ of the reflection submatrix. At the topological phase transition $\mathrm{Det}\, r = 0$, implying a perfectly transmitted mode and a quantized peak in the thermal conductance [33].

We study the effect of the phase transition on the statistics of the electrical conductance, measured by contacting one end of the nanowire (terminal 1) to a metal electrode at voltage V, while the superconductor and the other end of the nanowire (terminal 2) are at ground. Terminal 1 is connected to the nanowire via a point contact, thus creating a confined region (quantum dot) with chaotic scattering. The minimal dimensionality of the scattering matrix S of the quantum dot is 3×3: One electron and one hole mode connected to terminal 1 and one Majorana

mode connected to terminal 2.

To minimize the number of free parameters we assume ballistic coupling through the point contact, so the matrix r_B in the Poisson kernel (4.27) is $r_B = \text{diag}\,(1, 1, r_2)$. The reflection amplitude r_2 at terminal 2 is tuned through zero by some external control parameter ξ, typically magnetic field or gate voltage. Near the transition (conveniently shifted to $\xi \equiv 0$) this dependence can be conveniently parameterized by [33]

$$r_2(\xi) = \tanh(\xi/\xi_0). \tag{4.57}$$

(The width ξ_0 of the transition is system dependent.) The corresponding coupling constant κ_2 in Eq. (4.5) then has an exponential ξ-dependence,

$$\kappa_2 = \frac{1 - r_2}{1 + r_2} = \exp(-2\xi/\xi_0). \tag{4.58}$$

The probability distribution of the Andreev conductance (in units of e^2/h) follows from Eq. (4.53),

$$\begin{aligned}
P(g_A) &= \tfrac{1}{2}(1 - r_2^2)[1 + (g_A - 1)r_2]^{-2} \\
&= \tfrac{1}{2}[\cosh(\xi/\xi_0) + (g_A - 1)\sinh(\xi/\xi_0)]^{-2}, \\
& \qquad\qquad 0 < g_A < 2.
\end{aligned} \tag{4.59}$$

The delta-function limits (4.54) are reached for $\xi \to \pm\infty$ (keeping $\nu = 0$, because the entire system is topologically trivial). Right at the transition, at $\xi = 0$, the distribution is uniform in the interval $0 < g_A < 2$. The average conductance varies through the transition as

$$\langle g_A \rangle = 1 - \frac{1}{\tanh(\xi/\xi_0)} + \frac{\xi/\xi_0}{\sinh^2(\xi/\xi_0)}, \tag{4.60}$$

see Fig. 4.7.

4.10 Conclusion

In conclusion, we have investigated a variety of observable consequences of the fact that the scattering matrix of Majorana fermions is real orthogonal rather than complex unitary. Of particular interest is the identification of observables that can detect the sign of the determinant, since $\text{Det}\,S = -1$ signifies the presence of a Majorana bound state. The obvious signal of such a zero-mode, a midgap peak in the density of states [42,43], is broadened by tunnel coupling to the continuum. We find that the peak remains hidden if the coupling is ballistic (unit transmission) in even a single scattering channel. The thermal conductance is likewise insensitive

Figure 4.7: Variation of the ensemble-averaged Andreev conductance in the geometry of Fig. 4.6, as the nanowire is driven through a topological phase transition (controlled by a parameter ξ, which can be thought of as the deviation of the magnetic field from the critical field strength). The curve is the result (4.60) for a single-channel ballistic point contact.

to the presence or absence of a Majorana bound state, but the electrical conductance retains this sensitivity when the coupling is ballistic.

These results for the effect of a tunnel barrier on the midgap spectral peak are derived from the distribution $P(S, Q)$ of scattering matrix and time-delay matrix under the assumption of chaotic scattering, due to disorder or due to irregularly shaped boundaries. The appropriate ensemble in the absence of time-reversal and spin-rotation symmetry has symmetry class D in the Altland-Zirnbauer classification[1]. Chiral symmetry would change this to class BDI, in which multiple zero-modes can overlap without splitting[32]. The effect of chiral symmetry on the joint distribution $P(S, Q)$ is known for ballistic coupling[24] — but not yet for tunnel coupling. This seems a worthwhile project for future research.

4.11 Appendix A. Joint distribution of scattering matrix and time-delay matrix

We calculate the joint distribution $P(S, Q)$ of scattering matrix and time-delay matrix in the presence of a tunnel barrier, starting from the known distribution $P(S_0, Q_0)$ without a barrier[22,23]. The application in the main text concerns symmetry class D, but for the sake of generality and for later reference we give results for all four Altland-Zirnbauer[1]

	Altland-Zirnbauer				Wigner-Dyson		
	D	**DIII**	**C**	**CI**	**A**	**AI**	**AII**
α	-1	-1	2	1	0	0	0
β	1	2	4	2	2	1	4
t_0/τ_{H}	1	1	$\frac{1}{2}$	$\frac{1}{2}$	1	1	1
degeneracy d	1	2	2	2	1	1	2

Table 4.1: Parameters that appear in the distribution of the scattering matrix and time-delay matrix, for each of the Altland-Zirnbauer and Wigner-Dyson symmetry classes. Notice that a different set of indices α', β' govern the energy level statistics [11]. The degeneracy factor d refers to the Kramers degeneracy of the scattering channels and the delay times, ignoring uncoupled spin bands. (The energy levels may have a different degeneracy.)

symmetry classes D, DIII, C, CI, as well as for the three Wigner-Dyson [7,50] symmetry classes A, AI, AII. The symmetry indices that distinguish the ensembles are listed in Table 4.1, see Ref. 11 for an overview of this classification.

The unitary matrix S and the Hermitian matrix Q are real in class D, complex in class A, and quaternion in class C. We consider these three symmetry classes without time-reversal symmetry first, and then include the constraints of time-reversal symmetry in classes DIII, CI, AI, AII.[*]

4.11.1 Broken time-reversal symmetry

Without the barrier S_0 is independent of Q_0 and uniformly distributed,

$$P(S_0, Q_0)d\mu(S_0)d\mu(Q_0) = P(Q_0)d\mu(S_0)d\mu(Q_0). \qquad (4.61)$$

The differential $d\mu$ indicates the Haar measure for the unitary matrix S_0 and the Euclidean measure for the Hermitian matrix Q_0. The ballistic time-delay matrix distribution is given by [22,23]

$$P(Q_0^{-1}) \propto (\mathrm{Det}' \, Q_0^{-1})^{\alpha + N\beta/2}$$
$$\times \Theta(Q_0) \exp(-\tfrac{1}{2}\beta t_0 \, \mathrm{Tr}' \, Q_0^{-1}), \qquad (4.62\mathrm{a})$$
$$\Leftrightarrow P(Q_0) \propto (\mathrm{Det}' \, Q_0)^{-\beta(N-1)-2-\alpha-N\beta/2}$$
$$\times \Theta(Q_0) \exp(-\tfrac{1}{2}\beta t_0 \, \mathrm{Tr}' \, Q_0^{-1}). \qquad (4.62\mathrm{b})$$

Degenerate eigenvalues of Q_0 are counted only once in Tr' and Det'. In terms of the degeneracy factor d from Table 4.1 this can be written as

$$\mathrm{Det}' \, Q_0 = (\mathrm{Det} \, Q_0)^{1/d}, \quad \mathrm{Tr}' \, Q_0 = \frac{1}{d} \, \mathrm{Tr} \, Q_0. \qquad (4.63)$$

---

[*]The seven symmetry classes in Table 4.1 do not exhaust the tenfold way classification of random-matrix theory: There are three more chiral classes [51] (labeled AIII, BDI, CII) that require separate consideration [24].

	D	**C**	**A**	**AI**	**CI**	**AII**	**DIII**
	broken time-reversal symmetry			preserved time-reversal symmetry			
	$\delta S \equiv S^\dagger dS = -\delta S^\dagger$			$\delta S \equiv \tilde{U}^\dagger dSU^\dagger = -\delta S^\dagger = \delta \tilde{S}$			
				$\tilde{U} \equiv U^{\mathrm{T}}$		$\tilde{U} \equiv U^{\mathrm{D}} \equiv \sigma_y U^{\mathrm{T}} \sigma_y$	
δS_{nm}	q_0	$q_0 \sigma_0 + i\boldsymbol{q} \cdot \boldsymbol{\sigma}$	$a + ib$	ia	$ia\sigma_x + ib\sigma_z$	$iq_0\sigma_0 + \boldsymbol{q} \cdot \boldsymbol{\sigma}$	$a\sigma_x + b\sigma_z$
$(n \neq m)$	$\beta = 1$	$\beta = 4$	$\beta = 2$	$\beta = 1$	$\beta = 2$	$\beta = 4$	$\beta = 2$
δS_{nn}	0	$i\boldsymbol{q} \cdot \boldsymbol{\sigma}$	ib	ia	$ia\sigma_x + ib\tau_z$	$iq_0\sigma_0$	0
	$\alpha + 1 = 0$	$\alpha + 1 = 3$	$\alpha + 1 = 1$	$\alpha + 1 = 1$	$\alpha + 1 = 2$	$\alpha + 1 = 1$	$\alpha + 1 = 0$
	$Q \equiv -i\hbar S^\dagger dS/dE = Q^\dagger$			$Q \equiv -i\hbar \tilde{U}^\dagger (dS/dE) U^\dagger = Q^\dagger = \tilde{Q}$			
Q_{nm}	q_0	$q_0 \sigma_0 + i\boldsymbol{q} \cdot \boldsymbol{\sigma}$	$a + ib$	a	$a\sigma_0 + ib\sigma_y$	$q_0 \sigma_0 + i\boldsymbol{q} \cdot \boldsymbol{\sigma}$	$a\sigma_0 + ib\sigma_y$
Q_{nn}	q_0	$q_0 \sigma_0$	a	a	$a\sigma_0$	$q_0 \sigma_0$	$a\sigma_0$

Table 4.2: Characterization of the scattering matrix differential δS and of the time-delay matrix Q. All coefficients q_n, a, b are real, and σ_i is a Pauli matrix. The symmetry indices β and $\alpha + 1$ count, respectively, the number of degrees of freedom of the off-diagonal and diagonal components of the anti-Hermitian matrix δS. The off-diagonal elements of the Hermitian matrix Q have β degrees of freedom, while the diagonal elements have one single degree of freedom in each symmetry class.

The channel number N also does not include degeneracies, so the total number of eigenvalues of Q_0 is $d \times N$. The characteristic time t_0 differs from the Heisenberg time t_{H} by a numerical coefficient,* see Table 4.1.

Insertion of the barrier, with unitary scattering matrix

$$S_{\mathrm{B}} = \begin{pmatrix} r_{\mathrm{B}} & t'_{\mathrm{B}} \\ t_{\mathrm{B}} & r'_{\mathrm{B}} \end{pmatrix}, \tag{4.64}$$

transforms S_0 into

$$\begin{aligned} S &= r_{\mathrm{B}} + t'_{\mathrm{B}} S_0 (1 - r'_{\mathrm{B}} S_0)^{-1} t_{\mathrm{B}} \\ \Leftrightarrow S_0 &= {t'_{\mathrm{B}}}^{-1} S (1 - S^\dagger r_{\mathrm{B}})(1 - r_{\mathrm{B}}^\dagger S)^{-1} t_{\mathrm{B}}^\dagger. \end{aligned} \tag{4.65}$$

Variations of S and S_0 are related by [9]

$$S^\dagger dS = \Sigma(S_0^\dagger dS_0)\Sigma^\dagger, \quad \Sigma = (1 - S^\dagger r_{\mathrm{B}}) t_{\mathrm{B}}^{-1}. \tag{4.66}$$

The differentials

$$\delta S = S^\dagger dS, \quad \delta S_0 = S_0^\dagger dS_0, \tag{4.67}$$

are anti-Hermitian matrices, $\delta S^\dagger = -\delta S$. The number of degrees of freedom of the off-diagonal elements are given by β and the number of

---

*We define $t_{\mathrm{H}} = 2\pi\hbar/\delta_0$, with δ_0 the mean spacing of *nondegenerate* levels. The ratio t_0/t_{H} then equals the degeneracy of energy levels divided by the degeneracy of delay times [23]. It is unity in all symmetry classes except C and CI, where the delay times have a Kramers degeneracy that the energy levels lack [11].

degrees of freedom of the diagonal elements by $1 + \alpha$. As summarized in Table 4.2, real matrices (class D) have $\alpha = -1$, $\beta = 1$, complex matrices (class A) have $\alpha = 0$, $\beta = 2$, and quaternion matrices (class C) have $\alpha = 2$, $\beta = 4$. These parameters determine the Jacobian [44]

$$
\begin{aligned}
J_S = \frac{d\mu(S)}{d\mu(S_0)} &= \left\| \left| \frac{\Sigma \delta S_0 \Sigma^\dagger}{\delta S_0} \right| \right\| \\
&= (\text{Det}' \, \Sigma\Sigma^\dagger)^{(N-1)\beta/2+1+\alpha}.
\end{aligned}
\tag{4.68}
$$

Eq. (4.66) also implies the relation between the time-delay matrices,

$$
Q = \Sigma Q_0 \Sigma^\dagger \Rightarrow dQ = \Sigma dQ_0 \Sigma^\dagger + \mathcal{O}(dS).
\tag{4.69}
$$

The off-diagonal elements of the Hermitian matrix Q have β degrees of freedom, the diagonal elements have one single degree of freedom in each symmetry class. The Jacobian is then given by

$$
\begin{aligned}
J_Q = \frac{d\mu(Q)}{d\mu(Q_0)} &= \left\| \left| \frac{\Sigma dQ_0 \Sigma^\dagger}{dQ_0} \right| \right\| \\
&= (\text{Det}' \, \Sigma\Sigma^\dagger)^{(N-1)\beta/2+1}.
\end{aligned}
\tag{4.70}
$$

The joint probability distribution $P(S, Q)$ now follows upon division of $P(S_0, Q_0)$ by the product of Jacobians,

$$
\begin{aligned}
P(S, Q) &= \frac{P(Q_0)}{J_S J_Q} \\
&= P(Q_0)(\text{Det}' \, \Sigma\Sigma^\dagger)^{-\beta N + \beta - 2 - \alpha}.
\end{aligned}
\tag{4.71}
$$

Substituting $Q_0 = \Sigma^{-1} Q {\Sigma^\dagger}^{-1}$ into Eq. (4.62) we thus arrive at the joint distribution

$$
\begin{aligned}
P(S, Q) \propto\ & (\text{Det}' \, \Sigma\Sigma^\dagger)^{\beta N/2}(\text{Det}' \, Q)^{-3\beta N/2+\beta-2-\alpha} \\
& \times \Theta(Q) \exp(-\tfrac{1}{2}\beta t_0 \, \text{Tr}' \, \Sigma^\dagger Q^{-1}\Sigma).
\end{aligned}
\tag{4.72}
$$

The class-D result (4.24) from the main text follows for $\alpha = -1$, $\beta = 1$, $t_0 = \tau_\text{H}$, $d = 1$, $\Sigma^\dagger = \Sigma^\text{T}$.

4.11.2 Preserved time-reversal symmetry

Time-reversal symmetry equates the scattering matrix to its transpose S^T in class AI and CI and to its dual S^D in class AII and DIII. (The dual of a matrix is $S^\text{D} = \sigma_y S^\text{T} \sigma_y$.) We use a unified notation $S = \tilde{S}$, where the tilde indicates the transpose or the dual, whichever is appropriate for

that symmetry class. The symmetry $S = \tilde{S}$ allows for the "square root" factorization

$$S = \tilde{U}U = \tilde{S}, \tag{4.73}$$

with unitary U.

The time-delay matrix in these symmetry classes is constructed such that it satisfies the same symmetry,

$$Q = -i\hbar \lim_{E \to 0} \tilde{U}^\dagger \frac{dS}{dE} U^\dagger = \tilde{Q}. \tag{4.74}$$

This redefinition of Q differs from Eq. (4.8) by a unitary transformation, so the delay times are not affected.

The ballistic Q_0 and S_0 are again independent[22,23], distributed according to Eqs. (4.61) and (4.62) with the appropriate values of α and β from Table 4.1. These numbers now count the diagonal and off-diagonal degrees of freedom of the symmetrized differential

$$\delta S = \tilde{U}^\dagger dSU^\dagger, \tag{4.75}$$

constrained by $\delta S = -\delta S^\dagger$, $\delta \tilde{S} = \delta S$. The matrix elements of δS are imaginary in class AI ($\alpha = 0$, $\beta = 1$), i times a quaternion[*] in class AII ($\alpha = 0$, $\beta = 4$), and of the form $a\sigma_x + b\sigma_z$ with a, b imaginary in class CI ($\alpha = 1$, $\beta = 2$) and a, b real in class DIII ($\alpha = -1$, $\beta = 2$).

The elements of the Hermitian matrix Q are real in class AI, quaternion in class AII, and of the form $a\sigma_0 + ib\sigma_y$ with a, b real in both classes CI and DIII. The off-diagonal elements of Q have the same number of β degrees of freedom as δS, but the diagonal elements have only a single degree of freedom irrespective of α. All of this is summarized in Table 4.2.

The symmetrization of the differential modifies the relation (4.66), which now reads

$$\delta S = U\Sigma U_0^\dagger \delta S_0 U_0 \Sigma^\dagger U^\dagger, \quad \Sigma = (1 - U^\dagger \tilde{U}^\dagger r_{\rm B}) t_{\rm B}^{-1}. \tag{4.76}$$

The relation (4.69) between Q and Q_0 is similarly modified by the symmetrization,

$$Q = U\Sigma U_0^\dagger Q_0 U_0 \Sigma^\dagger U^\dagger. \tag{4.77}$$

Because the matrices U, U_0 are unitary, the Jacobians (4.68) and (4.70) are unchanged,

$$J_S = (\mathrm{Det}'\, \Sigma\Sigma^\dagger)^{(N-1)\beta/2+1+\alpha}, \tag{4.78}$$

$$J_Q = (\mathrm{Det}'\, \Sigma\Sigma^\dagger)^{(N-1)\beta/2+1}. \tag{4.79}$$

---

[*]A quaternion has the form $a_0\sigma_0 + ia_1\sigma_x + ia_2\sigma_y + ia_3\sigma_z$, with four real coefficiients a_n. The matrix σ_0 is the 2×2 unit matrix.

We thus obtain the joint distribution

$$P(S,Q) \propto (\mathrm{Det}' \, \Sigma\Sigma^\dagger)^{\beta N/2} (\mathrm{Det}' \, Q)^{-3\beta N/2+\beta-2-\alpha}$$
$$\times \, \Theta(Q) \exp(-\tfrac{1}{2}\beta t_0 \, \mathrm{Tr}' \, \Sigma^\dagger U^\dagger Q^{-1} U \Sigma). \qquad (4.80)$$

4.11.3 Poisson kernel

The marginal distribution of the scattering matrix resulting from the Jacobians (4.68) and (4.78) is

$$P(S) = \int dQ \, P(S,Q) = 1/J_S$$
$$= (\mathrm{Det}' \, \Sigma\Sigma^\dagger)^{-(N-1)\beta/2-1-\alpha}$$
$$= \left(\frac{\mathrm{Det}'(1 - r_{\mathrm{B}}^\dagger r_{\mathrm{B}})}{|\mathrm{Det}'\,(1 - r_{\mathrm{B}}^\dagger S)|^2} \right)^{(N-1)\beta/2+1+\alpha}, \qquad (4.81)$$

including the normalization constant. This formula combines the known expressions for the Poisson kernel* in the Wigner-Dyson ensembles [15] and in the Altland-Zirnbauer ensembles [16].

The present analysis confirms that Eq. (4.81) holds without modification in the two symmetry classes D and DIII that support Majorana zero-modes, depending on the sign of the determinant $\mathrm{Det}\,S = \pm 1$ in class D and the sign of the Pfaffian $\mathrm{Pf}\,(i\sigma_y S) = \pm 1$ in class DIII [52]. As a check, we can take $N = 1$, when $S = \pm 1$ in class D and $S = \pm\sigma_0$ in class DIII. The $\pm$ sign determines the presence or absence of a Majorana bound state (twofold degenerate in class DIII). Since there is only a single element in the ensemble we should have $P(S) = 1$, which is indeed what Eq. (4.81) gives for $N = 1$, $\alpha = -1$.

4.12 Appendix B. Calculation of the ensemble-averaged scattering matrix

4.12.1 Symmetry class D

According to Eq. (4.37), the effect of a tunnel barrier on the average density of states follows directly once we know the average scattering matrix. Simple expressions can be obtained if we assume that the tunnel probabilities are mode-independent, $\Gamma_n = \Gamma$ for $n = 1, 2, \ldots N$.

---

*The name "Poisson kernel" applies strictly speaking only to the Wigner-Dyson ensembles, when $r_{\mathrm{B}} = \int SP(S)dS$. In the Altland-Zirnbauer ensembles the average scattering matrix differs from r_{B}, see Ref. 16 and App. 4.12.

4.12 Appendix B. Calculation of the ensemble-averaged scattering matrix

The scattering matrix of the barrier has the polar decomposition

$$S_{\mathrm{B}} = \begin{pmatrix} O_1 & 0 \\ 0 & O_3 \end{pmatrix} \begin{pmatrix} \sqrt{1-\Gamma} & \sqrt{\Gamma} \\ \sqrt{\Gamma} & -\sqrt{1-\Gamma} \end{pmatrix} \begin{pmatrix} O_2 & 0 \\ 0 & O_4 \end{pmatrix}, \qquad (4.82)$$

with $O_1, O_2, O_3, O_4 \in \mathrm{SO}(N)$. The block structure corresponds to Eqs. (4.22) and (4.64), in particular, $r_{\mathrm{B}} = \sqrt{1-\Gamma}\, O_1 O_2$. From Eq. (4.65) we obtain the scattering matrix S of the quantum dot,

$$S = O_1 \left[\sqrt{1-\Gamma} + \Gamma U (1 + \sqrt{1-\Gamma}\, U)^{-1} \right] O_2, \qquad (4.83)$$

in terms of a matrix $U = O_4 S_0 O_3$ that is uniformly distributed in $\mathrm{O}_{\pm}(N)$.

Because the average of U^p for any power $p = 1, 2, \dots$ is proportional to the identity matrix, we may write the average of S in the form of a power series,

$$\langle S \rangle_{\pm} = r_{\mathrm{B}} \left(1 - \frac{\Gamma}{1-\Gamma} \sum_{p=1}^{\infty} (-1)^p (1-\Gamma)^{p/2} \frac{1}{N} \langle \mathrm{Tr}\, U^p \rangle_{\pm} \right). \qquad (4.84)$$

If the average of U would be over the entire unitary group, then all terms in the power series would vanish and we would simply have $\langle S \rangle = r_{\mathrm{B}}$. But averages over orthogonal matrices do not vanish, in the nontrivial way calculated* by Rains[53]:

$$\langle \mathrm{Tr}\, U^p \rangle_{\pm} = \frac{1 + (-1)^p}{2} \pm \begin{cases} (-1)^{N+1} & \text{if } p - N = 0, 2, 4, \dots \\ 0 & \text{otherwise.} \end{cases} \qquad (4.85)$$

We substitute Eq. (4.85) into Eq. (4.84) and sum the geometric series, to arrive at the average scattering matrix

$$\langle S \rangle_{\pm} = r_{\mathrm{B}} \left(1 - \frac{1}{N} \pm \frac{1}{N} (1-\Gamma)^{-1+N/2} \right), \qquad (4.86)$$

used in Sec. 4.6 to obtain the average density of states in class D.

---

*For the record, we note that Eq. (4.85) differs from the formula in Ref. 53 by a minus sign ($\pm$ instead of $\mp$).

4.12.2 Symmetry class C

In a similar way we can derive the average scattering matrix in other symmetry classes. We give the result for class C. The matrix U then varies over the unitary symplectic group $\mathrm{Sp}(2N)$. Ref. 53 gives the required average:

$$\langle \mathrm{Tr}\, U^p \rangle_{\mathrm{C}} = \begin{cases} -1 & \text{if } p \leq 2N \text{ and even,} \\ 0 & \text{otherwise.} \end{cases} \tag{4.87}$$

Eq. (4.84) still holds with the factor $1/N$ replaced by $1/2N$. We thus find the average scattering matrix in class C,

$$\langle S \rangle_{\mathrm{C}} = r_{\mathrm{B}} \left(1 + \frac{1}{2N}[1 - (1-\Gamma)^N] \right). \tag{4.88}$$

For $N = 1$ this gives $\langle S \rangle_{\mathrm{C}} = (1 + \Gamma/2)r_{\mathrm{B}}$, in agreement with Ref. 16.

The average density of states in class C follows from Eq. (4.3), where we again account for the doubling of the dimensionality $N \mapsto 2N$:

$$\langle \rho \rangle_{\mathrm{C}} = \langle \rho \rangle_{\text{ballistic}} \left(1 - \frac{1}{N\Gamma} \mathrm{Tr}\, r_{\mathrm{B}}^\dagger [\langle S \rangle_{\mathrm{C}} - r_{\mathrm{B}}] \right)$$

$$= \frac{N}{(N+1)\delta_0} \left(1 - \frac{1-\Gamma}{N\Gamma}[1 - (1-\Gamma)^N] \right). \tag{4.89}$$

In the second equation we have substituted the ballistic class-C result from Ref. 23. The tunneling limit $\Gamma \to 0$ gives a vanishing density of states,

$$\langle \rho \rangle_{\mathrm{C}} = \frac{N\Gamma}{(N+1)\delta_0} + \mathcal{O}(\Gamma^2), \tag{4.90}$$

consistent with the class-C result for a closed system[42,43].

Bibliography of chapter 4

[1] A. Altland and M. R. Zirnbauer, Phys. Rev. B **55**, 1142 (1997).

[2] J. Alicea, Rep. Progr. Phys. **75**, 076501 (2012).

[3] M. Leijnse and K. Flensberg, Semicond. Sci. Technol. **27**, 124003 (2012).

[4] T. D. Stanescu and S. Tewari, J. Phys. Cond. Matt. **25**, 233201 (2013).

[5] C. W. J. Beenakker, Annu. Rev. Con. Mat. Phys. **4**, 113 (2013).

[6] S. Das Sarma, M. Freedman, and C. Nayak, NPJ Quantum Inf. **1**, 15001 (2015).

[7] E. P. Wigner, SIAM Review **9**, 1 (1967).

[8] M. L. Mehta, *Random Matrices* (Elsevier, Amsterdam, 2004).

[9] P. J. Forrester, *Log-Gases and Random Matrices* (Princeton University Press, 2010).

[10] F. J. Dyson, J. Math. Phys. **3**, 140 (1962).

[11] C. W. J. Beenakker, Rev.Mod.Phys. **87**, 1037 (2015).

[12] T. J. Krieger, Ann. Phys. **42**, 375 (1967).

[13] P. A. Mello, P. Pereyra and T. Seligman, Ann. Phys. **161**, 254 (1985).

[14] W. A. Friedman and P. A. Mello, Ann. Phys. **161**, 276 (1985).

[15] P. W. Brouwer, Phys. Rev. B **51**, 16878 (1995).

[16] B. Béri, Phys. Rev. B **79**, 214506 (2009).

[17] V. A. Gopar, P. A. Mello, and M. Büttiker, Phys. Rev. Lett. **77**, 4974 (1996).

[18] P. W. Brouwer and M. Büttiker, Europhys. Lett. **37**, 441 (1997).

Bibliography of chapter 4

[19] M. Büttiker, in *Time in Quantum Mechanics*, edited by J. G. Muga, R. Sala Mayato, and I. L. Egusquiza (Springer, Berlin, 2002).

[20] P. W. Brouwer, S. A. van Langen, K. M. Frahm, M. Büttiker, and C. W. J. Beenakker, Phys. Rev. Lett. **79**, 913 (1997).

[21] S. F. Godijn, S. Möller, H. Buhmann, L. W. Molenkamp, and S. A. van Langen, Phys. Rev. Lett. **82**, 2927 (1999).

[22] P. W. Brouwer, K. M. Frahm, and C. W. J. Beenakker, Phys. Rev. Lett. 78, 4737 (1997).

[23] M. Marciani, P. W. Brouwer, and C. W. J. Beenakker, Phys. Rev. B **90**, 045403 (2014).

[24] H. Schomerus, M. Marciani, and C. W. J. Beenakker, Phys. Rev. Lett. **114**, 166803 (2015).

[25] D. V. Savin, Y. V. Fyodorov, and H.-J. Sommers, Phys. Rev. E **63**, 035202 (2001).

[26] H.-J. Sommers, D. V. Savin, and V. V. Sokolov, Phys. Rev. Lett. **87**, 094101 (2001).

[27] J. P. Dahlhaus, B. Béri, and C. W. J. Beenakker, Phys. Rev. B **82**, 014536 (2010).

[28] C. W. J. Beenakker, J. P. Dahlhaus, M. Wimmer, and A. R. Akhmerov, Phys. Rev. B **83**, 085413 (2011).

[29] C. Mahaux and H. A. Weidenmüller, Phys. Rev. **170**, 847 (1968); *Shell-model Approach to Nuclear Reactions* (North-Holland, Amsterdam, 1969).

[30] L. Fu and C. L. Kane, Phys. Rev. Lett. **100**, 096407 (2008).

[31] M. Titov, A. Ossipov, and C. W. J. Beenakker, Phys. Rev. B **75**, 045417 (2007).

[32] J. J. M. Verbaarschot, H. A. Weidenmüller, and M. R. Zirnbauer, Phys. Rep. **129**, 367 (1985).

[33] A. R. Akhmerov, J. P. Dahlhaus, F. Hassler, M. Wimmer, and C. W. J. Beenakker, Phys. Rev. Lett. **106**, 057001 (2011).

[34] E. P. Wigner, Phys. Rev. **98**, 145 (1955).

[35] F. T. Smith, Phys. Rev. **118**, 349 (1960).

[36] Y. V. Fyodorov and H.-J. Sommers, J. Math. Phys. **38**, 1918 (1997).

[37] M. Sh. Birman and M. G. Krein, Soviet Math. Dokl. **3**, 740 (1962).

[38] E. Akkermans, A. Auerbach, J. E. Avron, and B. Shapiro, Phys. Rev. Lett. **66**, 76 (1991).

[39] N. Lehmann, D. V. Savin, V. V. Sokolov, and H.-J. Sommers, Physica D **86**, 572 (1995).

[40] A. F. Andreev, Sov. Phys. JETP **19**, 1228 (1964).

[41] K. Schwab, E. A. Henriksen, J. M. Worlock, and M. L. Roukes, Nature **404**, 974 (2000).

[42] M. Bocquet, D. Serban, and M. R. Zirnbauer, Nucl. Phys. B **578**, 628 (2000).

[43] D. A. Ivanov, J. Math. Phys. **43**, 126 (2002); arXiv:cond-mat/0103089.

[44] A. M. Mathai, *Jacobians of Matrix Transformations and Functions of Matrix Argument* (World Scientific Publishing, 1997).

[45] D. Bagrets and A. Altland, Phys. Rev. Lett. **109**, 227005 (2012).

[46] J. Li, G. Fleury, and M. Büttiker, Phys. Rev. B **85**, 125440 (2012).

[47] B. Béri, Phys. Rev. B **79**, 245315 (2009).

[48] R. M. Lutchyn, J. D. Sau, and S. Das Sarma, Phys. Rev. Lett. **105**, 077001 (2010).

[49] Y. Oreg, G. Refael, and F. von Oppen, Phys. Rev. Lett. 105, 177002 (2010).

[50] F. J. Dyson, J. Math. Phys. **3**, 1199 (1962).

[51] J. J. M. Verbaarschot and T. Wettig, Ann. Rev. Nucl. Part. Sci. **50**, 343 (2000).

[52] I. C. Fulga, F. Hassler, A. R. Akhmerov, and C. W. J. Beenakker, Phys. Rev. B **83**, 155429 (2011).

[53] E. M. Rains, Probab. Theory Relat. Fields **107**, 219 (1997).

5 General scheme for stable single and multiatom nanomagnets according to symmetry selection rules

5.1 Introduction

In recent years, great effort has been made to scale down the dimension of spintronic devices able to store classical bits of information. For this purpose, current research is devoted to understand the physics of single atoms and small clusters absorbed on non-magnetic metallic [1–4] or insulating [5–9] surfaces. The theoretical description of the dynamics of such systems is challenging as it lies at the intersection of classical [10–12] and quantum [13] mechanics.

The low temperature dynamics of suitable adatoms, without applied magnetic field, may be described by two degenerate low-energy states with opposite magnetization. These states can be naturally regarded as the bit constituents. Unfortunately, not all adatoms present this feature as it relies on specific environmental conditions like the hybridization mechanism with the surface and the symmetry of the crystal field produced by the substrate [14,15]. In particular, some systems exhibit no degenerate groundstate and the two lowest-energy states have no magnetization at all. This feature is referred to as groundstate splitting (GSS) and is due to the coupling of the orbital degree of freedom of the adatom with the crystal field.

To be suitable as memory storage [16], an engineered bit is required to retain its state over an extended time period [17]. Hyperfine interactions inside the adatom [18] and the contact with the substrate induce the atomic state to have an incoherent dynamics. In particular, the scattering of electrons and phonons off the adatom may be such that the stability of its state is affected drastically due to frequent switching between the groundstates.

With time the scientific community has started to recognize the role played by the symmetries of the system [3,17,19]. Their implications are
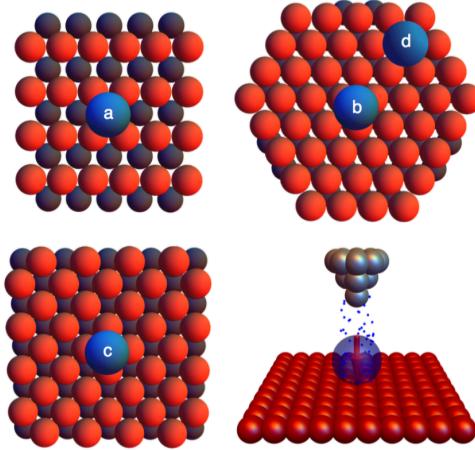
Figure 5.1: *(a)-(d)* Atoms deposited on different surfaces with $C_{\chi v}$ symmetry. $\chi = 2, 3, 4, 6$, respectively for the adatoms (a),(b),(c),(d). (*bottom right*) Sketch of a scanning tunneling microscope current measurement to infer the total momentum of the adatom. The tip of the microscope (in grey) exchanges electrons with the surface through the adatom.

extremely relevant not only in determining whether the two low-energy atomic states are magnetized but also in constraining their stochastic dynamics. In particular, first order processes mediated by the substrate electrons that make the adatom in one low-energy state to jump to another one - usually called single-electron (SE) switching processes - may be inhibited by symmetry selection rules[20]. However, symmetry information alone is not always sufficient. According to models currently in use[13,21], it must be contrasted with the magnitude of the effective total angular momentum of the adatom.

In this paper we present a general scheme to explain and predict exceptional long lifetimes of spin orientation in single and multi atomic systems. Hereby we provide a complete and rigorous map of such combinations of symmetries and total angular momentum magnitude, valid for small transversal crystal field. The symmetries we consider are the spatial point group $C_{\chi v}$ of the surface (see Fig. 5.1) and time-reversal. We consider the possibility that the time-reversal symmetry could be broken by a finite magnetic field perpendicular to the surface. Our findings are in agreement with existing experimental[3,9] results and previous numerical[19] and analytical[22] studies. With the restriction to time reversal symmetry a classification scheme[23] was presented, which is related to a non-trivial geometric phase. However, we noticed a difference in the prediction of stable systems in the common case of zero magnetic field.

Further, we generalize our findings to multiatom clusters where adatoms are coupled with each other via bipartite Heisenberg interactions. This extension creates also a link between our work and classical research on general properties of spin systems [24,25].

5.2 Single atom nanomagnet

5.2.1 Model

The Hamiltonian we consider can be decomposed as summation of parts related to the atom (A), to the electrons in the substrate (S) and their mutual interaction

$$H = H_A + H_S + H_t. \tag{5.1}$$

The atom is assumed to be described, at low temperature, by a magnetic moment of magnitude J. For instance, this is the case of some rare-earth atoms [26], whose strong internal spin-orbit coupling is such that only one multiplet of the total angular momentum plays a role in the low energy physics, and transition metal ions [27]. The atom, affected by the substrate crystal field and subject to an external magnetic field $\vec{B}$, can be described by the single-spin Hamiltonian

$$H_A = H_A^{(0)} + H_A^{(1)} + \vec{B} \cdot \vec{J}, \quad H_A^{(0)} = -|D|\, J_z^2 \tag{5.2}$$

where $H_A^{(0)}$ represents the so-called uniaxial (longitudinal) anisotropy (at second order) and $H_A^{(1)}$ contains higher order uniaxial and transversal anisotropy terms. The coefficient $|D|$ has been found as big as $1.5\,meV$ in Fe deposited on CuN [28] and $0.1\,meV$ in Fe deposited on Cu(111) [4]. In the rest of the paper we will refer to J as a spin degree of freedom for brevity; however, the reader must intend that we mean total angular momentum. The substrate Hamiltonian is that of a single-band metallic Fermi liquid with no self-interactions:

$$H_S = \sum_{k,\sigma} \varepsilon_k \; c_{k,\sigma}^\dagger \, c_{k,\sigma}. \tag{5.3}$$

Finally, we describe the effective interaction between metal and adatom by the Appelbaum Hamiltonian [29]

$$H_t = \kappa\, \vec{J} \cdot \vec{j} \tag{5.4}$$

where κ is a momentum-independent coupling strength and $\vec{j} = c_{x=0}^\dagger \vec{\sigma} c_{x=0} \propto \sum_{k,k'} c_k^\dagger \vec{\sigma} c_{k'}$ is the effective spin degree of freedom of the metal electrons coupled to the atom. Here and later σ_i are the Pauli matrices and $\hbar = 1$.

We assume the temperature to be large enough, to justify a perturbative master equation approach [30] and neglect strong correlations with the bath, such as the Kondo effect or energy renormalization [31]. On the other hand, thermal excitations should be small enough to ensure only the ground states to be occupied and resemble switching dynamics of a two level system. According to the Boltzmann distribution, the temperature should verify $k_\mathrm{B}T \lesssim 0.1\Delta$, where $\Delta \propto |D|$ is the energy gap between the two lowest-energy levels and the other ones. We will not treat atomic hyperfine interactions.

5.2.2 Operators

Three physical operations on the system are relevant for our analysis of the stability of the atomic nanomagnet: rotation with discrete angles with axis perpendicular to the surface, time reversal (TR) and mirror across a certain mirror plane. We define here their representations in the atomic spin space. In the next sections, we will regard these operations as symmetries of the atomic system and analyze the consequences on the stability of the groundstate.

Rotation generator. The rotational symmetry of the adatom within the crystal field maps onto a rotational symmetry into the spin space. The generator of the rotation group is represented by

$$R_{z,2\pi/\chi} = \exp\{i\frac{2\pi}{\chi}\,J_z\}. \tag{5.5}$$

The rotation generator has the property $R^\chi = \pm 1$ (we will omit the subscript in $R_{z,2\pi/\chi}$ for the rest of the paper), where the plus refers to integer spin systems and the minus to half-integer ones. This generator has at most χ distinct unit eigenvalues, equal to $r_\chi = \exp\{i\,2\pi n/\chi\}$ with $n \in \mathbb{Z}$, for integer momentum systems, and $n \in \mathbb{Z}+1/2$, for a half-integer ones.

Time reversal operator. Time reversal is represented by the antiunitary operator

$$T = \exp\{i\pi\,J_y\}\,K, \tag{5.6}$$

acting on the basis $\{|J, j_z\rangle\}$, where K is the conjugation operator. In the following we will shorten the notation of the basis states as $\{|j_z\rangle\}$.

The action of T can be defined such that $T|j_z\rangle = (-1)^{\lfloor j_z \rfloor}|-j_z\rangle$, where $\lfloor \cdot \rfloor$ is the floor function. The square of the TR operator acting on a integer or half-integer momentum Hilbert space gives 1 or -1, respectively[32].

T commutes with R. Nonetheless its antiunitarity hinders the possibility to find a common eigenbasis. Indeed, suppose $|\psi\rangle$ is an eigenstate of R with eigenvalue r, then $T R |\psi\rangle = T r |\psi\rangle = r^* T |\psi\rangle$. At the same time $T R |\psi\rangle = R T |\psi\rangle$ and we conclude that $T|\psi\rangle$ is an eigenstate of R but with eigenvalue r^*. Considering the quantity $\langle T\psi|R|\psi\rangle$ and applying R in the bracket first to the left and then to the right state, one immediately concludes that $T|\psi\rangle \perp |\psi\rangle$ when r is non real. Only if r is real we can find a $|\psi\rangle$ which is eigenstate of both T and R. We will use this feature later, in section 5.2.4.

In other words, even though two commuting symmetries are present, eigenstates cannot be in general labeled with two well defined quantum numbers at the same time.

Mirror operator. Freedom in choosing the coordinate axes allows to set one mirror plane along yz. We call M the operator that reflects across this plane. Then, all other possible reflections with the other mirror planes are constructed conjugating it with the elements of the rotation group.

Since $\vec{J}$ is a pseudo-vector, M acts on the spin fundamental algebra transforming $J_{y,z}$ to $(-J_{y,z})$ while keeping J_x unchanged. To obtain the explicit representation, we notice that this operator is equivalent to a π rotation around x. Therefore,

$$M = e^{i\pi J_x}. \tag{5.7}$$

Notice that $M^2 = \pm 1$ (the plus refer to integer spins systems and the minus for half-integer ones) and that $M R = R^\dagger M$.

5.2.3 Hamiltonian symmetry constraints and Stevens operator expansion

Using all symmetries we can characterize the most general structure that the Hamiltonian can have. In Ref. 26 a general tesseral harmonic expansion of H compatible with a number of point symmetry groups is discussed and relative constraints are found. Here, we stick to the point group $C_{\chi v}$ symmetry and analyze the Stevens operator expansion of the Hamiltonian H_A in Eq. (5.1). We start considering the spatial symmetries constraints, then we show the one due to the TR symmetry.

A generic Stevens operator[33] O_p^q (with $q < p$) is expressed in a closed form in Ref. 34. These operators are Hermitian by construction and, after trivial manipulations, we can write them in the following form:

$$O_p^q = \frac{1}{2} \sum_{r=0}^{\lfloor (p-q)/2 \rfloor} c(p,q,r) \left\{ J_+^q + J_-^q, J_z^{p-q-2r} \right\},$$

$$O_p^{-q} = \frac{i}{2} \sum_{r=0}^{\lfloor (p-q)/2 \rfloor} c(p,q,r) \left\{ J_+^q - J_-^q, J_z^{p-q-2r} \right\}, \qquad (5.8)$$

where q and p are natural numbers and $c(p,q,r)$ are real prefactors whose magnitude is not relevant for our discussion.

Since the atomic system has spatial symmetry $C_{\chi v}$, the equations

$$[H_A, R] = 0,$$
$$[H_A, M] = 0 \qquad (5.9)$$

must hold.

The first equation implies that all matrix elements of H between states with different eigenvalue r_χ must vanish. Moreover, we can expand H_A using the operators in Eq. (5.8). Each operator O_p^q or O_p^{-q}, when applied to the basis state $|j_z\rangle$, transforms it to a superposition $\alpha|j_z+q\rangle + \beta|j_z-q\rangle$. The superposition retains the rotation eigenvalue of the latter state only if $r_\chi(J_z \pm q) = r_\chi(J_z)$ i.e. if $q = m\chi, m \in \mathbb{N}^*$. Therefore, only terms proportional to $O_p^{\pm m\chi}$, are allowed in the expansion.

Notice that rotational symmetry in our problem is analogous to translation symmetry in one dimensional periodic crystals. The Hamiltonian eigenstates can be labeled with their eigenvalues r and the latter are in one to one correspondence with a set of *quasi*-spin[†] defined in a one dimensional Brillouin zone (BZ). Such a set is isomorphic to $\mathbb{Z}_\chi$ and can be defined as $\{-\lfloor \chi/2 \rfloor + 1, -\lfloor \chi/2 \rfloor + 2, \ldots, \lfloor \chi/2 \rfloor\}$, for systems with integer J, and $\{-\lceil \chi/2 \rceil + 1/2, -\lceil \chi/2 \rceil + 3/2, \ldots, \lceil \chi/2 \rceil - 1/2\}$ for systems with half-integer J (notice the use of floor and ceiling functions here). For instance, for half-integer spin systems with $\chi = 3$ the BZ is $\{-1/2, 1/2, 3/2\}$; for integer ones with $\chi = 4$, the BZ is $\{-1, 0, 1, 2\}$. Clearly, every spin state has a well defined *quasi*-spin in the above defined BZs and this is equal to

$$J_{J_z}^{(q)} := ([J_z + (\chi - 1)/2] \bmod \chi) - (\chi - 1)/2. \qquad (5.10)$$

---

[*]In our convention, $\mathbb{N}$ includes the zero unless further specifications are present.

[†]Our definition of *quasi*-spin must not be confused with the one used in nuclear physics. See B.H. Flowers, S. Szpikowski, Proc. Roy. Soc. **84** (1964) 193 for details.
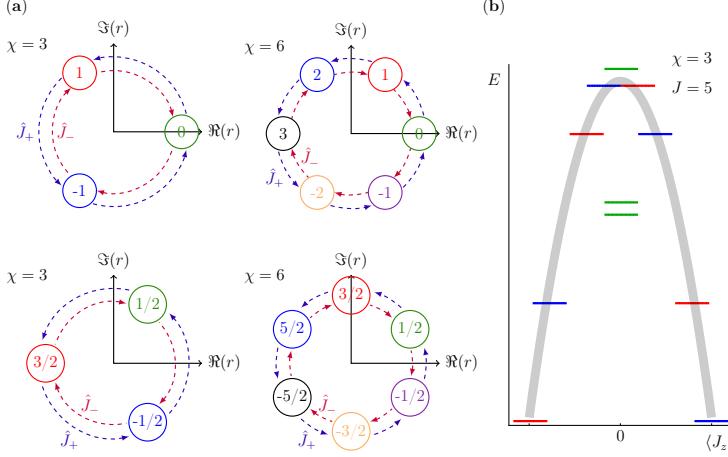
Figure 5.2: (*a*) Periodic Brillouin Zones (BZs) for integer spin systems (top) and half-integer ones (bottom). To better visualize the periodicity of the BZs, their elements (the little circles) are placed at the complex eigenvalues of R and the number they contain indicates the associated *quasi*-spin. Blue(red) arrows indicate SE transitions with transfer of positive(negative) *quasi*-spin. (*b*) Typical spectrum of a three-fold rotation symmetric system with small transversal anisotropy. On horizontal axis is the average magnetization along z of the levels. The color code of the level indicates its *quasi*-spin according to the top left case in (a). All figures are adapted from Ref. 22.

where we make use of the modulo operation ($x \bmod y$ indicates the value of x modulo y).

For instance, the spin state with $J_z = -4$ in a system with $\chi = 3$ has $J^{(q)} = -1$. More "bands" are present as soon as $J \geq \chi/2$ i.e. when J is such that at least two different spin states have the same *quasi*-spin. Fig. 5.2(a) shows the periodic BZs for $\chi = 3, 6$.

The mirror operator M acts with the transformations $(J_z, J_\pm) \rightarrow (-J_z, J_\mp)$. Eq. (5.9) implies $[M, O_p^{\pm q}] = 0$ and the latter equation constrains the difference $p - q$ to be even(odd) when the superscript of O is positive(negative). Hence, combining this constraint with the rotational one, we see that only operators of the form $O_{m\chi+2n}^{m\chi}$ and $O_{m\chi+2n+1}^{-m\chi}$ with $m, n \in \mathbb{N}$ are allowed.

Finally, TR operator acts with the transformation $(J_\pm, J_z) \rightarrow -(J_\mp, J_z)$ and $i \rightarrow (-i)$. Consequently, TR symmetry, if present, implies the label p to be even.

To be explicit, when all symmetries are present, the allowed Stevens operators in the expansion of H_A only $O_{2n}^{(-1)^{m\chi} m\chi}$, $(m, n \in \mathbb{N})$. Notice that the Hamiltonian would be always real (in the spin eigenbasis $\{|j_z\rangle\}$)

for $\chi \neq 3$, but is in general not real for $\chi = 3^{*}$.

In the following, we will use the *quasi*-spins as quantum numbers to label the atomic eigenstates. In some cases, the eigenvalues of the mirror operator M could be added to the set of the quantum numbers. However, its eigenstates present no magnetization along the z direction[†] and are not suitable for the analysis of the next sections. Thus, the rotational symmetry is a central ingredient in determining the stability of the nanomagnet.

In the rest of the paper we will allow also for TR symmetry breaking due to magnetic field. However, only the component B_z is allowed as is the only one which preserves rotational symmetry. *Per contra*, the mirror symmetry gets broken. Notice that the antiunitary product operator TM would still represent a symmetry for the system. We have checked the implications of this symmetry. It is antiunitary and surprisingly allows for an additional quantum number for the Hamiltonian eigenstates. However, since it does not provide strong selection rules for GSS or SE switching processes, we limit ourselves to briefly mention them in App. 5.6.

5.2.4 Groundstate splitting at $H_t = 0$

We now turn our attention to the first goal: to show that, *assuming $H_t = 0$ and $\vec{B} = 0$, it is possible to tell whether the groundstate of the atom is degenerate or it is allowed not to be, only by knowledge of the symmetries and the magnitude J of its spin.*

First, switch off momentaneously $H_A^{(1)}$ in H (with $H_t = 0$ and $\vec{B} = 0$). The two degenerate groundstates are $|\psi_{GS}\rangle := |j_z = J\rangle$ and $|\tilde{\psi}_{GS}\rangle := T|\psi_{GS}\rangle \propto |-J\rangle$ (we will omit '$j_z =$' for the rest of the paper). Even though $H_A^{(0)}$ has symmetry $C_{\infty v}$, it is convenient to identify already their eigenvalues under the action of the rotation generator $R_{z,2\pi/\chi}$ (where χ is defined as the maximum value for which $[H_A^{(1)}, R_{z,2\pi/\chi}] = 0$ holds). They are $r_{GS} = (r_{\widetilde{GS}})^* = \exp\{i\,J\,2\pi/\chi\}$ ($r_{\widetilde{GS}}$ is the eigenvalue for $|\tilde{\psi}_{GS}\rangle$) and their *quasi*-spin are defined in Eq. (5.10).

---

[*]The allowed Stevens operators depend, if $\chi = 3$, on the choice of the mirror axis as clarified in C. Rudowicz, Chem. Phys. **97**, 43–50 (1985). Our convention follows Ref. 26, other authors (for instance Ref. 3 and Y. M. Chang, T. H. Yeom, Y. Y. Yeung, and C. Rudowicz, J. Phys. **5**, 6221 (1993)) follow a different convention according to which the Hamiltonian is real.

[†]To see this, let $|\psi\rangle$ be an eigenstate of M. Its eigenvalue is a unit complex number (see App. 5.6 for details). Considering that $\{J_z, M\} = 0$, the magnetization of the state along z satisfies $\langle\psi|J_z|\psi\rangle = -\langle\psi|M^\dagger J_z M|\psi\rangle = -\langle\psi|J_z|\psi\rangle$. Thus, the magnetization is vanishing.

Now, we switch on $H_A^{(1)}$ adiabatically to its actual value. Energies and eigenstates change along the process, but the *quasi*-spin of all eigenstates are preserved since $[H_A^{(1)}, R] = 0$. At the end of the process the groundstates of the system would have retained their initial *quasi*-spins unless some state with different *quasi*-spin crossed the groundstates along the process, becoming lower in energy. Since $H_A^{(1)}$ is left generic in our analysis, we can not have control on the final value of the groundstate *quasi*-spin after such crossings. To prevent these inconvenience, we assume $H_A^{(1)}$ to be small enough (roughly speaking, $H_A^{(1)} \ll H_A^{(0)}$ is sufficient).

Using the properties of the TR operator illustrated Sec. 5.2.2, we claim that *eigenstates $|\psi\rangle$ of both H_A and R with non-real r are degenerate in presence of TR symmetry.*

Clearly, this statement is non-trivial only for integer spin systems because half-integer spin ones under TR symmetry always exhibit groundstate degeneracy by Kramers theorem. To prove the claim, remind that if r is non-real then $|\tilde{\psi}\rangle := T|\psi\rangle \perp |\psi\rangle$. Subsequently, $[H, T] = 0$ implies that, on one hand $TH|\psi\rangle = \varepsilon_0 T|\psi\rangle = \varepsilon_0|\tilde{\psi}\rangle$ and on the other hand $TH|\psi\rangle = HT|\psi\rangle = H|\tilde{\psi}\rangle$. Hence, joining together the two equations, we get $H|\tilde{\psi}\rangle = \varepsilon_0|\tilde{\psi}\rangle$.

The statement above applies to the groundstate. We conclude that it can get split by tranversal anisotropy terms only if r_{GS} is real or, in other words, if its associated *quasi*-spin is a TR invariant point of the Brillouin zone ($|J_{GS}^{(q)}| = -|J_{GS}^{(q)}| + m\chi, m \in \mathbb{N}$). Thus, the splitting happens when

$$\exists m \in \mathbb{N} \; : \; J = \frac{m\chi}{2}. \tag{5.11}$$

This constraint determines the columns GSS in the Tables 5.1 and 5.2. When the system features GSS in presence of TR symmetry, the two lower states are also non magnetic. They have to be eigenstates of the TR operator, therefore, $\{J_z, T\} = 0$ implies $\langle\psi_{GS}|J_z|\psi_{GS}\rangle = 0$. We stress that the splitting may be also seen as a consequence of lowering the symmetry from the $C_{\infty v}$ subgroup of the free atom point group to the $C_{\chi v}$ subgroup of the atom within the crystal field.

5.2.5 Single-electron switching process at $H_t \neq 0$

Finally, we switch on the interaction with the metal, $H_t \neq 0$. When the substrate gets coupled with the atom, the energy and *quasi*-spin of the atomic state are not preserved anymore, because of scattering with

the metal electrons. Since the metal has many degrees of freedom with respect to the atom, it is usually assumed to thermalize quickly and its Boltzmann distribution, being a classical one, leads the atom to have also an associated classical distribution [35]. The approximated Markovian law, that describes the dynamics of energy-defined states of the atom (the pointer basis of the nanomagnet [36]), is well known in literature [37,38]. However, there is an ambiguity in the definition of the pointer basis when the atom presents pairs of degenerate states (which is the case when the atom has no GSS and applied magnetic field). There are indications [39] that the states of the pointer basis are those with maximum magnitude of the average magnetization, as the dephasing due to the scattering is the largest for these states. Thus, we are allowed to assume that the pointer basis coincides with the atomic eigenstates considered in the previous sections, with well defined quasi-spin.

It was shown [31] that the GSS feature might be destroyed when the Kondo coupling times the substrate electronic density of states gets large via a mechanism of gap quenching. However, such a mechanism is not effective in most of the experiments performed, therefore here we limit the discussion to small Kondo couplings i.e. $H_t \ll H_A$.

The rate of switching between two atomic eigenstates, say $|\psi_a\rangle$ and $|\psi_b\rangle$, at lowest order in H_t, i.e. due to a SE scattering with the atom, is

$$\Gamma_{ab} = \frac{2\pi\kappa^2}{\hbar} \sum_{\mu,\nu} |\langle \psi_a, \nu | H_t | \psi_b, \mu \rangle|^2 \, e^{-\beta E_\mu} \delta(x)$$

$$= \frac{2\pi\kappa^2}{\hbar} \sum_{\mu,\nu} \left| \sum_{s \in \{+,-,z\}} \langle \psi_a | J_s | \psi_b \rangle \langle \nu | j_{\bar{s}} | \mu \rangle \right|^2 e^{-\beta E_\mu} \delta(x) \qquad (5.12)$$

where μ, ν are states in the substrate, the bar in $j_{\bar{s}}$ indicates that the subscript takes opposite sign if $s = \pm$ and $x = E_\nu - E_\mu + E_a - E_b$. It is clear that transitions are possible only when the states are connected by an operators J_s, with $s = +, -, z$.

We show that the rotational symmetry provides a selection rule on SE switching processes. The commutation relations between J_s and R are $RJ_s = e^{i\varphi_s} J_s R$, where $\varphi_s = 0, \pm 2\pi/\chi$ respectively for $s = z, \pm$. Since the states $\psi_{a,b}$ are also eigenvalues of R, one gets:

$$\left[e^{i(\varphi_b - \varphi_a + \varphi_s)} - 1 \right] \langle \psi_a | J_s | \psi_b \rangle = 0. \qquad (5.13)$$

Thus, given $\psi_{a,b}$, at most one value of s is such that $\varphi_s = \varphi_a - \varphi_b$. This means that a SE transition produces a *quasi*-spin change equal to either $0, 1$ or -1. When the *quasi*-spins of the states differ by more than one, we are guaranteed that $\Gamma_{ab} = 0$ and there is no SE transition between

the two states. For instance, systems with $\chi = 6$ and $J = 15/2$ have groundstates with $J^{(q)} = \pm 3/2$ therefore at least three SE transitions are needed for a groundstate switching. One could easily check it using Fig. 5.2(a) (SE transitions from the eigenstates are shown with arrows).

A second selection rule comes from the TR symmetry. It protects degenerate groundstates of integer spin systems from SE switching. Given $|\psi_{GS}\rangle$ and $|\tilde{\psi}_{GS}\rangle$ as the two time-reversal groundstate partners and making use of $\{J_z, T\} = 0$ and $J_+ T = -T J_-$ one finds[3,20] for all $s \in \{+, -, z\}$

$$\langle \psi_{GS}|J_s|\tilde{\psi}_{GS}\rangle = 0 \quad \text{for integer spin.} \tag{5.14}$$

Actually, this constraint is non-trivial only with $\chi = 3$. In the other cases the groundstates are either already split by transversal anisotropy or have *quasi*-spin difference greater than one. For instance, in the experimental set of Ref. 28 (Fe atoms on CuN substrate with $J = 2, \chi = 2$) GSS is present and SE transitions between the two lowest-energy states are indeed observed even at $B = 0$.

Other weak constraints come from the mirror symmetry but they are not enough to make SE switching to vanish. We leave this discussion to App. 5.6.

As a final remark, we notice that also small spin systems with $\chi > 2J > 1$ are protected against SE switching process. This happens because there are no pairs of states with the same phase or, in other words, there is only one "band" in the Brillouin zone. Only if $J = 1/2$, the system groundstates can be connected by SE transitions.

5.2.6 Suppression of SE switching process at $H_t \lesssim H_A^{(1)} \ll H_A^{(0)}$

As an application of the tools of analysis developed in the previous sections, we describe here a feature related to the suppression of SE switching rate in some systems, when the terms in $H_A^{(1)}$ gets *uniformly* small. We assume, therefore, that $H_t \lesssim H_A^{(1)} \ll H_A^{(0)}$, making the further assumption that the different prefactors in front of each J_s^n ($n \geq 0; s = +, -, z$), in the expansion of $H_A^{(1)}$, have all the same order of magnitude $\varepsilon \ll 1$. In this regime we can treat $H_A^{(1)}$ as perturbation of the system with Hamiltonian $H_A^{(0)}$.

Consider now $\Gamma_{\psi_{GS}, \tilde{\psi}_{GS}}$ in Eq. (5.12), the transition rate of the SE switching process between the true groundstates. The groundstates can

be expressed as a perturbation series in ε:

$$|\psi_{GS}\rangle = |J\rangle + \varepsilon \sum_m \alpha_m |J - m\chi\rangle + \mathcal{O}\left(\varepsilon^2\right)$$

$$|\tilde{\psi}_{GS}\rangle \propto |-J\rangle + \varepsilon \sum_n \alpha'_n |-J + n\chi\rangle + \mathcal{O}\left(\varepsilon^2\right) \qquad (5.15)$$

where $m(n)$ is a natural number such that $J - m(n)\chi > -J$ and $\{\alpha_{m(n)}\}$ are expansion coefficients[*].

The quantity $\langle \psi_{GS} | J_s | \tilde{\psi}_{GS}\rangle$ in $\Gamma_{\psi_{GS}, \tilde{\psi}_{GS}}$ gets contributions of different perturbative orders, of the form $\varepsilon \, \alpha'_n \langle J - m\chi | J_s | -J\rangle$ or $\varepsilon \, \alpha_m \langle J | J_s | -J + n\chi\rangle$ and $\varepsilon^2 \, \alpha_m \alpha'_n \langle J - m\chi | J_s | -J + n\chi\rangle$. We notice that, inside the sets of systems which exhibit SE switching, we can distinguish two subsets. The systems in the first one presents the $\mathcal{O}(\varepsilon)$ contributions while the systems in the second one not. The first subset contains systems in which the unperturbed groundstate $|-J\rangle$, call it the left one, has the same *quasi*-spin of either $|J\rangle$ (in the half-integer case only) or $|J-1\rangle$. On the contrary, systems of the second subset possess a left groundstate which would have the same *quasi*-spin of the state $|J + 1\rangle$. Of course this state is not allowed, thus, the $\mathcal{O}(\varepsilon)$ contributions are vanishing. A systems falls in the second group when the difference between the *quasi*-spin of $|\tilde{\psi}_{GS}\rangle$ and $|\psi_{GS}\rangle$ (modulo χ) is equal to one. The magnitude of its spin, then, must verify (we make use of Eq. (5.10))

$$(2J) \bmod \chi = \chi - 1. \qquad (5.16)$$

In this perturbative regime the SE switching rates are

$$\Gamma_{\psi_{GS}, \tilde{\psi}_{GS}} \propto \begin{cases} \kappa^2(\varepsilon^2 + \mathcal{O}(\varepsilon^3)) & \text{for the first subset,} \\ \kappa^2(\varepsilon^4 + \mathcal{O}(\varepsilon^5)) & \text{for the second subset.} \end{cases} \qquad (5.17)$$

where $\kappa \lesssim \varepsilon$ (the assumption $H_A^{(1)} \gtrsim H_t$ is to guarantee that the dominant switching path for the second subset remains the SE one and not a multiple-electrons one). From this expression is clear how systems in the second subset have smaller SE switching rates in the perturbative limit. They are listed in the column "Supp" in Tables 5.1 and 5.2.

5.2.7 Numerical simulations

We demonstrate the consequences of the symmetry considerations on the switching rate of a single-atom nanomagnet when experimentally

---

[*]To be precise, for the approximation to be valid, the second-order terms must be smaller then the first order ones. This happen if ε verifies $\varepsilon \ll 1/(2J\alpha_{\max})$, with $\alpha_{\max} = \max_k \alpha_k$.
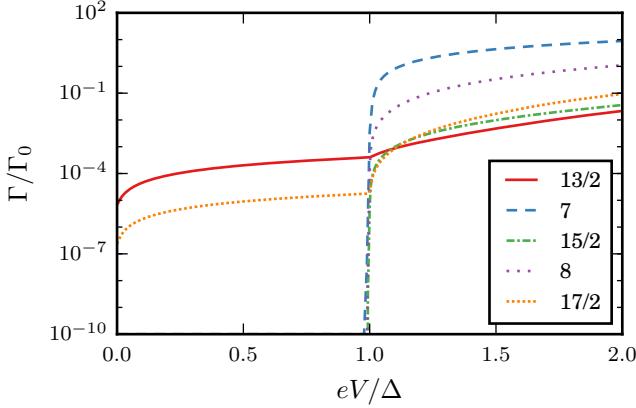
Figure 5.3: Bias-dependent switching rate of a spin with $J = 13/2 \ldots 17/2$ in a six-fold rotational symmetric crystal ($\chi = 6$). Other parameters are $\kappa^2/D = 0.1$, $\alpha_6^6/D = 5 \cdot 10^{-5}$, $kT/D = 0.01$, $P = 0.1$ (P is the tip polarization) and Δ is the first excitation energy of the spin.

measured by spin-resolved scanning tunneling microscopy (STM). In previous experiments, the stability of few-atoms clusters was investigated by means of this technique[4,6,17]. In particular, the switching rate between groundstates has been observed in the telegraph noise. Such an experimental setup can be described by adding the STM tip Hamiltonian to Eq. (5.1) while accessible quantities like the bias voltage, temperature and external magnetic field are varied. For this purpose we solve the master equation (see Refs. 4,19) for a six-fold rotational symmetric system with small transversal anisotropy, $H_A^{(1)} = \alpha_6^6 O_6^6$, and several different spin magnitudes. As already mentioned before, we neglect the small energy renormalization of the atomic levels due to the coupling with the tip. All rates will be given in units of the direct tunneling rate $\Gamma_0 = \pi v_S^4(\rho_{T\uparrow}\rho_{S\uparrow} + \rho_{T\downarrow}\rho_{S\downarrow})$.

Fig. 5.3 shows the bias-dependent switching rate for several spin magnitudes. We observe that in all cases an increasing switching rate is observed for voltage higher than the spin excitation energy Δ of the magnet (Δ is the energy difference between the first excited state and the groundstate of the system with $B = 0$). For the protected cases $J = 7, 15/2, 8$, however, the switching rate becomes negligible for low temperatures $kT \ll \Delta$ in accordance to Tables 5.1 and 5.2. In contrast, $J = 13/2$ and $17/2$ show SE switching even at low bias voltages resulting in a finite switching time $\tau = \Gamma^{-1}$.

Temperature-dependent switchings are investigated often by X-ray
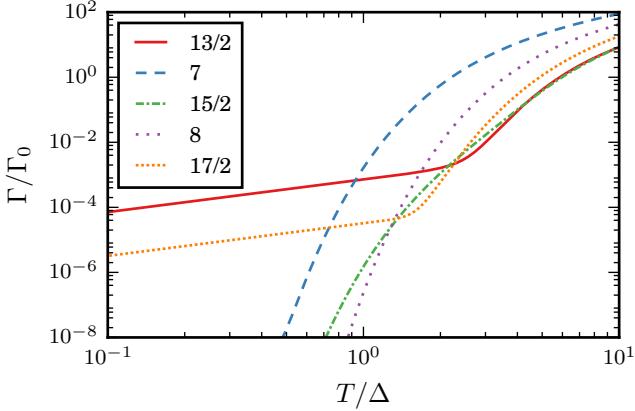
Figure 5.4: Zero-bias temperature dependence of the switching rate of a spin with $J = 13/2 \ldots 17/2$ in a six-fold rotational symmetric crystal ($\chi = 6$). Other parameter as in in Fig. 5.3.

absorption spectroscopy and magnetic circular dichroism (XCMD) measurements to infer the stability of an atom or cluster (Fig. 5.4). Similar to the bias-dependent measurement, one can observe, in all cases, an onset of the switching rate for temperatures high enough to excite the spin. At low temperature, the switching rate becomes negligible for the stable cases while remaining finite for unstable ones. In contrast to the bias dependence where the switching sets in abruptly at $eV = \Delta$ for stable atom configurations, the onset of the switching with temperature appears continuous and monotonously.

In a next step, we break TR symmetry by applying magnetic field of strength B along the z axis (Fig. 5.5). For the chosen magnetic field range, the cases $J = 13/2$ and $J = 17/2$ show SE switching as they are not protected by symmetry. In particular, $J = 13/2$ shows a Lorentzian-like peak at the magnetic field strength at which one of the former groundstates gets degenerate with one of the former first excited states. The specific shape has to be associated to the fact that the two states have the same *quasi*-spin and hybridize. In contrast, $J = 7$ is stable for low magnetic field. However, spin switching gets activated at higher applied fields when the former groundstate is brought in resonance with one excited state. In this case the curve profile is different since the two states have different *quasi*-spins.
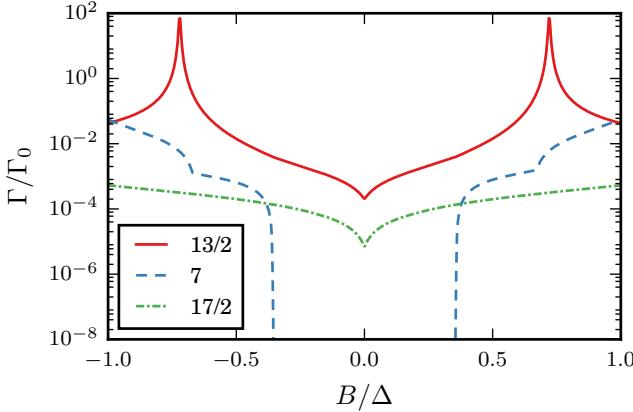
Figure 5.5: Magnetic field dependence of the switching rate of a spin with $J = 13/2, 7, 17/2$ in a six-fold symmetric crystal ($\chi = 6$) for $eV/D = 6$ and other parameters as in Fig. 5.3.

5.2.8 Discussion

The results of our single-atom analysis are summarized in Tables 5.1 and 5.2.

From our considerations, we can conclude that the higher the symmetry the more stable will be the bit encoded in the groundstates. To substantiate this statement we bring to the attention of the reader the cases of $\chi = 2$ and $\chi = 6$. The former case does not host good nanomagnets as either their groundstates are split or present SE switching processes. On the contrary, the latter case hosts nanomagnets with high stability against both SE and single-phonons switching processes[*]. Indeed, in half-integer spin systems with $J = \frac{3}{2} + 3n$, ($n \in \mathbb{N}$) the difference between the groundstates *quasi*-spins is maximal, equal to 3.

We remark the advantage in working with the *quasi*-spin formalism, analog to the *quasi*-momentum formalism in crystal theory, in order to get universal formula for the presence of GSS and other features. The *quasi*-spin would also be a more natural horizontal axis in typical spectrum plots encountered in literature, like the one in Fig. 5.2(b).

Notice that the mirror symmetry plays only a marginal role in our qualitative discussion: it does not provide strong constraints to GSS or

---

[*]About the phonon contribution to $\Gamma_{a,b}$ (cf. Eq. (5.12)) the reader may consult Refs. 13 and M. Mannini *et al.*, Nature **468**, 417–421 (2010). In first approximation, single-phonon processes induce *quasi*-spin changes equal to $|\Delta J^{(q)}| = 1, 2$. Moreover, notice that they induce no groundstate switching if $\vec{B} = 0$, as their density of state at zero energy vanishes.

χ	GSS	SES(T)	SES(BT)	Protected	Supp
2	$\{n\}$	$\{\}$	$\{n\}$	$\{\}$	$\{\}$
3	$\{3n\}$	$\{\}$	$\{n\}\setminus\{1\}$	$\{1\}$	$\{1+3n\}$
4	$\{2n\}$	$\{\}$	$\{2n\}$	$\{1,3,5\}$	$\{\}$
6	$\{3n\}$	$\{\}$	$\{3n\}$	$\{1,2,4,5\}$	$\{\}$

Table 5.1: Sets of integer spin magnitudes $\{J_n\}$, with $n \in \mathbb{N}_{>0}$, which exhibit ground-state splitting (GSS) or SE switching processes (SES), at given system symmetry $C_{\chi v}$. The etiquette "(T)" and "(BT)" differentiate on whether time reversal symmetry is, respectively, present or broken. "$\{\}$" indicates the empty set and the notation "$\{a\}\setminus\{b\}$" stands for the set subtraction of $\{b\}$ from $\{a\}$. The fourth column (Protected) shows instances of magnitudes which are protected from both GSS and SES. The last column (Supp) shows the sets with suppressed SE switching processes at very small $H^{(1)}$ and H_t, as described in Sec. 5.2.6.

χ	GSS	SES(T,BT)	Protected	Supp
2	$\{\}$	$\{n+1/2\}$	$\{\}$	$\{\}$
3	$\{\}$	$\{n+1/2\}\setminus\{\frac{3}{2}\}$	$\{\frac{3}{2}\}$	$\{\frac{5}{2}+3n\}$
4	$\{\}$	$\{n+1/2\}\setminus\{\frac{3}{2}\}$	$\{\frac{3}{2}\}$	$\{\frac{3}{2}+2n\}$
6	$\{\}$	$\{n+1/2\}\setminus\{\frac{5}{2},\frac{3}{2}+3n\}$	$\{\frac{3}{2},\frac{5}{2},\frac{9}{2},\frac{15}{2}\}$	$\{\frac{5}{2}+3n\}$

Table 5.2: Same as in Table 5.1, but for half-integer spin magnitudes. Notice that TR symmetry does not provide additional protection from SE switching processes as it does in integer spin systems.

SE switching processes. However, its inclusion is relevant for quantitative numerics where the correct (symmetry preserving) Stevens operators must be taken into account.

We warn the reader that our results refer to "generic" Hamiltonians, that is, within a non-zero measure subset of the set of all possible symmetry preserving Hamiltonian. For example, a system with $J = 9/2$ and $\chi = 3$ would not present SE switching processes (in contrast with Table 5.2) if only the Stevens operator O_4^3 is included in $H_A^{(1)}$. However, inclusion of higher order Stevens operators like O_6^6 would restore the agreement with our theory.

The absence of SE switching processes in the case $J = 3/2$ and $\chi = 3$ is explained at the end of App. 5.5.

As a final remark, we comment a few relevant, recent experiments.

One experiment is Ho on Pt(111) where the substrate has 3-fold degeneracy. One experimental group[3] found the adatom spin magnitude to be $J = 8$ and measured low groundstates switching rate. According to our theory, such system would be protected from both GSS and SE switching if the transversal anisotropy is not too big (see Table 5.1). The latter was actually computed by the authors by means of *ab-initio*

calculations. The ratio between the uniaxial anisotropy term and the biggest transversal anisotropy term was found to be approximately 0.1%. Such value is compatible with the absence of level crossing and allows the usage of our theory. However, another experimental group [14] found a strong fourth-order uniaxial term inducing a groundstate level crossing. The system groundstate then does not occupy the spin state $|J_z| = 8$ anymore but rather it occupies the spin state $|J_z| = 6$. In this case we can still use our theory in this way: the groundstate quasi-spin can be inferred using Eq. (5.10) with $J_z = 6$ and not with $J_z = 8$. Table 5.1 can be used assuming the system as effective spin $J = 6$. However, the suppression feature of Sec. 5.2.6 does not take place anymore. According to our table, GSS had indeed to be expected.

Another experiment [9] is Ho on MnO. Here, $\chi = 4$ while spin magnitude is found to be $J = 8$. Also in this case *ab-initio* calculations reveal the presence of a groundstate level crossing. The ratio between the uniaxial anisotropy term and the biggest transversal anisotropy term is found to be as big as 5%. The latter term favours a groundstate occupation of the spin state with $|J_z| = 7$, rather than $|J_z| = 8$. With the prescriptions above indicated, Table 5.1 can still be exploited (using $J = 7$) and protection from GSS and SE switching are found, in agreement with the statements of the authors.

A similar situation happens in a third experiment. Dy atoms are deposited on graphene [40]. Hence $\chi = 6$ and $J = 8$. Again, a strong uniaxial field leads to a groundstate occupation of the spin state $|J_z| = 7$. The authors found protection from GSS and SE switching, which agrees to the indication of Table 5.1 (using $J = 7$).

This comparison with real experiments shows that level crossing is likely to happen. When this is case, the groundstate quasi-spin can not be inferred from the spin magnitude (and χ) only. Nonetheless, as shown above, our theory can still be applied, for a deep understanding of the system properties, if additional independent informations, e.g. from *ab-initio* calculations or direct measurements, give access to the groundstate quasi-spin.

5.3 Multiatom cluster systems

Since not only single-atom nanomagnets but also multiatom clusters are under the attention of researchers [1,4,6,41], we generalize the single atom results to non-frustrated multiatom configurations.

5.3.1 Model

We assume that the atoms interact through Heisenberg-like couplings due to e.g. direct ferromagnetic exchange or indirect Ruderman-Kittel-Kasuya-Yosida interaction [42,43]. For simplicity, we do not include Dzyaloshinsky-Moriya interactions [44]. As they might play a role when dealing with rare-earth adatoms and in general with systems with broken inversion-symmetry [45], their inclusion is left to future investigations. Thus, the total Hamiltonian

$$H_A = \sum_i \left[H_A^{(0)}(i) + H_A^{(1)}(i) + \vec{B}_i \cdot \vec{J}(i) \right]$$
$$+ \sum_{i>j} H_A^{int}(i,j) \tag{5.18}$$

includes the uniaxial anisotropy felt by the $i-$th atom

$$H_A^{(0)}(i) = - |D_i| \, J_z^2(i), \tag{5.19}$$

further anisotropy terms $H_A^{(1)}(i)$, and the multiatom Heisenberg interaction

$$H_A^{int}(i,j) = G_{ij} \, J(i) \cdot J(j). \tag{5.20}$$

The effective interaction between the electrons in the metallic surface and the atoms is

$$H_t = \sum_l \kappa_l \, J(l) \cdot j_{x_l} \tag{5.21}$$

where $j_{x_l} = c_{x_l}^\dagger \sigma c_{x_l} \propto \sum_{k,k'} e^{i \, (k-k') \cdot x_l} c_k^\dagger \sigma c_{k'}$ is the effective spin degree of freedom of the metal electrons coupled to the atom at position x_l.

To avoid magnetically frustrated configurations, we restrict the discussion to clusters where one can distinguish two groups of atoms, say A and B, such that they have intragroup ferromagnetic coupling ($G_{ij} < 0$ if the $i - th$ and the $j-$th atoms are in the same group) and intergroup antiferromagnetic couplings ($G_{ij} > 0$ if the $i - th$ and the $j-$th atoms are in different groups). A part from this restriction, the clusters are not required to have other additional properties like, for instance, a specific symmetric spatial configuration of the adatoms that compose it.

5.3.2 Operators

Similarly to R in Eq. (5.5), the rotation generators for every atom may be defined as $R(l) = \exp\{i \, J_z(l) \, 2\pi/\chi\}$. We define the operator associated

to the rotation of all spins as

$$R_{tot} = \otimes_l R(l) = \exp\{i\, J_{z,tot}\, 2\pi/\chi\} \qquad (5.22)$$

where $J_{z,tot} = \sum_l J_z(l)$ is the projection along the z-axis of the total spin.

The mirror operators $M(l)$ at mirror planes by each atom may be defined analogously.

The time-reversal operator is also trivially generalized to act on multiple spins.

5.3.3 Groundstate splitting for $H_t = 0$

As a first step, we show that a *quasi*-spin can be associated to the groundstates of the multiatom configuration.

With $H_A^{(1)}(i) = H_A^{(int)}(i,j) = \vec{B}_i = 0$ ($\forall i, j$), the non-interacting groundstates of the system are products of the groundstates of every independent atom. For instance, with only two atoms, the four groundstates are $|\pm J_1\rangle |\pm J_2\rangle$, J_i being the magnitude of the spin of the i-th atom.

We now switch on adiabatically all the interactions $H_A^{int}(i,j)$. These terms have actually a higher symmetry than C_χ, namely they are isotropic, and preserves $J_{z,tot}$. Since the non-interacting groundstate has high degeneracy, at first sight it is not clear a priori which states remain groundstate of the system after the switching process. However, such clusters seam to have the following, *per se* interesting, feature:

Conjecture. *Given the Hamiltonian in Eq.* (5.18) *with vanishing* $H_A^{(1)}(i)$, *the groundstate is an eigenstate of* $J_{z,tot}$, *with eigenvalue in modulus equal to* $|J_A - J_B|$, *where* $J_{A(B)} := \sum_{i \in A(B)} J(i)$. *By TR symmetry, the groundstate is doubly degenerate if* $J_A \neq J_B$.

Through the analysis of the spectrum of several H_A and numerical simulations (see Sec. 5.3.5), we got evidence that this conjecture[46] holds true. We are able to give a rigorous proof only in first order perturbation theory in the intergroup couplings of the matrix G (the intragroup couplings being allowed to have arbitrary magnitude). This regime is enough to understand how the single-atom features, found in Sec. 5.2, appear also in the multiatom case. Notice that purely ferromagnetic configurations fall into the range of our proof (as either group A or B is empty). Due to the technical character of the proof, we present it in App. 5.7.

The Marshall theorem, in the generalized fashion by Lieb and Mattis[24], ensures that, at $H_A^{(0,1)} = \vec{B}_i = 0$, for each $l \geq |J_A - J_B|$, the lowest

Hamiltonian eigenvalue with total spin magnitude J_{tot} equal to l is a monotone increasing function of l while, for $l \leq |J_A - J_B|$, it is monotone decreasing. Lieb and Mattis have proven that a magnetic field, proportional to J_{z_i}, destroys this order. Our conjecture regards the same kind of systems but with an additional finite and negative definite TR symmetric term, the uniaxial anisotropy (also higher order negative definite uniaxial terms may be added). The magnitude of the total spin is not anymore a good quantum number and the ordering of levels is destroyed. Still, according to our conjecture, the groundstates have the property

$$|J_{z,GS}| = |J_A - J_B| \tag{5.23}$$

and, crucially, we can associate them well defined *quasi*-spins. The latter are inferred by their eigenvalue under R_{tot} (see Eq. (5.22)) and are computed via Eq. (5.10) inserting J_z according to Eq. (5.23).

As a further step in the discussion upon the presence of GSS, we switch on the $H_A^{(1)}(i)$ terms. As in Sec. 5.2.4, if we assume these terms to be small enough such that the initial groundstates are not crossed (in energy) by other levels, then the groundstates *quasi*-spins are preserved. At this point the discussion about the GSS is identical to one done for the single-atom case: when the groundstates *quasi*-spins are integers and are at the TR invariant points of the Brillouin Zone, then GSS takes place. Notice that, according to the conjecture, equal-spin dimers have zero $J_{z,tot}$ (and *quasi*-spin) and their groundstate is generically non-degenerate. We conclude that dimers present GSS even with vanishing $H_A^{(1)}(i)$ terms.

5.3.4 Single-electron switching process at $H_t \neq 0$

We now switch on the small interaction with the metal. Similarly as before (cf. Eq. (5.12))

$$\Gamma_{ab} = \frac{2\pi}{\hbar} \sum_{\mu,\nu} |\langle \psi_a, \nu | H_t | \psi_b, \mu \rangle|^2 \, e^{-\beta E_\mu} \delta(x)$$

$$= \frac{2\pi}{\hbar} \sum_{\mu,\nu} \left| \langle \psi_a, \nu | \sum_{\substack{i \\ s \in \{+,-,z\}}} \kappa_i J_s(i) \cdot j_{x_i \bar{s}} | \psi_b, \mu \rangle \right|^2 e^{-\beta E_\mu} \delta(x)$$

$$= \frac{2\pi}{\hbar} \sum_{\mu,\nu} \left| \vec{\kappa} \cdot \vec{V} \right|^2 e^{-\beta E_\mu} \delta(x) \tag{5.24}$$

where $\left(\vec{V}\right)_i = \sum_{s\in\{+,-,z\}}\langle\psi_a|J_s^{(i)}|\psi_b\rangle\,\langle\nu|j_{x_i\bar{s}}|\mu\rangle$, $(\vec{\kappa})_i = \kappa_i$ and $x = E_\nu - E_\mu + E_a - E_b$.

$\Gamma = 0$ only when $\vec{V}\cdot\vec{\kappa} = 0$ for all possible μ, ν states i.e. when $\langle\psi_a|\,J_s^{(i)}|\psi_b\rangle$ are vanishing for every i. Fortunately, an analog of Eqs. (5.13) and (5.14), with J_s replaced by $J_s^{(i)}$, does hold and, in particular we get again protection from SE switching process for integer spin system. The protection here may be subtle. Consider, for instance, a system with $\chi = 6$ made up of two atoms with spins $J = 7/2$. If their coupling G is ferromagnetic, the total spin is $J = 7$ and the system presents no SE switching process, according to Eq. (5.24) and Table 5.1. In particular, this fact holds true even when the atoms are set at big reciprocal distance. However, in this situation the two atoms may be regarded as non-interacting and present individually SE switching processes, according to Table 5.2. We remark that there is no contradiction between the two viewpoints: the full groundstate, being a product of the groundstates of the two atoms in the non-interacting limit, needs two electrons to be fully switched. Even though quantitatively, the dimer has a big rate of switching, qualitatively it remains SE switching protected.

We warn the reader that switching transitions between degenerate groundstates of integer spin systems can be observed. However, these transitions must be attributed to $2n$-electrons processes, with n integer, (as one can see generalizing Eq. 5.14) and not to single-electron ones[*].

Finally, we notice that the suppression feature of Sec. 5.2.6 is not present for the multiatom case. The difference with the single-atom case lies in the fact that the state $|1 + J\rangle$ was a forbidden state there, while here its analog, $|1 + |J_A - J_B|\rangle$ is, in general, allowed.

5.3.5 Numerical simulations

We perform numerical simulations similar to the ones shown in section 5.2.7, focusing only on the bias dependence of the switching rate. We analyze the cases of two dimers with same *quasi*-spins when they are in a ferromagnetic configuration but different when in a antiferromagnetic one (see Figs. 5.6,5.7). Since we are interested only in the stability features, we assume vanishing distance between the atoms.

When the coupling is ferromagnetic ($G_{12} < 0$), both dimers are predicted to be unstable, as in both cases $|J_{GS}^{(q)}| = 5/2$. Both our simulations

---

[*]An example of multiatom systems, in which the switching has been measured, are antiferromagnetic chains with an even number of atoms (see Ref. 6). A special mechanism sets in as the chains become longer for which the GSS disappears and a degenerate groundstate is restored[31]. The effective groundstates of these chains are the Néél (time reversal partner) states.

confirm the expectation. The case $G_{12} = -0.1$ in Fig. 5.7 points to an important feature of multiatom configurations: the rate (at zero voltage) can be very small. Notice that, in order to get rates Γ comparable with the single-atom case, we need to increase the transversal anisotropy (α_6^6/D) about two orders of magnitude.

When the coupling is antiferromagnetic ($G_{12} > 0$) the case in Fig. 5.6 is predicted to be stable, as $|J_{GS}^{(q)}| = 3/2$, while the other one unstable, as $|J_{GS}^{(q)}| = 1/2$.

Notice that the cases $G_{12} = \pm 0.1$ in Fig. 5.7 present the first kink at higher voltage than the one which corresponds to the first excitation energy (Δ). This interesting phenomenon is a prerogative of multiatom systems (with $\chi = 6$): the first excited states can be not SE-connected to the groundstates. When it happens, the transition rates between these states are suppressed and a new channel of switching opens only at higher voltage when second excited states can get excited. This feature may be exploited to increase the energy-window of stability (in units of Δ). For instance, a dimer with $J_1 = 4$ and $J_2 = 2$ with the same parameter set as in the figures and antiferromagnetic coupling $G_{12} = -0.1$ has groundstate *quasi*-spin $|J_{GS}^{(q)}| = 2$ while the first excited states have $|J_{GS}^{(q)}| = 0$. The groundstates are then SE-switching protected and the switching (at small T) activates only at $eV \sim 2\Delta$ in correspondence with the second excited states.

As a final remark, we see that our numerical simulations support the conjecture in Sec. 5.3.3. Indeed, the cases with $G_{12} = 1$ fall outside the range of validity of our proof (see App. 5.7), but the numerics confirms our expectations in terms of the stability of the groundstates.

5.3.6 Discussion

Clusters seem to behave as single atoms as far as our analysis is concerned. We can associate them a *quasi*-spin and they have analogous selection rules for SE switching processes. A difference with the single-atom case is that the magnitude of total spin of the groundstates is not well defined anymore (a part in the ferromagnetic case). Nonetheless, this is of no consequence since the unique quantum number needed to determine the symmetry selection rules is the *quasi*-spin.

One other caveat is that the feature of missing SE switching process for small spin systems (see Sec. 5.2.5) is not present here unless for all atoms, that compose the cluster, $\chi > 2J > 1$ holds. These systems do not follow our tables but could be addressed separately as they are relatively simple to be studied. Moreover, also the suppression feature of Sec. 5.2.6 is not present.
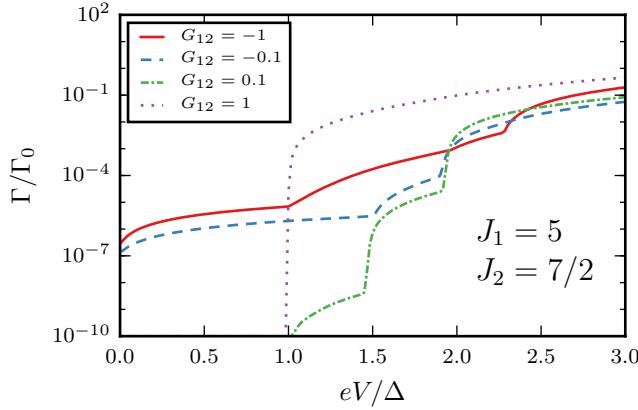
Figure 5.6: Bias-dependent switching rate of a dimer with spin magnitudes J_1 and J_2 in a six-fold symmetric crystal ($\chi = 6$), at different strength of the exchange coupling G_{12} (in unit of D). The tip is placed on top of the first atom i.e. $\kappa_1^2/D = 0.1$ and $\kappa_2^2/D = 0$. Here, $\alpha_6^6/D = 1 \cdot 10^{-3}$, all other parameters are as in Fig. 5.3 .

To conclude, we inform that Tables 5.1 and 5.2 can be used for the multiatom case. However, the spin magnitude of the single atom has to be replaced with an effective groundstate spin magnitude $|J_A - J_B| + \chi$, where the "$+\chi$" term is conveniently added to avoid those small spins constraints, as illustrated above.

5.4 Summary and Outlook

We focused on the dynamic properties of generic nanomagnets made of absorbed adatoms on metallic or insulating surfaces. We presented a complete and comprehensive discussion on the implications of the symmetries of the system on the stability of the magnetic states. In particular, the symmetries of interest are the rotational, the mirror and the time-reversal symmetry. All our results are summarized in Tables 5.1 and 5.2. Given the effective spin magnitude of the adatoms and the symmetries of the system, our main results, the Tables 5.1, 5.2, indicate whether a nanomagnet is stable by its desirable properties: absence of groundstate splitting and single-electron switching processes. Further, we discovered the interesting feature of suppression of single-electron switching process in some systems with uniform and weak transversal anisotropy.

Finally, we presented an extension of our symmetry considerations to a rather generic class of multiatom clusters. The Tables 5.1, 5.2 can still
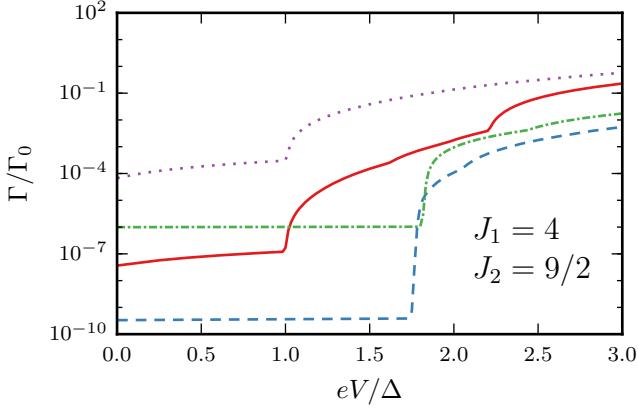
Figure 5.7: Same as in Fig. 5.6 but for a dimer with different spin magnitudes.

be used if the effective spin magnitude of each adatoms composing the cluster is known. Here, we limited our study to generic non-frustrated configurations. Our analysis of the multiatom clusters could be in future extended to many other symmetries (for example to systems where the adatoms form chains or lattices).

All our results are supported by numerical simulations which show the switching behavior of these nanomagnets and offer guidance for experimental measurements, e.g. by scanning tunneling microscopy.

We notice that high rotational symmetry is desirable for the stability of nanomagnets. Indeed, the Brillouin zone associated to the adatom or cluster eigenstates has many elements and systems with a big difference between the grounstates' *quasi*-spin can be found.

We found that the mirror symmetry does not influence qualitative results.

As one rules out the translation symmetry of the substrate, χ is not restricted anymore by the crystallographic restriction theorem [47]. However, our expressions, been generic, are still valid and applicable. For instance, if a single adatom is put at the high symmetric point of a pentagonal *quasi*-crystal, our expressions apply with $\chi = 5$ and we expect the system to have similar (but richer) properties compared to a system with $\chi = 3$. Moreover, the adatom could be put on top of an high symmetric molecule with $\chi > 6$ [48]. However, a quantitative analysis that ensures that environmental crystal field (the one due to the support of the molecule) is negligible must be attached to the study.

Future work may be done in this direction or to prove the conjecture

in section 5.3.3 at arbitrary Heisenberg intergroup couplings.

5.5 Appendix A. Matrix representation of the Hamiltonian in the single-atom case

Here, we analyze an explicit matrix representation of H_A in the single-atom case. This is an alternative to the most straightforward Stevens operator expansion presented in the main text. It proves to be useful for finding the weak constraints on SE switching due to the mirror symmetry and for checking calculations done with other approaches. It may be used for statistical analysis of the system with the tools of Random Matrix Theory[49,50].

As in Sec. 5.2.3, we start considering the spatial symmetry constraints, then we show the one due to TR symmetry.

Rotational symmetry. The symmetry $[R, H] = 0$ imposes all matrix element between different elements with different r to be zero. Clearly the unspecified H can be represent in an hermitian block diagonal form which has, in general, 3 kinds of blocks: blocks associated to R-eigenspaces with real eigenvalue r and pairs of blocks associated to eigenspaces with conjugated pairs of eigenvalues r. To simplify the discussion, assume one real r block, call it $\mathcal{Q}$, and one pair of blocks, call them $\mathcal{X}$ and $\mathcal{Y}$, then:

$$H = \begin{bmatrix} \mathcal{Q} & 0 & 0 \\ 0 & \mathcal{X} & 0 \\ 0 & 0 & \mathcal{Y} \end{bmatrix} \tag{5.25}$$

Mirror symmetry. When acting on the spin eigenbasis $\{|j_z\rangle\}$, the mirror operator in Eq. (5.7) can be written as

$$M = \begin{cases} A & \text{for integer spin} \\ iA & \text{for half integer spin} \end{cases} \tag{5.26}$$

with A a matrix with antidiagonal filled with ones and zeros outside.

The Hamiltonian elements get the simple constraint:

$$\langle j_z | H | j_z \rangle = \langle -j_z | H | - j_z' \rangle. \tag{5.27}$$

It is convenient, to order the elements of this basis in each block by putting states with descending order in j_z, for blocks $\mathcal{Q}$ and $\mathcal{X}$, and with ascending order for $\mathcal{Y}$. For instance, with $J = 3$ and $\chi = 3$ such

basis is $\{|j_z\rangle\} = \{|3\rangle, |0\rangle, |-3\rangle, |2\rangle, |-1\rangle, |-2\rangle, |1\rangle\}$. This choice will be particularly useful when we will implement the TR symmetry.

We see clearly that the mirror symmetry creates a constraint between the elements of block $\mathcal{Q}$ and implies that the block $\mathcal{X}$ must be equal to the block $\mathcal{Y}$.

Time reversal symmetry. We show the constraint due to TR symmetry alone; spatial symmetries are not necessarily present. We order the states of the spin eigenbasis such that TR-partners are grouped together. For instance, with $J = 3$ and $\chi = 3$ such basis is $\{|j_z\rangle\} = \{|3\rangle, |-3\rangle, |2\rangle, |-2\rangle, |1\rangle, |-1\rangle, |0\rangle\}$. In this basis the operator T is represented as

$$T = K \ \oplus_{j \neq 0}^{J} \left[\sigma_x^{(j)} \cos(\pi j) + i\sigma_y^{(j)} \sin(\pi j) \right]$$

$$\oplus \begin{cases} 1^{(j=0)} & \text{for integer spin} \\ -- & \text{for half integer spin} \end{cases} \tag{5.28}$$

where the superscript (j) indicates that the operator acts on the time reversal pair $\{|j\rangle, |-j\rangle\}$ (or on the singlet state when $j = 0$). For the sake of the discussion, we discard the presence of the $J_z = 0$ state for integer spin systems; we reintroduce it next paragraph. The TR symmetry constraint reads

$$\bar{h}_{lk} = \begin{cases} (-1)^{l+k} \sigma_x \, \bar{h}_{lk}^* \, \sigma_x & \text{for integer spin} \\ (-1)^{l+k-1} \sigma_y \, \bar{h}_{lk}^* \, \sigma_y & \text{for half integer spin} \end{cases} \tag{5.29}$$

here all $\bar{h}_{lk}$s are 2×2 Hamiltonian submatrices acting on time reversal pairs with $|j_z| = l, k$.
We see that, for integer systems,

$$\bar{h}_{lk} = \begin{cases} \begin{pmatrix} a & b \\ b^* & a^* \end{pmatrix}, & \text{for l + k even} \\ \begin{pmatrix} a & b \\ -b^* & -a^* \end{pmatrix}, & \text{for l + k odd} \end{cases} \tag{5.30}$$

For half-integer systems

$$\bar{h}_{lk} = \begin{cases} \begin{pmatrix} a & b \\ b^* & -a^* \end{pmatrix}, & \text{for l + k even} \\ \begin{pmatrix} a & b \\ -b^* & a^* \end{pmatrix}, & \text{for l + k odd} \end{cases} \tag{5.31}$$

General form with all symmetries. When TR symmetry is added to the spatial symmetries, the Hamiltonian structure in Eq. (5.25) becomes

$$
H = \begin{cases}
\left[\begin{array}{c|c|c} P & 0 & 0 \\ \hline 0 & S & 0 \\ \hline 0 & 0 & S \end{array}\right], & \text{for } \chi \neq 3 \\[2em]
\left[\begin{array}{c|c|c} C^\dagger PC & 0 & 0 \\ \hline 0 & C^\dagger SC & 0 \\ \hline 0 & 0 & C^\dagger SC \end{array}\right], & \text{for } \chi = 3
\end{cases}
\tag{5.32}
$$

where P is a real matrix where the superdiagonals have components disposed in a palindromic way[*]; S is a symmetric matrix; $C = \text{diag}\{1, i, 1, i, \dots\}$ where the alternating pattern is limited by the dimension of the block. Notice that block $\mathcal{Q}$ is not present for half-integer spin systems with $\chi \neq 3$ (hence P is null), since there are not TR invariant *quasi*-spins in the BZ.

We remark that, for $\chi \neq 3$, the eigenvectors can be chosen to be real, since the Hamiltonian matrix is real and symmetric. For $\chi = 3$, the eigenvectors are complex but can be written in the form $\vec{w} = C^\dagger \vec{v}$ with $\vec{v}$ a real vector. In Dirac notation, the eigenstates could be written as

$$
|\psi\rangle = \begin{cases}
\sum_{j \in block} v_j |j\rangle, & \text{for } \chi \neq 3 \\
\sum_{j \in block} c_{jj} v_j |j\rangle & \text{for } \chi = 3
\end{cases}
\tag{5.33}
$$

Hermiticity constraints the diagonal elements of the half-integer cases bringing to Kramers degeneracy. One relevant consequences of this fact is that systems with $J = 3/2$ and $\chi = 3$ are protected from SE switching processes (as indicated in Table 5.2).

5.6 Appendix B. Weak constraints on the SE switching processes

Here, we show the constraints to the quantity

$$
\langle \psi_{GS} | J_s | \tilde{\psi}_{GS} \rangle, \ (s = +, -, z)
\tag{5.34}
$$

---

[*]We define superdiagonal of order m, ($m \in \mathbb{Z}$), the vector with component $v_i = H_{ij}$ with $i - j = m$. For palindromic vector we mean, for instance $v = (4, 2, -1, 9, -1, 2, 4)$.

coming from the mirror symmetry and the symmetry under the operator TM, effective in a specific regime. The analysis is restricted to the single-atom case. As these constraints appear to affect the SE switching rates only quantitatively we call them "weak" as opposed to the constraints due to time reversal and rotational symmetries. We do not generalize them to the multiatom case as we expect, also for this case, similar weak constraints.

Constraint from the mirror symmetry. Consider the quantity in the expression (5.34) when the mirror symmetry is present. The Hamiltonian eigenstates $|\psi\rangle$ can be chosen to be also eigenstates of R, since $[H, R] = 0$. The commutation relation $RM = MR^\dagger$, then, implies $R\left(M|\psi\rangle\right) = r^* M|\psi\rangle$. This means that $M|\psi\rangle$ is an eigenstate of R but with different *quasi*-spin if r is non real. On the other hand $M|\psi\rangle$ and $|\psi\rangle$ must have the same energy since $[H, M] = 0$. Therefore, when r is not real $M|\psi\rangle \perp |\psi\rangle$ i.e. $M|\psi\rangle = a|\tilde\psi\rangle := aT|\psi\rangle$, with a a unit complex number. Applying M to both sides of the previous equation and using $M^2 = \pm 1$, after a trivial manipulation one gets $M|\tilde\psi\rangle = \pm a^*|\psi\rangle$, where plus(minus) sign refers to integer(half integer) spin systems. About a we only need to know whether it is real or imaginary, as it will be clear in a moment. From Eq. (5.28) and the specification of the form of $|\psi\rangle$ in Eq. (5.33), we see that T maps the vector v, for $\chi \neq 3$, in another real vector, and $w = C^\dagger v$, for $\chi = 3$, to the vector $C^\dagger v'$ (with $v' \neq v$). Differently, M maps the vectors to same-shape vectors but multiplied by the imaginary unit for half-integer spins (see Eq. (5.26)). Therefore, a is real(imaginary) for integer(half-integer) spin systems. We are now ready to obtain the SE switching constraint:

$$\begin{aligned}
\langle\psi_{GS}|J_\pm|\tilde\psi_{GS}\rangle &= \langle\psi_{GS}|M^\dagger J_\mp M|\tilde\psi_{GS}\rangle \\
&= \pm\,(a^*)^2\langle\tilde\psi_{GS}|J_\mp|\psi_{GS}\rangle \\
&= \pm\,(a^*)^2\langle\psi_{GS}|J_\pm|\tilde\psi_{GS}\rangle^* \\
&= \langle\psi_{GS}|J_\pm|\tilde\psi_{GS}\rangle^*
\end{aligned} \tag{5.35}$$

where the external plus(minus) sign refers to integer(half integer) spin systems.

Finally, we conclude

$$\mathrm{Im}\langle\psi_{GS}|J_\pm|\tilde\psi_{GS}\rangle = 0. \tag{5.36}$$

When r is real, it is of interest to consider whether there is a constraint on $\langle\psi_{GS}|J_z|\tilde\psi_{GS}\rangle$, for half-integer spin systems (then with $\chi = 3$). We

show first that

$$\langle\psi|M|\psi\rangle = 0. \tag{5.37}$$

Using Eq. (5.33), we can rewrite the the l.h.s of the previous equation as the scalar product $(w, Mw) = (C^\dagger v, MC^\dagger v)$. Remember, now, that $M = iA$ and notice that the dimension of the block $\mathcal{Q}$ must be even, therefore $iAC^\dagger = CA$ holds. The quantity, then, simplifies to $(v, C^2 Av)$ which vanishes since v is real and $C^2 A$ antisymmetric. Similarly as when r is non-real, we conclude that $M|\psi\rangle = b|\tilde\psi\rangle$.

One could show that b, like a is real(imaginary) for integer(half-integer) spin systems and, with similar passages as before, conclude

$$\mathrm{Re}\langle\psi_{GS}|J_z|\tilde\psi_{GS}\rangle = 0. \tag{5.38}$$

Notice that the constraints (5.36) and (5.38) are not enough to make SE switching processes vanish since, respectively, the real and imaginary parts are left unconstrained and, unfortunately, they are different from zero, given a generic systems.

Constraint from the TM symmetry operation. Here, we show the weak constraint on the expression (5.34) coming from the symmetry operator TM, relevant when the time reversal symmetry is broken by a (rotational symmetry preserving) magnetic field along the z axis. In this situation, the groundstate is non degenerate. However, for small enough B_z, the two lower energy eigenstates retain the same quasi spins and eigenvalues under the action of TM as the ones of the two groundstate at $B_z = 0$. Calling (improperly) these two lower eigenstates $|\psi_{GS}\rangle$ and $|\tilde\psi_{GS}\rangle$ one can find:

$$\begin{cases} \mathrm{Im}\langle\psi_{GS}|J_z|\tilde\psi_{GS}\rangle = 0 \\ \mathrm{Re}\langle\psi_{GS}|J_\pm|\tilde\psi_{GS}\rangle = 0 \quad \text{for integer spin} \\[2mm] \mathrm{Re}\langle\psi_{GS}|J_z|\tilde\psi_{GS}\rangle = 0 \\ \mathrm{Im}\langle\psi_{GS}|J_\pm|\tilde\psi_{GS}\rangle = 0 \quad \text{for half integer spin.} \end{cases} \tag{5.39}$$

We limit ourselves to just show this result because its proof is lengthy and the result is just weak constraints which are not enough to make SE switching processes vanish. The reader may appreciate how, at $B_z = 0$, these constraints plus the constraints in Eq. (5.36) and (5.38) imply the time reversal one in Eq. (5.14).

5.7 Appendix C. Prove of the conjecture in Sec. 5.3.3 at small intragroup couplings

We show a proof of the conjecture that appears in Sec. 5.3.3, restricted to the case when intragroup couplings of the matrix G are small in comparison to all other energies in H_A.

At zeroth order in the intergroup terms in H_A^{int}, without uniaxial anisotropy and magnetic field but with finite intragroup terms, the ground-states are $(2J_A + 1) \times (2J_B + 1)$ product states of the form $J_{-,A}^m |GS_A\rangle \otimes J_{+,B}^n |GS_B\rangle$ with $m(n) = 0, \ldots, 2J_{A(B)}$, $J_{\pm,X} = \sum_{i \in X} J_\pm(i)$ and $|GS_X\rangle$ is the state with all spin aligned up, for $X = A$, and down, for $X = B$. Clearly, once the uniaxial anisotropy is switched on, $|GS_A\rangle \otimes |GS_B\rangle$, along with the other three states obtained by applying the TR operator to the state in either to A, to B or to both, remains the unique ground-state. Indeed, they are eigenstates with maximum eigenvalue of both $\sum_{ij} H_A^{int}(i,j)$ and $\sum_i H_A^{(0)}(i)$. Then, we add small intergroup coupling terms in H_A^{int}, small with respect to the other energies involved. It is straightforward to see that configurations in which the spin of the two groups are oppositely aligned i.e. $|GS_A\rangle \otimes |GS_B\rangle$ along with its TR partner, gain a negative first-order perturbation energy. This energy is equal to $-\sum_{i \in A, j \in B} G_{ij} J(i) J(j)$. On the contrary, the other two states (aligned) gain the same term but with opposite sign. Since the intergroup coupling preserves the value of $J_{z,tot}$ of the perturbed states, the new groundstates will have the same $J_{z,tot}$ of $|GS_A\rangle \otimes |GS_B\rangle$ and its TR partner, given by $\pm(J_A - J_B)$. Thus, the conjecture is proven for small intergroup couplings as claimed in the main text.

Bibliography of chapter 5

[1] P. Gambardella, S. Rusponi, M. Veronese, S. S. Dhesi, C. Grazioli, A. Dallmeyer, I. Cabria, R. Zeller, P. H. Dederichs, K. Kern, C. Carbone, and H. Brune, Science, **300**, 5622, 1130–1133 (2003).

[2] A. A. Khajetoorians, S. Lounis, B. Chilian, A. T. Costa, L. Zhou, D. L. Mills, J. Wiebe, and R. Wiesendanger, Phys. Rev. Lett. **106**, 037205 (2011).

[3] T. Miyamachi, T. Schuh, T. Märkl, C. Bresch, T. Balashov, A. Stöhr, C. Karlewski, S. André, M. Marthaler, M. Hoffmann, M. Geilhufe, S. Ostanin, W. Hergert, I. Mertig, G. Schön, A. Ernst, and W. Wulfhekel, Nature **503**, 242 (2013).

[4] A. A. Khajetoorians1, B. Baxevanis, C. Hübner, T. Schlenk, S. Krause, T. O. Wehling, S. Lounis, A. Lichtenstein, D. Pfannkuche, J. Wiebe, and R. Wiesendanger, Science **339**, 55 (2013).

[5] A. F. Otte, M. Ternes, K. von Bergmann, S. Loth, H. Brune, C. P. Lutz, C. F. Hirjibehedin, and A, J. Heinrich, Nature Physics **4**, 847 – 850 (2008).

[6] S. Loth, S. Baumann, C. P. Lutz, D. M. Eigler, and A. J. Heinrich, Science **335**, 196 (2012).

[7] I. G. Rau, S. Baumann, S. Rusponi, F. Donati, S. Stepanow, L. Gragnaniello, J. Dreiser, C. Piamonteze, F. Nolting, S. Gangopadhyay, O. R. Albertini, R. M. Macfarlane, C. P. Lutz, B. A. Jones, P. Gambardella, A. J. Heinrich, and H. Brune, Science **344**, 988 (2014).

[8] S. Loth, M. Etzkorn, C. P. Lutz, D. M. Eigler, and A. J. Heinrich, Science **329**, 1628–1630 (2010).

[9] F. Donati, S. Rusponi, S. Stepanow, C. Wäckerlin, A. Singha, L. Persichetti, R. Baltic, K. Diller, F. Patthey, E. Fernandes, J. Dreiser, Ž. Šljivančanin, K. Kummer, C. Nistor, P. Gambardella, and H. Brune, Science **352**, 318 (2016).

[10] D. M. Apalkov and P. B. Visscher, Phys. Rev. B **72**, 180405(R) (2005).

Bibliography of chapter 5

[11] Z. Li and S. Zhang Phys. Rev. B **69**, 134416 (2004).

[12] T. Taniguchi, Y. Utsumi, and H. Imamura Phys. Rev. B **88**(21), 214414 (2013).

[13] Gatteschi, R. Sessoli, and J. Villain, *Molecular Nanomagnets* (Oxford University Press, New York, 2006).

[14] F. Donati, A. Singha, S. Stepanow, C. Wackerlin, J. Dreiser, P. Gambardella, S. Rusponi, and H. Brune, Phys. Rev. Lett. **113**, 237201 (2014).

[15] M. Steinbrecher, A. Sonntag, M. dos Santos Dias, M. Bouhassoune, S. Lounis, J. Wiebe, R. Wiesendanger, and A. A. Khajetoorians, Nat. Comm. **7**, 10454 (2016).

[16] F.E. Kalff, M. P. Rebergen, E. Fahrenfort, J. Girovsky, R. Toskovic, J. L. Lado, J. Fernández-Rossier, and A. F. Otte, Nat. Nanotech. **11**, 926 (2016).

[17] A. A. Khajetoorians and A. J. Heinrich, Science **352**, 296 (2016).

[18] W. Wernsdorfer, A. Caneschi, R. Sessoli, D. Gatteschi, A. Cornia, V. Villar, and C. Paulsen, Phys. Rev. Lett. **84**, 2965 (2000).

[19] C. Hübner, B. Baxevanis, A.A. Khajetoorians, and D. Pfannkuche, Phys. Rev. B **90**, 155134 (2014).

[20] J. von Delft, and C. L. Henley, Phys. Rev. Lett. **69**, 3236 (1992).

[21] J. Bartolome, F. Luis, and J. F. Fernández, Molecular Magnets: Physics and Applications (Springer, New York, 2014).

[22] C. Hübner, Ph.D. Thesis, Hamburg University, Germany (2015).

[23] M. Prada, arXiv:cond-mat/1605.03371 (2017).

[24] W. Marshall, Proc. Roy. Soc. A 232 48 (1955); E. H. Lieb and D. Mattis, J. Math. Phys. 3, 749 (1962).

[25] B. Nachtergaele and R. Sims, Markov Processes Rel. Fields (J.T. Lewis special edition), **13** ,315–329 (2007).

[26] B. G. Wybourne, *Spectroscopic Properties of Rare Earths*, Ch. 6.1, 166 (Wiley, New York 1965).

[27] A. Abragam and B. Bleaney, *Electron Paramagnetic Resonance of Transition Ions* (Oxford University Press, Oxford, 1970).

[28] C. F. Hirjibehedin, C. Lin, A. F. Otte, M. Ternes, C. P. Lutz, B. A. Jones, and A. J. Heinrich, Science **317**, 1199–1203 (2007).

[29] J.A. Appelbaum, Phys.Rev. **154**, 633 (1967).

[30] C. Timm, Phys. Rev. B **77**, 195416 (2008).

[31] F. Delgado, S.Loth, M.Zielinski and J. Fernández-Rossier, EPL **109**, 57001 (2015).

[32] E. P. Wigner, *Group Theory and Its Application to the Quantum Mechanics of Atomic Spectra*, Ch. 26 (Academic Press Inc., New York,1959).

[33] K. W. H. Stevens, Proc. of the Phys. Soc., A **65**, 209–215 (1952).

[34] I.D. Ryabov, J. of Mag. Res. **140**, 141 (1999).

[35] C. Cohen-Tannoudji, G. Grynberg, and J. Dupont-Roc, *Atom-Photon Interactions* (Wiley, New York, 1998).

[36] W. H. Zurek, Rev. Mod. Phys. **75**, 715 (2003).

[37] J. Fernández-Rossier, Phys. Rev. Lett. **102**, 256802 (2009).

[38] F. Delgado, J. J. Palacios, and J. Fernández-Rossier, Phys. Rev. Lett. **104**, 026601 (2010).

[39] F. Delgado, J. Fernández-Rossier, Prog. in Surface Science **92**, 40 (2017).

[40] R. Baltic, M. Pivetta, F. Donati, C. Wäckerlin, A. Singha, J. Dreiser, S. Rusponi, and H. Brune, Nano Lett., **16** (12), 7610–7615 (2016).

[41] F. Delgado, J. Fernández-Rossier, Phys. Rev. B **95**, 094431 (2017).

[42] M. A. Ruderman and C. Kittel, Phys. Rev. **96**, 99–102 (1954).

[43] L. Zhou, J. Wiebe, S. Lounis, E. Vedmedenko, F. Meier, S. Blügel, P. H. Dederichs, and R. Wiesendanger, Nature Phys. **6**, 187–191 (2010).

[44] I. E. Dzyaloshinsky, J. Phys. Chem. Solids **4**, 241 (1958); T. Moriya, Phys. Rev. Lett. **4**, 228 (1960).

[45] M. Bode, M. Heide, K. von Bergmann, P. Ferriani, S. Heinze, G. Bihlmayer, A. Kubetzka, O. Pietzsch, S. Blügel, and R. Wiesendanger, Nature **447**, 190 (2007).

Bibliography of chapter 5

[46] Similar theorems on spin systems are under current attention of mathematical physicists. For instance, see B. Nachtergaele, W. Spitzer, and S. Starr, arXiv:math-ph/1509.00907 and Ref. 25.

[47] J. Bamberg, G. Cairns, and D. Kilminster, The American Mathematical Monthly Vol. 110, No. 3, pp. 202–209 (2003).

[48] K. R. Meihaus and J. R. Long, J. Am. Chem. Soc. **135**, 17952 (2013); L. Ungur, J. J. Le?Roy, I. Korobkov, M. Murugesu, and L. F. Chibotaru, Angew. Chem. Int. Ed. **53**, 4413 (2014); Y. Zhang, Appl. Phys. Lett. **108**, 132407 (2016).

[49] Mehta, M.L., *Random Matrices* (Elsevier, Amsterdam, 2004).

[50] V. A. Marchenko and L. A. Pastur, Math. USSR-Sb. **1**(4), 457–483 (1967).

Summary

The 2016 Nobel Prize in Physics was awarded for the theoretical discovery in the 1970's and 1980's of topological states of matter. In the last decade, experimental discoveries have placed topological insulators, semimetals, and superconductors at the center of attention. Applications, in the area of spintronics and quantum computing, are still in the future, but at present these materials offer a wealth of fundamentally new effects to explore.

In this thesis we focus on topological superconductors. The topology manifests itself in the presence of gapless excitations bound to edges or surfaces, which cannot be removed by disorder or other perturbations. The excitations are so-called Majorana bound states, charge neutral particles that are their own antiparticles. A pair of Majorana fermions bound to two magnetic vortices can be used to store quantum information in a way that is nonlocal, insensitive to decoherence. Because of this potential application to quantum computing their properties are under intense investigation. The approach taken in this thesis is to study the universal, model-independent properties of Majorana fermions by means of random-matrix theory: a statistical approach in which only fundamental symmetries enter. The model system to which we apply the theory is a superconducting quantum dot coupled to metal leads (a so-called Andreev billiard).

Random-matrix theory was previously applied to condensed matter systems that were governed by the presence or absence of time-reversal symmetry, producing the three Wigner-Dyson symmetry classes. Chiral symmetry, studied mostly in the context of particle physics, doubled this to six symmetry classes. In a superconductor the particle-hole symmetry gives rise to the four Altland-Zirnbauer symmetry classes, for a total of 10 — the celebrated "tenfold way" of random-matrix theory. The central objective of this thesis is to investigate how particle-hole symmetry modifies the statistics of spectral properties and transport properties, in particular in systems where there is an additional chiral symmetry.

In Chapter 2, we investigate how the coupling to metal leads broadens the midgap spectral peak in a superconducting quantum dot. This peak is a key signature of the presence of a Majorana bound state, observed in conduction experiments as a peak in the differential conductance around zero voltage. A surprising result of our calculation is that ballistic

coupling, without a tunnel barrier, completely hides the Majorana peak in the background density of states. The technical ingredient that enables us to arrive at this result is the calculation of the eigenvalue statistic of the so-called time-delay matrix, the energy derivative of the scattering matrix. With that knowledge we can also access thermo-electric properties such as the Seebeck coefficient, and we find that it is similarly insensitive to the presence or absence of a Majorana bound state.

In Chapter 3 we include the effect of chiral symmetry, which is present at the surface of a topological insulator with induced superconductivity. Chiral symmetry stabilizes multiple Majorana bound states, by preventing a splitting of the midgap states. In contrast to the situation without chiral symmetry, we now find that the density of states and the thermo-electric properties do become sensitive to the Majorana bound states. At the technical level this chapter is more demanding than the previous one, where we could directly apply a technique developed for the Wigner-Dyson ensembles. With the chiral symmetry a new "trick" was needed.

In Chapter 4 we turn to an alternative way to restore the sensitivity to the Majorana bound states in the density of states, which is to introduce a tunnel barrier in the metal leads. While indeed the Majorana peak returns when the ballistic coupling is removed, one needs tunnel coupling in all leads attached to the quantum dot. The Majorana signature remains hidden if only a single metal lead has a ballistic coupling.

Finally, the last chapter is devoted to a problem in a different field: the search for adatomic nanomagnets with stable magnetization. These systems provide a benchmark for studies of decoherence effects and may provide the smallest-size logic unit possible in a condensed matter system. Since a few years, it has been recognized that symmetries are important to qualitatively characterize the stability of the magnetization. However, a complete study of the typical substrate symmetries (rotational and mirror ones) combined with time-reversal symmetry was missing, even for the single-adatom case. We have identified all combinations of symmetry groups that allow for a magnetized doubly degenerate ground state, robust under small crystal field-induced transversal anisotropies and first-order scattering from the substrate electrons. We could generalize the classification to arbitrary bipartite multiadatom nanomagnets with Heisenberg couplings. Our results can be seen as an extension of the celebrated Lieb-Mattis theorem on the ordering of energy levels in magnetic systems.

Samenvatting

In 2016 is de Nobelprijs natuurkunde toegekend aan de theoretische ontdekking van topologische fase van materie in de jaren '70 en '80 van de vorige eeuw. De afgelopen tien jaar hebben experimentele ontdekkingen zulke topologische fasen, isolatoren, half-metalen en supergeleiders, in het middelpunt van de belangstelling geplaatst. Toepassingen op het gebied van spintronica en quantumcomputers zijn nog toekomstmuziek, maar nu al bieden deze materialen een weelde aan fundamentele nieuwe effecten die we kunnen gaan verkennen.

In dit proefschrift richten we ons op de topologische supergeleiders. Topologie toont zichzelf daar door de aanwezigheid van excitaties zonder energie-gap, die gebonden zijn aan randen of oppervlakten van het materiaal, en die niet verwijderd kunnen worden door wanorde of andere verstoringen. Deze excitaties zijn zogenaamde Majorana-toestanden, ladingsneutrale fermiondeeltjes die hun eigen antideeltje zijn. Een paar Majorana-fermionen gebonden aan twee magnetische vortices kan worden gebruikt om quantuminformatie op te slaan op een manier die niet-lokaal is, en daardoor ongevoelig voor decoherentie. Vanwege deze mogelijke toepassing in quantumcomputers worden de eigenschappen van Majorana's intensief onderzocht. De aanpak die we in dit proefschrift volgen is om de universele, model-onafhankelijke eigenschappen van Majorana-fermionen te onderzoeken door middel van de theorie van toevalsmatrices: dat is een statistische aanpak waar enkel de fundamentele symmetrieën een rol spelen. Het modelsysteem waar we de theorie op toepassen is een supergeleidende "quantum dot" met metalen contacten (een zogenaamd "Andreev biljart").

Toevalsmatrix-theorie is in het verleden toegepast op systemen in de gecondenseerde materie waar de aanwezigheid of afwezigheid van tijds-omkeersymmetrie bepalend is. Zo ontstaan de drie symmetrieklassen van Wigner en Dyson. Chirale symmetrie, afkomstig uit de elementaire deeltjesfysica, verdubbelde dit tot een zestal symmetrieklassen. In een supergeleider zorgt de deeltje-gat symmetrie ervoor dat er nog vier symmetrieklassen bijkomen, genoemd naar Altland en Zirnbauer. Het totaal aan 10 symmetrieklassen staat bekend als de "tienvoudige weg" van de toevalsmatrix-theorie. Het centrale doel van dit proefschrift is om te onderzoeken hoe de deeltje-gat symmetrie de statistiek verandert van spectrale eigenschappen en transporteigenschappen, in het bijzonder in

systemen waar de chirale symmetrie ook een rol speelt.

In hoofdstuk 2 onderzoeken we hoe de koppeling aan metalen contacten de spectrale piek in het midden van de energie-gap verbreedt. Deze piek in de toestandsdichtheid is een karakteristiek kenmerk van een gebonden Majorana-toestand, die in geleidingsexperimenten is waargenomen als een piek rond spanning-nul in het geleidingsvermogen. Een verrassend resultaat van onze berekening is dat de ballistische koppeling aan de contacten, zonder tunnelbarrière, de Majorana-piek compleet doet opgaan in de achtergrond. De technische stap die het ons mogelijk maakt om dit resultaat te bereiken is de berekening van de statistiek van de eigenwaarden van de zogenaamde tijd-vertragingsmatrix, namelijk de afgeleide van de verstrooiingsmatrix naar de energie. Met deze kennis hebben we ook toegang tot thermo-elektrische eigenschappen zoals de Seebeck-coëfficiënt, en we vinden dat deze ook ongevoelig is voor de aanwezigheid of afwezigheid van de gebonden Majorana-toestand.

In hoofdstuk 3 nemen we het effect van chirale symmetrie in rekening, die aanwezig is op het oppervlak van een topologische isolator waar supergeleiding is geïnduceerd. Chirale symmetrie stabiliseert meerdere gebonden Majorana-toestanden, door de opsplitsing van de toestanden te voorkomen. In tegenstelling tot de situatie zonder chirale symmetrie, vinden we nu dat de toestandsdichtheid en de thermo-elektrische eigenschappen wel degelijk gevoelig zijn voor de Majorana's. Vanuit technisch oogpunt is dit hoofdstuk lastiger dan het vorige, waar we direct gebruik konden maken van bestaande technieken voor de Wigner-Dyson matrixensembles. De chirale symmetrie benodigde een nieuwe "rekentruuk".

In hoofdstuk 4 vervolgen we met een alternatieve manier om de gevoeligheid voor de gebonden Majorana-toestanden te herstellen, namelijk het toevoegen van een tunnelbarrière in de contacten. Zodra de ballistische koppeling verwijderd wordt keert de Majoranapiek in de toestandsdichtheid terug, mits alle contacten een tunnelbarrière krijgen. De Majoranapiek blijft in de achtergrond verborgen als er ook maar een enkel ballistisch contact overblijft.

Het laatste hoofdstuk, ten slotte, is gewijd aan een probleem uit een wat ander vakgebied: de zoektocht naar nanomagneten met een stabiele magnetisatie. Zulke systemen kunnen gebruikt worden om decoherentie te meten en vormen de kleinste logische rekeneenheid in de gecondenseerde materie. Sinds enkele jaren onderkent men dat symmetrieën belangrijk zijn om de stabiliteit van de magnetisatie te karakteriseren. Een volledige klassificatie van de symmetrieën van het substraat (rotatiesymmetrie, spiegelsymmetrie) in samenspel met tijd-omkeersymmetrie ontbrak, zelfs voor het geval van een enkele geïsoleerde nanomagneet. In hoofdstuk 5 worden alle combinaties van symmetrieën gevonden die een magnetisch tweevoudig ontaarde grondtoestand toestaan. Deze ont-

aarding blijft bestaan in aanwezigheid van anisotropiën ten gevolge van het kristalveld en verstrooiing aan geleidingselektronen. De klassificatie is gegeneraliseerd naar willekeurige multi-atomaire nanomagneten met Heisenberg-koppeling. Deze resultaten vormen een uitbreiding van de beroemde stelling van Lieb en Mattis over de ordening van energieniveaux in magnetische systemen.

Curriculum Vitæ

I was born in Rome, Italy, on the 28th of January 1989. There, I received my primary education and completed it with scientific-oriented high school studies.

In 2007, I enrolled in the Physics department at the university "La Sapienza" (Rome). As a bachelor student I attended additional courses associated to an "Excellence program". In 2010 I graduated *cum laude* at the bachelor level with the dissertation "An essay on Bianchi's Universes and their isotropic limit" with prof. Giovanni Montani. After that, I enrolled in the master program on general theoretical physics and, in early 2013, I obtained the master degree in Physics *cum laude* with the thesis "Collective modes in multiband superconductors" under the supervision of dr. Lara Benfatto. After the graduation I spent a few months working with prof. Claudio Castellani's group with a grant subsidized by the Centro Nazionale di Ricerca (CNR).

In September 2013 I became employed by the University of Leiden, The Netherlands, as a Ph.D. student at the Instituut-Lorentz in the group of prof. Carlo Beenakker. For my thesis I worked mostly on the random-matrix theory applied to topological superconductors. For three consecutive years, I have served as teaching assistant to the master-degree course "Quantum Theory". During my Ph.D. I have attended a number of courses, a summer school and several workshops presenting my work in the Netherlands, Italy, Spain, France, Germany and Israel.

List of publications

- M. Marciani, L. Fanfarillo, C. Castellani, L. Benfatto. *Leggett modes in iron-based superconductors as a probe of Time Reversal Symmetry Breaking.* Phys. Rev. B **88**, 214508, (2013).

- M. Marciani, P. W. Brouwer, C. W. J. Beenakker. *Time-delay matrix, midgap spectral peak, and thermopower of an Andreev billiard.* Phys. Rev. B **90**, 045403, (2014).   [Chapter 2]

- Shuo Mi, D. I. Pikulin, M. Marciani, C. W. J. Beenakker. *X-shaped and Y-shaped Andreev resonance profiles in a superconducting quantum dot.* JETP **119**, 1018–1027, (2014).

- H. Schomerus, M. Marciani, C. W. J. Beenakker. *Effect of chiral symmetry on chaotic scattering from Majorana zero modes.* Phys. Rev. Lett. **114**, 166803, (2015).   [Chapter 3]

- M. Marciani, H. Schomerus, C. W. J. Beenakker. *Effect of a tunnel barrier on the scattering from a Majorana bound state in an Andreev billiard.* Physica E **77**, 54–64, (2016).   [Chapter 4]

- M. Marciani, C. Hübner, B. Baxevanis. *General scheme for stable single and multiatom nanomagnets according to symmetry selection rules.* Phys. Rev. B **95**, 125433 (2017).   [Chapter 5]

Acknowledgements

First of all, I thank my thesis advisors Prof. Carlo Beenakker and Prof. Henning Schomerus. They taught me how to approach daily work with enthusiasm and efficiency, to be proactive and to embark on new projects with courage, to have no resentment after intellectual discussions, to put generously professional skills at others' disposal and many other things. I am grateful to them.

Secondly, I thank my research group and in general all colleagues of the Instituut-Lorentz. During these years I have greatly enjoyed to work and share with them laughters, bureaucratic problems, parties and quite some science. I must confess I began this experience with several prejudices about other countries cultures. I would not say now they were totally wrong, however I have learned (and even began to enjoy) that differences might be difficult to accept but make us richer and more aware of personal limits. I want to give a special thanks to Nicandro who made me realize that social interactions and a relaxed attitude are important and can not be neglected in the name of career and success seeking.

I also want thank the secretaries Fran and Marianne without whom an important Appendix would have never reached the Beadle, I would have never gotten a discount on my first bike and many other things.

How not to mention Lola and my housemate Gyllion, with whom I have shared my deepest thoughts and who have on a daily basis endured my complexes of superiority and inferiority.

I would like to thank also the neocathecumenal communities I am part of, both the Dutch and the Italian ones, for constantly reminding me that God loves me.

Finally, I thank my beautiful family. Their support and love have been the only certainty I had during the toughest periods, a wonderful cherry on the cake during the best moments.

Stellingen
behorende bij het proefschrift
"On the random-matrix theory of Majorana fermions
in topological superconductors"

1. Unlike the conductance, the density of states of a superconducting quantum dot with ballistic contacts cannot be used to detect a Majorana zero-mode.

   Chapter 2

2. In the chiral ensembles, the time-delay matrix contains more information about the number of Majorana zero-modes than the scattering matrix. In the Altland-Zirnbauer ensembles the opposite holds.

   Chapter 3

3. The thermal conductance of a superconducting quantum dot depends on the presence or absence of a Majorana zero-mode unless at least one of the scattering channels is coupled ballistically to the quantum dot.

   Chapter 4

4. When antisymmetric exchanges are negligible and transversal anisotropies small, the low-temperature magnetization stability of multiatom nanomagnets is determined by the symmetries, the spin magnitudes and the signs of the exchange terms.

   Chapter 5

5. The statistics of the compressibility of a chaotic Andreev billiard is not universal.

6. The attractor and repeller found by Gerasimenko *et al.* in non-linear 1D quantum walks must also be present if a (sign-definite) space dependence of the coefficient in front of the non-linear term is allowed.

   Y. Gerasimenko, B. Tarasinski, and C. W. J. Beenakker,
   Phys. Rev. **A** 93, 022329 (2016).

7. Particle-hole entanglement can be detected via Bell inequalities if one uses Andreev reflection to rotate the Nambu pseudospin.

8. The protection of some magnetized adatoms with half-integer spin from Kondo-assisted tunnelling, predicted by Prada, stems from a mistaken anticommutation in equation (14).

   M. Prada, arXiv:1605.03371.

Marco Marciani
21 June 2017